Università degli Studi di Cagliari

**DOTTORATO DI RICERCA**

Scienze e Tecnologie Chimiche

Ciclo XXIX

# BIOPHYSICAL CHARACTERIZATION OF A NOVEL CLASS OF MEMBRANE-ACTIVE BRANCHED POLYPEPTIDES

CHIM/02


| | |
|---|---|
| Presentata da: | Ilaria Serra |
| Coordinatore Dottorato | Prof. Stefano Enzo |
| Tutor | Prof. Mariano Casu<br>Dr. M. Andrea Scorciapino |



Esame finale anno accademico 2015 – 2016

Tesi discussa nella sessione d'esame marzo – aprile 2017

PON Ricerca e Innovazione 2014- 2020
Unione Europea
Ministero dell'Istruzione, dell'Università e della Ricerca
REGIONE AUTONOMA DELLA SARDEGNA
POR SARDEGNA
Unione Europea
Fondo Sociale Europeo

Università degli Studi di Cagliari
Università degli studi di Sassari

**DOTTORATO DI RICERCA**

Scienze e Tecnologie Chimiche

Ciclo XXIX

# BIOPHYSICAL CHARACTERIZATION OF A NOVEL CLASS OF MEMBRANE-ACTIVE BRANCHED POLYPEPTIDES

CHIM/02

Presentata da: Ilaria Serra

Coordinatore Dottorato: Prof. Stefano Enzo

Tutor: Prof. Mariano Casu
Dr. M. Andrea Scorciapino

Esame finale anno accademico 2015 – 2016
Tesi discussa nella sessione d'esame marzo – aprile 2017

*La presente tesi è stata prodotta durante la frequenza del corso di dottorato in Scienze e Tecnologie Chimiche dell'Università degli Studi di Cagliari, a.a. 2015/2016 - XXIX ciclo, con il sostegno di una borsa di studio finanziata dall'Università degli Studi di Sassari con le risorse del P.O.R. SARDEGNA F.S.E. 2007-2013 - Obiettivo competitività regionale e occupazione, Asse IV Capitale umano, Linea di Attività l.3.1 "Finanziamento di corsi di dottorato finalizzati alla formazione di capitale umano altamente specializzato, in particolare per i settori dell'ICT, delle nanotecnologie e delle biotecnologie, dell'energia e dello sviluppo sostenibile, dell'agroalimentare e dei materiali tradizionali*

*“Posteriores enim cogitationes sapientiores solent esse”*

(Cicerone*, Filippiche)*

Ever increasing number of resistant pathogens is seriously threatening global health care. With a possible new dark era of medicine at the horizon, new classes of antimicrobials and alternative strategies are urgently needed. In this scenario, Nature can provide prototypes of potential solutions. Biologically active molecules can be rationally modified in order to tailor their activity for specific therapeutic applications. To this aim, structure-function relationships have to be clearly identified and characterized at a molecular level. Among different new molecular classes investigated during the last decades, antimicrobial peptides have received particular attention from the scientific community. However, beside great potentialities and versatility, severe drawbacks limit their actual application and developments as drugs. Usually, high activity is accompanied by not negligible toxicity. This unlikely comes from the main potential advantage of antimicrobial peptides action when compared to conventional anti-infectives. Instead of specific and often intracellular targets, antimicrobial peptides typically exploit their activity by targeting and altering the fundamental physical properties of biological membranes, more specifically, the lipid bilayers. However, these represent the ubiquitous constitutive element of any biomembrane, meaning that often peptides specificity for the pathogen's membrane cannot be guaranteed. This issue, among others, has prevented development of such class of natural compounds into real therapeutics so far. Although numerous synthetic and semi-synthetic strategies have met success in solving a variety of their drawbacks, the new class of direct microbicidal drugs has still to come. Possibly, the strategy is simply wrong, or to say better, is overoptimistic. Possibly, seek for the "magic bullet" has to be abandoned in favour of other approaches. As the World Health Organization suggested, we should also think about new adjuvants to help the already available antimicrobial drugs to overcome their current limitations in tackling resistant pathogens.

The present work was devoted to the characterization of a novel class of branched polypeptides, endowed with several advantages over typical natural antimicrobial peptides, like the lower susceptibility to proteases degradation. A lysine linker represented the core of the dendrimeric architecture, with two identical copies of the active 10-mer amino acid sequence bound on the α- and ε-nitrogen, respectively, and an octanamide tail at the C-terminus. In recent years, the research group has already performed investigations on this interesting class of membrane-active compounds, providing first fundamental information such as antimicrobial activity in standard media, qualitative estimation of bilayer affinity and 3D structure in simple membrane mimicking environments. An intensive biophysical characterization has been undertaken during the last three years within the present PhD programme, aimed at more comprehensive understanding of the behaviour of such unusual peptides by using lipid bilayers as more accurate membrane model and taking physiologic electrolytes concentration into consideration. Particular efforts were spent to unveil the mechanism of action, a difficult task that required combination of different methodologies. Spectroscopic techniques, like both absorbance and fluorescence UV-vis spectroscopy and attenuated total reflectance infrared spectroscopy represented the main investigation tools, together with surface pressure measurements of lipid monolayers at the air-water interface. In addition to dynamic light scattering, setup of numerical models to analyse the results completed the strategy. Different collaborations were also needed to provide further insight from microbiological assays and transmission electron microscopy.

The work comprised two complementary parts. The comparison of two analogues with the same tail and net positive charge, allows focusing on the effects of amphipathic profile regularization of the

amino acid sequence. By inverting the position of just two residues at the N-terminus, dramatic differences were found both in terms of structural order and activity. Overall, the investigated peptides were found to fold in β-hairpin like conformation at a monomeric level, and to form extended aggregations with increasing peptide local concentration on the membrane. The structural order was determined by the inherent characteristics of the peptide sequence as well as by system electrostatics, ultimately affecting peptide activity. The second research line focused on several analogues with highly hydrophobic tail of different length. Quite unexpectedly, a membrane-anchoring tail worsened peptide efficacy. Conversely, the original hydrophilic tail provided enough mobility in the bound phase, thus, allowing peptide to escape from local structural minima and to find the proper order to exploit its full activity.

To my opinion, the present work is not only interesting for the peculiarities specifically pertaining to the investigated peptide family, but because these represent the smallest prototypical dendrimeric peptides with lysine based core. Structure-function investigations on dendrimenric peptides are almost completely lacking, whereas biological activity studies are numerous, on the other hand. It is fundamental to fill in this gap and to understand what is really due to the specific peptide sequence, to the branching spacers or to the branches number, if rational design of such complex molecular architecture is the goal. In addition, the characteristic β-type folding makes the investigated peptides interesting as elements of a structural class of membrane-active peptides that has still to be fully understood.

***List of relevant publications:***

I. Serra, M.A. Scorciapino, G. Manzo, M. Casu, A.C. Rinaldi, S. Attoub, M. Mechkarska, J.M. Conlon "*Conformational analysis and cytotoxic activities of the frog skin host-defense peptide, hymenochirin-1Pa*" Peptides 61, 114-121 (2014).

G. Batoni, M. Casu, A. Giuliani, V. Luca, G. Maisetta, M.L. Mangoni, G. Manzo, M. Pintus, G. Pirri, A.C. Rinaldi, M.A. Scorciapino, I. Serra, A.S. Ulrich, P. Wadhwani "*Rational modification of a dendrimeric peptide with antimicrobial activity: consequences on membrane-binding and biological properties*" Amino Acids 48, 887-900 (2016).

G. Manzo, I. Serra, A. Pira, M. Pintus, M. Ceccarelli, M. Casu, A.C. Rinaldi, M.A. Scorciapino "*The singular behavior of a β-type semi-synthetic two branches polypeptide: three-dimensional structure and mode of action*" Physical Chemistry Chemical Physics 18, 30998-31011 (2016).

I. Serra, G. Manzo, M. Casu, M. Ceccarelli, P. Gameiro, A.C. Rinaldi, M.A. Scorciapino "*Dissecting the role of the peptide domain and the tail on the structure order of short β-type two branches membrane-active polypeptides*" (In preparation).

I. Serra, A. Ardu, M. Casu, C. Cannas, M. Ceccarelli, A.C. Rinaldi, M.A. Scorciapino "*Correlation between structure order and fusogenic activity for short β-type two branches membrane-active polypeptides*" (In preparation)

*Undertaking this PhD has been a truly life-changing experience for me. It would not have been possible to do this without the support and guidance from many people. Now, at the very end of my PhD period, I would like to thank all the people who supported and helped me in any way during the last three years. Sardinia Regional Government is greatly acknowledged for the financial support of my PhD scholarship (P.O.R. Sardegna F.S.E. Operational Programme of the Autonomous Region of Sardinia, European Social Fund 2007-2013 - Axis IV Human Resources, Objective l.3, Line of Activity l.3.1.).*

*First, I would like to express gratitude to my supervisor Prof. Mariano Casu. He encouraged and gave me the opportunity to undertake this important path and for his continuous support. He provided me with his years-long experience in molecular spectroscopy and taught me to never give up and always do my best in all situations.*

*Profound gratitude goes to my other supervisor Dr. Andrea Scorciapino, who assisted me during my PhD. He shared motivation and enthusiasm even when experimental work was not going as expected. His guidance was important to me during both research and writing activity. The best advisor I could wish for my PhD.*

*My sincere thanks to Prof. Andrea Rinaldi for support, encouragement, comments and critics provided during these three years.*

*Also, I have to thank Prof. Matteo Ceccarelli for his precious help and support.*

*I am very "obrigada" with Prof. Paula Gameiro of the Departamento de Química e Bioquímica of Porto University and all her research group, in particular, Mariana Ferreira, Filipa Sousa and Bárbara Magalhães, for hosting me during my stage period, which, beside extending my scientific knowledge, contributed to broaden my horizons.*

*Many thanks to Prof. Carla Cannas and Dr. Andrea Ardu for the TEM images and the fruitful discussions, Prof. Guido Ennas for his time and help during a campaign of differential scanning calorimetry, which I did not included in the manuscript but contributed to my professional growth, Prof. Anne Ulrich and Dr. Parvesh Wadhwani of the Karlsruhe Institute of Technology for the synthesis of some model peptides used during my work, Prof. Maria Luisa Mangoni and Dr. Vincenzo Luca of the University of Rome "Sapienza" for the microbiology assays on my peptides and Prof. Giovanna Batoni of Pisa University and her group for the fundamental collaboration on biofilm activity.*

*My special thanks to Dr. Giorgia Manzo who helped me during the first months of my PhD. I learnt lots of lab tips and tricks and I really enjoyed being your colleague and roommate.*

*Particular thanks goes to Dr. Cristina Piras, who shared coffee breaks, lunches and campus gossips (crastuli) during the whole PhD period. I really enjoyed the time spent with you.*

*Thanks to my colleague Alessandro Pira, and the other PhD students of the Department, who made every single day of these three years sustainable.*

*Thanks to every people who I met and gave any kind of contribution to the growth of my knowledge.*

*My best thanks goes to my family, my parents and my brothers, who, with many efforts and sacrifices, have allowed me to achieve this important goal.*

*Last but not least, thank you Andrea who have always believed in me and have been so patient when I was in my "Kurt Cobain" mood. You gave me the strength to overcome all difficulties of the last three years.*

*Finally, I would like to thank Oreste, who stared at me while I was writing this PhD thesis.*

# 1 Introduction

## 1.1 HDP (host defence peptides): background and perspectives

Every day we are constantly exposed to an incredible high number of potential pathogens, like bacteria, fungi, protozoa and viruses.[1] They could enter our body by several ways, like ingestion, inhalation or simply through a direct contact with the carrier of infection.[1] Our exposure can be prevented, but not completely eliminated, as pathogenic microbes are nowadays pervading the biosphere.[2] Fortunately, through the evolution, almost all multicellular organisms have developed a defence mechanism, the innate immune system, to ensure a primary protection against pathogenic agents.[2] Such host defence system is characterized by broad-range and non-specific spectrum of action.[2] Besides innate immune system, vertebrates have developed a more sophisticated defence system in addition, the adaptive immunity, which is composed by highly specialized cells and, after an initial response to a specific pathogen, creates immunological memory.[2]

Host defence peptides (HDPs) represent one of the most important components of innate immunity.[3] The term HDP is typically referred to a class of peptide molecules endowed with a wide range of biological activities, both direct antimicrobial and immunomodulatory activity.[3,4] Many studies demonstrated the importance of such peptides in the defence mechanism of almost all living organism, ranging from the simplest ones, like bacteria, to the more sophisticated multicellular organisms, as mammals, including humans.[3,5] HDPs are gene-encoded molecules that are expressed by different cells. In mammals, for instance, they can be expressed by monocytes, neutrophils, epithelial cells, mast cells etc.[6] Multicellular organisms express HDPs either systematically and/or localized in certain regions/tissues, usually those areas that are more susceptible to infections.[7]

HDPs are involved in the modulation of the immune response, as bolstered by the presence of a high number of these molecules in immune circulating cells and in the sites of starting infections.[1] On the contrary, when the production of HDPs is affected by genome mutations, higher susceptibility to infections is usually observed.[3,8–10] Among all the effects documented for HDPs, one of the most important function is the immune cells recruitment at the site of infection, followed by a direct contribution to clearance of the infection. The broad activity of HDPs includes also the anti-inflammatory response. In the literature there is a large number of peptides with anti-inflammatory activity, like cathelicidin LL-37, defensin hBD-2, IDR-1 and IDR-1002, that are able to modulate the host immune inflammatory response generated by pathogens.[8] Their action is typically the suppression of pro-inflammatory processes, like the induction of tumour necrosis factor TNF-α, pro-inflammatory cytokines, and nitric oxide through different specific mechanisms.[8] Defensins and cathelicidins are the two most important families of HDPs identified so far.[4] The former are cationic amphipathic peptides constituted by about 30 residues. Depending on the disulphide bond pattern, defensins can be classified in three subfamilies: α, β and θ defensins.[4] Some α-defensin, known as cryptidins, are activated after microbial stimulation are reach a concentration high enough to guarantee an effective microbicidal action.[4] β-defensins are typically expressed after pro-inflammatory stimuli and infection by epithelial cells, and are present in several mucosal secretions, like in the gastrointestinal and respiratory tract.[4] θ-defensins are less common. These and produced by neutrophils and monocytes, and are characterized by a cyclic structure.[4] Differently, cathelicidins are synthesised in non-active form, and present higher variability in terms of length, sequence and structure. They can be found either as extended α-helices or β-hairpins.[4]

Other important examples of HDPs are dermicidins present in human sweat, which have an overall negative charge, histatins, histidine-rich cationic peptide present in saliva and endowed with antifungal activity, lactoferricin, a cationic peptide generally found in muscular secretions, milk and in the granules of leukocytes.[4]

Overall, the class of HDPs have a remarkably broad range of functions, which is obviously reflected by a wide variety of mode of action. There are well-documented examples of peptides that translocate inside the cell, without damaging the outermost layers, and target key cellular processes.[10,11] The frog peptide buforin II, for instance, translocates through the outer and inner membrane of *Escherichia coli* cells and accumulates in the cytoplasm, then it binds to DNA and RNA interfering with their fundamental biochemical pathways.[7,11] Others examples of peptides interfering with nucleic acids metabolism are the β-sheet human defensin hNP-1 and the extended structure indolicidin.[7,11] The proline-rich insect peptides drosocin, apidaecin and pyrrhocoricin are thought to interact with intracellular proteins[7,11–13] On the other hand, a wide variety of peptides are known to act by directly disrupting the lipid bilayers or impairing its physical properties through a wide range of different mechanisms.[2,10,11,14,15] Examples are the cathelicidin-derived human amphipathic α-helical peptide LL-37,[16] the membrane-lysing α-helical peptide pardaxin isolated from the fish *Pardachirus marmoratus,*[17] protegrins with two-stranded antiparallel β sheet structure derived from *porcine neutrophils*,[18,19] the α-helical peptides magainins discovered in the skin of *Xenopus laevis*,[20,21] the β-sheet tachyplesin family peptides were isolated from the hemocytes of *horseshoe crabs*,[21] the cyclic peptide gramicidin S secreted by *Bacillus brevis*,[22] the extended α-helical melittin present in the venom of the bee *Apis mellifera*[23] and the flexible helix peptide alamethicin derived from the fungus *Trichoderma viride*.[23]

Regardless the action of the HDPs involves some specific intracellular targets, or is exploited through damage of a totally unspecific target like the lipid membrane, peptides-membrane interactions are fundamental.[11] Even if intracellular targets are the final goal, peptides must cross the cell membrane, with the majority of HDPs not having a specific receptor/transporter, while they are usually active against the lipid membranes.[24] Some HDPs are also known to act by more than a single mode of action, thus lowering the chances for the pathogen to develop resistance. Magainin and indolicidin have been extensively studied and represent typical examples of peptides endowed with multiple modes of action.[11]

Peptide-membrane interaction is a complex multivariate process. Beside extreme variability of amino acid sequence among the HDPs, also lipid membranes show remarkable variability, in terms of composition, local charge, density, fluidity, curvature, thickness, etc. The nature of the lipids in the bilayer influence membrane properties, both their polar head group and their acyl chains length and the degree of unsaturation.[25] For example, generally speaking, eukaryotic membranes are composed mainly by zwitterionic lipids, while bacterial membranes are characterized by a significant fraction of negatively charged lipids.[26] Peptides' mode of action strongly depends on the specific nature of the lipid bilayer but also on its environment. In particular, pH, ionic strength, presence of degradation enzymes and temperature impact peptide-membrane interaction. One example is given by clavanins, which are histidine-rich antimicrobial peptides originally isolated from the leukocytes of a tunicate (*Styela clava*). It was demonstrated that both clavanin A amide and clavanin A acid displayed a great activity against *E. coli*, *Listeria monocytogenes* and *Candida albicans* at pH 5.5, while being significantly less active at pH 7.4.[27]

On the contrary, a synthetic variant of clavanin A acid, clavanin AK, showed a substantial activity at both pH values.[27]

Thus, most HDPs are part of a larger group of bioactive peptides typically referred to as membrane-active peptides, as they are able to perturb the lipid packing which represents the fundamental element of biological membranes. The consequence of peptide activity is strictly dependent on the specific peptide's mode of action, but the bilayer usually undergo some structural changes that can be described as either extensive or local phase change. An example is given by the human cathelicidin peptide LL-37, who is able to change the phase of lipid aggregates composed by zwitterionic lipids from lamellar bilayers to disk-like micelles.[25]

Today, antimicrobial resistance is becoming an extremely complex and serious healthcare challenge worldwide. According to World Health Organization, Gram-negative bacteria are of particular concern, since the therapeutic alternatives in our hands to contrast infections from several multi-drug resistant strains have almost expired.[28] The term HDP is relatively new, while peptides of the innate immune system were typically referred to as antimicrobial peptides (AMPs). The first molecules were isolated around the 1980,[3] immediately attracting researchers' attention because of their ability to kill a variety of pathogens, including bacteria, viruses, fungi and protozoa.[29] Most of them were cationic and, thus, generally showed higher selectivity for bacterial than eukaryotic cell membrane, with such selectivity being one of the most interesting aspect for the development of a new class of antibacterial drugs.[3,7,11,30] In addition, due to their highly unspecific target, the lipid bilayer, it was believed that resistance to AMPs was less likely developed by bacteria, compared to the specific action of most of the available antibiotics. As already mentioned, AMPs are found in almost all living organisms, including bacteria, plants and animals, both invertebrate and vertebrate.[7] They have been originally isolated from insects and amphibians, as these were particularly abundant sources, making purification process easier and providing high yield. The granular glands of amphibian skin is an extremely rich source of AMPs, with the peptides isolated from frogs and toads skin secretions usually endowed with broad spectrum antimicrobial activity, both against Gram-positive and Gram-negative bacteria.[7] Megainins,[31] buforin II,[32] temporins[33] and esculentins[34] are just few examples.

Although the first studied AMPs showed interesting direct microbicidal effects, their important role also in the innate immune system and inflammatory response became clear more recently, and the term HDP was adopted as more appropriate and comprehensive, in order to take into account all of the different aspect of the complex activity of these peptides, including their immunomodulatory properties.[3] These posed much concern about possible side effects on HDPs therapeutic development. Their potentially high toxicity appeared also soon, inherently due to their unspecific primary target, the lipid bilayer, which is present also in host cells and sub-cellular organelles. This, in addition to other serious drawbacks, severely limits AMPs therapeutic applicability (see §1.4), such that only few peptides have advanced into clinical practice, mostly for topical applications. Among them, the magainin derivative MSI-78 (Pexiganan) for impetigo and diabetic foot ulcers, the cattle indolicidin variant CP-226 (Omiganan) for catheter-associated infections, the pig protegrin derivative IB-367 (Iseganan) for oral mucosaitis, and the human bactericidal permeability protein derivative $rBPI_{23}$ (Neuprex) for the treatment of sepsis.[5]

Possibly, the design of a new antibiotic class using natural HDPs as templates, characterized by high direct bactericidal potency and negligible side effects, will remain chimeric. As suggested also by the WHO, more scientific efforts should be spent on complementary solutions to the problem of antimicrobial resistance.[35] Membrane-active peptides can be taken as templates for the design of

new compounds to be used in combination with the already available antimicrobials. In the literature some examples are reported for the synergistic action of drugs belonging to different classes, like the β-lactamase inhibitor clavulanic acid used together with amoxicillin, or the more recent example of ceftazidime/avibactam, a 3rd generation cephalosporin and a novel non-β-lactam β-lactamase inhibitor, respectively.[35] For instance, peptides with good permeation through the lipid bilayer might be used as carriers for antimicrobials, or a good membrano-lytic activity might be exploited by other drugs to penetrate better into the pathogen cell. Polymyxin B nonapeptide, for example, and deacylpolymyxin B are characterised by a weak direct antimicrobial activity, but both of them have the capacity to improve up to 100 times the activity of rifampin, a macrolide antibiotic, fusidic acid and novobiocin, against *E. coli*.[36] Another example is given by the synthetic peptide KFFKFFKFF, which is able to decrease rifampin MIC against *E. coli* by a factor of 300.[36] An artificial peptide ($KLKL_5KLK$) showed adjuvant activity in animal models as a potent inducer of adaptive immunity.[37]

## 1.2 Structural features of natural HDPs

HDPs are typically cationic and comprise 12-50 amino acid residues. Their molecular mass is typically less than 10kDa,[14] and the overall positive net charge is between +2 and +7.[1] This cationic character (modulated by pH) is mainly responsible for HDPs selectivity towards microbial targets with respect to the host's cell, since the positive charge promotes the initial electrostatic attraction with the anionic lipids, that are typically absent in eukaryotic cells.[36,38] A fraction ≥50% of the amino acid residues are hydrophobic, especially leucine, tryptophane and valine. This ensures high peptide affinity for the lipid membrane, which is fundamental for their activity.[1] It was found that, without changing cationicity and overall amphipathic character of the peptide, a higher hydrophobicity caused selectivity reduction, by promoting the interaction with zwitterionic lipids and resulting in toxicity enhancement.[14]

The presence of both strongly hydrophilic and hydrophobic residues drives HDPs to adopt an amphipathic folding upon interaction with lipid membranes,[3] such that hydrophobic residues are embedded within lipid tails and protected from contacts with water molecules, while the hydrophilic ones within the polar head groups and water exposed. The amphipathic folding appeared a fundamental feature of HDPs, such that changes in the amino acid sequence, even subtle, are sometimes responsible of a deep alteration of peptide activity and/or mechanism.[3] In spite of the mentioned similarities among HDPs, different secondary structure motives are represented,[14] so that HDPs are typically divided into four broad structural classes: α-helical, β-sheets, extended conformation and loop peptides with disulfide bridges.[3]

*α-helical peptides.* The group of α-helical peptides is the largest and the most studied one. It is composed by more than 300 molecules discovered so far.[14] Most of the mechanism described in the literature were hypothesized on the basis of investigations carried out on this group. These linear peptides are usually composed by less than 40 amino acids, often with a kink or hinge in the central region, as seen for dermaseptins, and hymenochirin-1Pa.[14,39] Unfortunately, a high number of structure-function studies have shown that, although activity can be high, these peptides are also highly cytotoxic towards mammalian cells.[11] Both activity and toxicity appeared to correlate with

helicity, as shown by the introduction of either D amino acids in the peptide sequence,[40] or a Gly near the centre.[38] Often, α-helical peptides are long enough to span the thickness of the lipid bilayer and act through pores formation (see §1.3).[11] They have been found in numerous sources, like extracellular fluids of invertebrates, insects, nematodes, frogs and mammalian neutrophils, and examples of well characterised peptides are cecropins, magainins and melittin.[14] The family of cecropins have been extensively studied since their first isolation from the pupae of cecropia moth. Among the various members of this family, cecropin A was seen to adopt the typical amphipathic helical conformation in the presence of an appropriate membrane-mimicking environment.[14] Magainins are a group of membrane-active peptides that fold into an α-helical secondary structure upon binding to phospholipid membranes, as studied through numerous techniques, in particular with solid-state NMR.[14,41–43] These are immunogenic peptides isolated from both the skin and the intestine of frogs. These are 23-residues peptides endowed with a broad spectrum activity against bacteria and fungi, but they also showed anti-tumoral activity.[14] Melittin is found in bee venom and its derivatives are generally highly haemolytic, even though characterized by a broad spectrum activity. These peptides are typically composed by 26 residues and fold into a α-helix interrupted at the level of residues 11 and 12.[14]

*β-sheet peptides.* This group is both less abundant and less studied than the previous one. These peptides are characterized by a number of β-strands, sometimes with a few helical domains, but overall folded in an amphipathic structure.[14] This group is also characterized by the presence of cysteine residues in the amino acid sequence, which are responsible for disulphide bonds, like in the case of tachyplesins, protegrins and lactoferricin.[14] In peptides like gramicidin S, polymyxin B and tyrocidines, the peptide's backbone is cyclic.[14] Among the different families of peptides characterized by disulphide bridges, defensins are definitively the most important.[14] They are typically arranged into several antiparallel β-strands, which are stabilized by the presence of cysteine residues paired into up to six disulfide bonds.[14]

The study of β-sheet peptides is also important to understand the structural determinants of amyloid fibrils formation, which is thought to be one of the most important factor to neurodegeneration and clinical dementia typical, for instance, of Alzheimer disease.[44] Amyloidogenic peptides are found indeed as plaques in the parenchyma of the brain, and the characteristic amyloid-like-fibers are mostly composed by peptides in a predominantly β-sheet conformation.[44,45]

*Extended peptides*. Peptides belonging to this group show no regular secondary structure. These are typically rich in amino acids like proline and arginine (PR-39), tryptophan (indolicidin), and histidine (histatins).[11,14] They are characterized by a very flexible structure, and most of them are cell-penetrating instead of membrane active.[11]

*Loop peptides*. These peptides are definitely more unusual than those belonging to the classes presented above. Loop peptides are characterized by the cyclization of peptide backbone. Some examples are cattle bactenecin[46] and gramicidin.[47]

Figure 1.1 shows an example for each peptide group describes above.

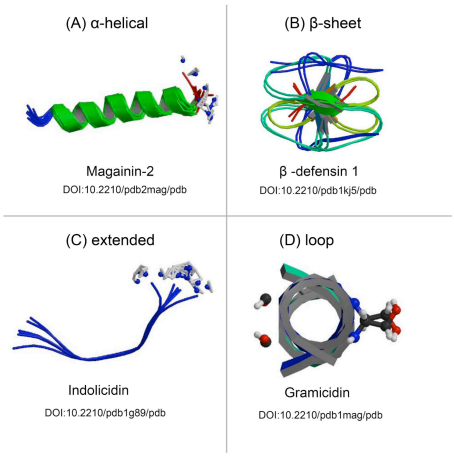


**Figure 1.1.** HDPs can be divided into four classes, depending on the structure they adopt upon interaction with the lipid bilayer: (a) α-helical, (b) β-sheet (c) extended and (d) loop peptides. Image taken from the reference.[48]

Usually, peptides with highly regular α-helical structure are highly haemolytic. Analogues of melittin and pardaxin, where one amino acid was substituted by its D enantiomer, showed a lower haemolytic character, without affecting the antimicrobial activity,[40] suggesting that a rigid and regular structure should be avoided in peptide design. On the contrary, when proline residues were incorporated in the N-terminal fragment of cecropin A and cecropin P1, helicity decrease was accompanied by reduction of antimicrobial activity against some bacterial strains.[40]

Tachyplesin-I is an arginine-rich β-hairpin antimicrobial peptide, which was isolated from the horseshoe crab *Tachyplesus tridentatus*.[49] The study of different analogues suggested that in this case a high structural order was necessary to prevent the formation of extended structures, which were considered responsible for the loss of peptide in-plane mobility and consequently the reduction in peptide activity.[49] A more regular β-hairpin conformation was found to prevent the formation of immobilized extended structures, while favouring a monomeric behaviour, which was responsible for a higher peptide lateral mobility and bilayer perturbing activity.

These are only few examples to stress how it is important to carry out specific studies on structure-function relationship. General roles to guide peptide design, if any, have not been unveiled yet.

## 1.3 Mechanisms of action

Some HDPs with immunomodulatory and antiviral effects are known to act through specific interaction with determined extra- and intracellular targets. However, most of the HDPs, especially the AMPs, exert their efficacy by directly acting against lipid membranes.[38] Such activity, largely unspecific, has been investigated for quite a long time and, although much have still to be deciphered, lots of information about different modes of action is documented in the literature, while immunoregulatory properties of HDPs are largely unclear. In many cases, multiple-mechanisms are used by peptides to kill pathogens.[5,7,11,50]

Regardless the specific mode of action, it is widely recognised that the interaction with the lipid bilayer is the very first step of peptides' activity.[7,11] Peptides are usually unstructured in the aqueous solution, but adopt a well defined amphipathic conformation upon interaction with the lipid

membrane.[14] This first step of adhesion is mostly driven by electrostatics, since the cationic peptide is attracted by the net negative charge of the membrane. Electrostatics determines peptide displacement the solution bulk to the membrane surface, and a partition equilibrium is thus generated between the two immiscible phases, the solution and the lipid bilayer.[7,14] In the case of intact bacteria, the precise mechanism used by peptides to reach the plasma membrane is not fully understood, but many authors consider fundamental for selectivity the negative charge of lipid A in lipopolysaccharides (LPS), in the case of Gram-negative bacteria, and teichoic and lipoteichoic acids, in the case of Gram-positive bacteria.[14,38] After crossing the outer membrane, peptides bind the plasma membrane and fold in their active structure. Again, the presence of negatively charge lipids is fundamental to attract peptides from the periplasm. The amphipathicity of AMPs secondary structure is fundamental to ensure thermodynamic stability of the bound state. As already mentioned, this is due to favourable interactions of both hydrophobic and hydrophilic residues. The former interact with the lipid tails and avoid contact with the water molecules, while the latter interact with both water molecules and the charged/polar lipid head groups.[11,14] Depending on the specific mechanism being adopted, peptides must reach a minimal local concentration on the membrane surface to exert their activity.[14]

After adhesion, several models have been proposed to explain the activity observed for the various peptides investigated so far. Some of them are really able to disrupt and/or permeabilize the lipid bilayer, like in the case of pore formation or the so-called carpet model. Other peptides do not cause effective disruption but, rather, alter lipid packing, order and physical properties, like the clustering of anionic lipids and membrane depolarization[7,12,14] Figure 1.2 summarizes the most common peptides' modes of action.

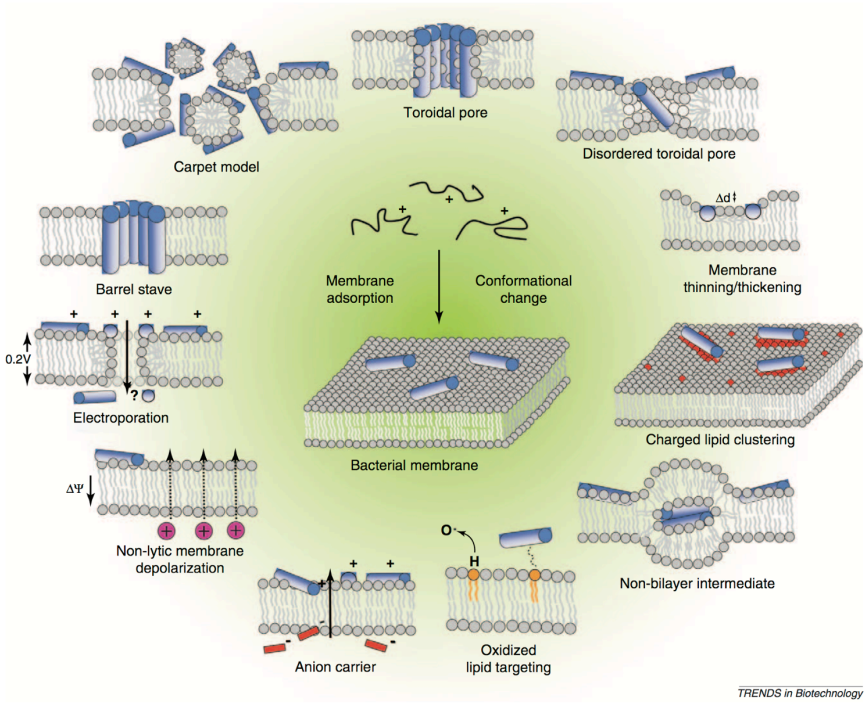


**Figure 1.2.** Most common modes of action of membrane-active peptides. Different mechanisms are not necessarily mutually exclusive, but more than a single one can be necessary for the peptide to kill the targeted microorganism. Image taken from the reference.[11]

Among the lytic models, peptides insert into the bilayer and form pores, or they disrupt the membrane into micelle structures through the carpet mechanism. Examples of non-lytic action are the clustering of anionic lipids, in which cationic peptides attract anionic lipids to form peptide-lipids domains that destabilize membrane equilibrium, or the non-lytic membrane depolarization, in which transmembrane potential is dissipated without any physical damage. Other mechanisms involve the variation of bilayer thickness, the attraction of small anions across the bilayer and their consequent efflux, the enhancement of peptide absorption on the membrane by targeting oxidized phospholipids, the accumulation of peptide on the outer leaflet over a certain threshold that causes a variation in the membrane potential and therefore in its permeability towards various molecules, including the peptide itself.[11] The most important mechanisms will be briefly discussed hereinafter.

The formation of pores is usually described with two main models: the "barrel-stave" and the "toroidal wormhole". According to the former, peptide molecules are arranged in a transmembrane pore, where the hydrophobic face of the peptide is exposed to the lipids acyl-chains, while the hydrophilic one point inward and constitute the wall of a water-filled pore.[14,51] After the starting binding stage, peptides fold on the membrane surface. Afterwards, peptides tilt and insert into the membrane through their hydrophobic side, and, above a certain concentration threshold, monomers start to form aggregates that are able to insert deeper into the hydrophobic membrane core.[14] As this process continues, the pore will be formed peptide molecules might also be brought on the inner membrane leaflet, mainly because of concentration gradient.[14] Alamethicin is an example of peptide that act through this mechanism.[11] It has to be stressed that pores are not described as stable entities, but a dynamic equilibrium of pores formation and relaxation is typically invoked. The second model proposed for pores formation is the "toriodal wormhole" mechanism.[47,52] After adhesion, peptide molecules force the outer leaflet to bend. This "defect" generated in the bilayer structure causes surrounding lipids to tilt and, ultimately, the connection between the two leaflets.[14] Finally, a water-filled pore is formed, whose wall is constituted both by peptide molecules and lipid head groups. Magainins and protegrins are typical examples.[14]

Another kind of lytic mode of action is the "carpet model".[51] Peptides are bound on the surface of the bilayer and do not insert but form a sort of disordered carpet.[14,51,52] When peptide concentration reaches a certain threshold, the membrane start to be disintegrated into small micelles. This is an inherently chaotic mechanism, which do not assume neither a defined order for peptide oligomerization nor peptides insertion into the hydrophobic core.[7,14,51] Some examples of peptides that act through a carpet mechanism are: ovispirin, natural analogues of dermaseptin, cecropins and caerin 1.1.[14]

One of the most quoted non-lytic mechanisms is the clustering of anionic lipids. This mechanism does not involve membrane disruption. It has been proposed that certain cationic peptides are able to perturb membrane local composition by segregating the negatively charged lipids. The consequent formation of non-native domains is accompanied by phase boundary defects, which are thought to cause an increased permeability, thus, impairing membrane correct functionality.[14,53] This is, for instance, the case reported by Arouri et al. for both linear and cyclic arginine- and tryptophan-rich peptides.[14,54] Obviously, both zwitterionic and negatively charged lipids are required to have anionic lipid clustering, otherwise no segregation of negative lipids would be possible.[53] It is generally observed that peptides acting through this mechanism are more active against Gram-negative than Gram-positive bacteria. This is possibly due to the fact that the latter usually have a higher content of negative lipids, therefore, a lower impact on membrane local composition is induced by the peptides.[14,53]

Some peptides are reported to be able to reduce transmembrane potential, a mechanism called "membrane depolarization". This requires that peptide molecules overcome a given concentration threshold, enough to depolarize the membrane potential. The consequence of such depolarization can be the variation in membrane permeability towards certain molecules, including the peptides themselves. Indeed, for some peptides, membrane depolarization is not considered as the primary goal, but a step needed to facilitate entry into the targeted microorganism.[55] Nisin is an example of such kind of peptides.[56] Daptomycin was demonstrated to act through the reduction of membrane potential and to kill bacteria by inducing them to release $K^+$.[55]

Membrane fusion is another important mechanism, in which two bilayers are fused together and the content of the two originally separated compartments is mixed. Lipids belonging to the two original bilayers coexist in the same bilayer after the fusogenic action of the peptides.[57] Some structural features have been suggested to be fundamental for such fusogenic activity, like the asymmetric distribution of hydrophilic and hydrophobic residues, which is thought to give peptides some membrane destabilizing properties.[58] Studies about fusogenic activity of WAE11, an 11-mer synthetic peptide, showed that for short peptides, a membrane anchoring element is of significant help for fusogenic activity.[58] Fusogenic activity is typically described as the approach between the two lipid bilayers, their destabilization in terms of lipids compactness and correct orientation, and final fusion into a mixed peptide-lipid phase.[59,60] This mechanism is commonly observed in viruses that make use of fusogenic terminal portion of anchoring proteins to fuse their membrane to that of the targeted cell, and ultimately favour the introduction of the viral material. An example is the simian immunodeficiency virus (SIV) fusion peptide, which is a 12-resiude N-terminal portion of the gp32 protein endowed with fusogenic activity.[61]

## 1.4 Drawbacks of natural peptides and possible alternatives

In the last two decades, HDPs have attracted much attention as natural templates for the design of a new class of antimicrobial drugs. However, the number of sequences reaching therapeutic use is very low, since most of them did not overcome or even reach the stage of clinical trials. One example is pexiganan MSI-78, developed by Genaera, which is a synthetic 22 amino acid variant of magainin-2, used in the treatment of diabetic foot ulcer.[5,10] Other examples are MX-226 (omiganan), an analogue of the bovine indolicidin, used against catheter-associated infections.[5,10,62]

Polymyxin B is sadly famous as the last resource against infections from multi-drug resistant Gram-negative bactaria, although highly toxic, or the lipopeptide daptomycin, which is still available against vancomycin-resistant *Staphylococcus aureus* strains.[5] An example of therapeutic application of an immunomodulatory HDP is IDR-1.[10]

There are several limitations to HDP development as a really applicable drug. As mentioned in previous sections, despite the putative selectivity towards microorganisms over eukaryotic cells, the level of cytotoxicity remains high for most of them. In the case of immunomodulatory peptides, the problem is the possible overstimulation of the immune system and inflammatory response.[5,63] These are the main reasons why the few HDPs that have reached clinics were mostly developed for topical applications.

Other important limitations come from the inherent peptide nature of these compounds and the high electrostatics contribution to the very first step of any mechanism of action (§1.3). In particular, HDPs are typically susceptible to proteases and peptidases degradation, and are

inactivated by pH and the presence of both mono- and divalent ions.[3,5,13] Since electrostatics play a major role in peptide binding to the membrane surface, every chemical species able to interfere with such interaction negatively affects peptide activity.[38] Physiological concentration of monovalent cations such as $Na^+$ and $K^+$ (at a concentration of 100 mM)[5] divalent cations (like $Mg^{2+}$ and $Ca^{2+}$, at concentrations of 1-2 mM)[5], serum components and, for instance, polyanionic glysoaminoglycans and mucins usually compromise peptide action.[3,5] The cathelicidin peptide LL-37, for example, shows low MIC values when the ionic strength is low, but the antimicrobial activity significantly decreases with increasing electrolytes concentration in the medium.[3] Electrolytes provide counter-ions to both cationic peptides and anionic lipids, thus, reducing their electrostatic long-range interaction.

Another aspect that cannot be neglected is the cost of peptides manufacturing on a large scale. In order to overcome this problem, many efforts were spent to produce peptides using bacteria, fungi, plants and animal production systems, but these did not completely meet pharmaceutical companies requirements.[5] Another option is the design of active sequence as short as possible, in order to keep the production costs down. This strategy was applied with success in the case of IDR analogues.[3,5,7,8]

Probably the most important limitation to HDPs development is represented by the degradative action of proteases and peptidases *in vivo*. These are enzymes specifically devoted to catalyse hydrolysis of linear polypeptides. Their action reduce peptides bioavailability and, therefore, lowers peptides activity.[3,5,7,8] A large number of strategies have been suggested in the literature to overcome this problem. Acetylation of the N-terminus resulted in a reduction of the activity of aminopeptidases.[3] Other examples are, the insertion of disulfide bridges, peptide cyclization, and introduction of D amino acids (all the standard amino acids have opposite chirality).[3] Great interest has been attracted by peptidomimetics, which are synthetic polymers that mimic key peptide structure features without involving α-amino acids.[15] Foldamers *N*,*N'*-linked oligoureas are an example of peptidomimetics characterized by a high activity against both Gram-negative and Gram-positive bacteria, resistance towards proteolytic degradation and a stable helical folding.[64–66] Arylamide foldamers are another interesting class of peptidomimetics composed by both charged and hydrophobic groups bound to an arylamide backbone.[64] The "defensin-mimetic" PMX-30063 developed by PolyMedix is one the most famous examples of this class, as it is used in the case of bacterial skin infections caused by *S. aureus*.[64] The class of α-AApeptides, that are typically active against both Gram-negative and Gram-positive bacteria as well as against fungi, are characterized by low cost of manufacture and are endowed with resistance to proteases degradation.[64,67] These are oligomers of *N*-acylated-*N*-aminoethyl amino acids. Also lipidated γ-AApeptides are reported in the literature, whose haemolytic activity was reduced by the introduction of an unsaturated lipid tail.[64,68]

Among all of these approaches, multiple antigenic peptides (MAP) are particularly interesting. These were developed in the '80s to prepare peptide immunogens,[15] compounds able to stimulate the immune system to produce the desired antibodies. Briefly, using standard solid-phase chemistry, it is possible to bind multiple copies of the same peptide sequence to a central core, which is usually composed by radially branched lysine residues.[15] The idea is to amplify the immunity response by having many copies of the active peptide unit per molecule. Basically the same approach was also brought to the field of AMPs, by attaching several copies of the selected amino acid sequence to a inner core.[15] The expected effect was an improved antimicrobial activity

together with an increased resistance to proteases degradation, due the steric hindrance provided by the branches architecture which does not allow the peptide to enter in the active site of the enzyme.[15,69,70] These peptides are also referred to as dendrimeric peptides, because of their structural analogy to dendrimeric polymers, and have found numerous different applications so far.[71–74]

The synthetic versatility of this class of compounds is certainly interesting. Both the number of active units and their sequence can be tuned, as well as the compactness of the structure by changing core and/or branching units. However, although a number of dendrimeric peptides were investigated and shown intriguing activity against different microbial pathogens,[70,75–79] little is known about the structure actually adopted in action. Knowledge of structure-function relationship is fundamental in order to tailor the properties of such compounds and keep both the activity and side effects under control.

## 1.5 The SB056 peptides family

The group of Applied Spectroscopy and the Biochemistry Unit of the University of Cagliari have been collaborating within a joint project on dendrimeric peptides since 2009. One of the first investigations in this field was focused on the dendrimeric peptide SB041. This was a tetra-branched peptide, whose four peptide units had the same peptide sequence [pyrEKKIRVRLSA], which was obtained by modification of a parent AMP [QEKIRVRLSA]. The latter was originally identified by selecting a random phage library against whole *E. coli* cells,[70] by the Spider Biotech company (this the reason why peptide name includes SB). The four branches were linked to a core constituted by a first lysine residue to which two additional lysines were bound to the alpha- and the epsilon- nitrogen, respectively. The K($K_2$) core presented four branching points, two alpha- and two epsilon nitrogens, so that up to four peptide sequences could be coupled in parallel through solid-state synthesis. The N-terminal pyroglutamic acid was introduced to confer more stability, avoiding the well known cyclization process involving a Gln residue at N-terminus.[70] The C-terminus of the first lysine of the core was functionalized by adding an amino valeric acid chain, which was finally amidated, aimed at improve membrane affinity.[70] SB041 was found to be particularly active against Gram-negative strains, with high affinity for both *E. coli* and *Pseudomonas aeruginosa* lipopolysaccharide (LPS) in-vitro.[70] Then, the company tried to obtain a more compact dendrimer by using a single lysine for the core and, thus, only two peptide branches. Also the peptide sequence was further changed into [WKKIRVRLSA], finally obtaining the compound SB056 (figure 1.3).[35]

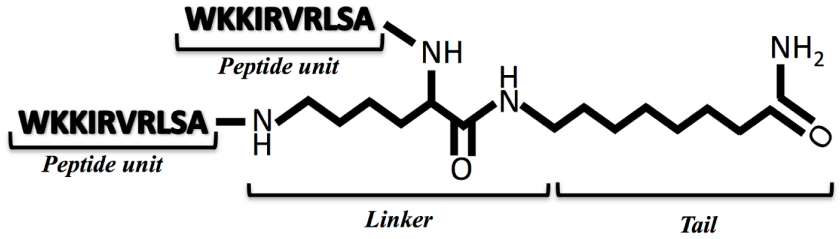


**Figure 1.3.** Schematic representation of SB056 structure.

Such a two-branches peptide can be actually considered as the smallest prototypical dendrimeric peptide and, from the point of view of the research group, it was particularly interesting because it offered the opportunity to compare easily both the activity and the structure-activity relationship in comparison to the simple linear sequence. In other words, when multi-branches dendrimers are investigated, it is difficult to assess what is due to the peptide sequence per-se or to the dendrimeric architecture in no comparative studies are performed. In addition, systematic investigations of the same compound with a different number of the same unit are very few.

SB056 is characterized by two copies of the amino acid sequence [WKKIRVRLSA] bound to the lysine linker. Similarly to SB041, there is also a tail at the C-terminus of the linker, which is longer in SB056, i.e. 8-aminooctanamide. SB056 was found to be more active against Gram-negative bacteria, with potency similar to that of colistin and polymyxin B (on a molar basis). It was endowed with a broader spectrum of activity, having some limited activity also against Gram-positive bacteria, possibly related to the very high net positive charge (+10) given by the high number of lysine and arginine residues.[80] The first biophysical characterization, with nuclear magnetic resonance (NMR), molecular dynamics (MD) simulations, measurements of the surface pressure of lipid monolayers and circular dichroism (CD) spectroscopy, showed interesting membrane affinity and the tendency to fold into β-type conformation in the presence of lipid membrane models.[80] Remarkably, the CD spectra did not perfectly match the canonical spectra shape of a β-sheet structure, probably because the branched architecture of SB056, like any dendrimeric peptide, is inherently not canonical and, possibly, the results coming from techniques usually employed in Biophysics, should be looked carefully before giving conclusive interpretations.

The amino acid sequence of SB056 is characterized by the alternation of hydrophilic and hydrophobic residues, with the only exception of the two first residues. This profile resembles the β-sheet model peptide $[KIGAKI]_3$, which was specifically designed to form amphipathic β-sheets,[81] as demonstrated from electron microscopy, CD and solid-state NMR. Interestingly, KIGAKI assembles and form crossed β-sheet amyloid fibrils already in solution, representing also a suitable model system to study the behaviour of β-amyloid peptides.[82,83] On the antimicrobial activity side, this appeared to be directly influenced by the formation of such ordered aggregates, whose formation depended on peptide length.[84] In fact, it was demonstrated that β-sheet content increased with sequence length, following a sigmoidal trend.[84] The midpoint was found at 10-12 amino acids, so that peptides with more than 10 residues easily formed β-structures, while shorter peptides showed only poor structuration.[84] These observations were particularly interesting for the research group, since the amino acid sequence of SB056 is composed by just 10 residues, which is almost half length compared to KIGAKI and equal to the lowest limit for structuration.

The research group performed a comparative study on SB056 and its linear counterpart, which will be referred to as SB056-linear in the whole thesis. The latter was found to be definitely less active than SB056 against all tested strains of both Gram-positive and –negative bacteria.[80] CD measurements confirmed that also the linear analogue has the same tendency to fold as β-type structures in the presence of lipid unilamellar vesicles,[80] as further confirmed by solid-state NMR.[85] The almost perfect alternation of charged/polar and hydrophobic residues along the amino acid sequence of SB056, with the already mentioned exception of the first two positions, suggested a possible optimization. By exchanging the position of the first two residues, namely, tryptophan and lysine, respectively, a new dendrimeric analogue was obtained with sequence [KWKIRVRLSA]

(figure 1.4). This regularization of the amphipathic profile was specifically designed to obtain a more regular β-sheet like structure and, hopefully, an improved activity, also in the light of the reports on the model peptide KIGAKI.[84] For this reason, the new analogue was called β-SB056.

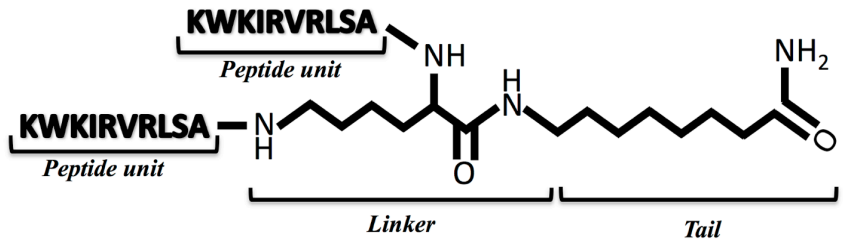


**Figure 1.4.** Schematic representation of β-SB056 structure.

First, the corresponding linear analogue β-SB056-linear was studied in comparison to SB056-linear. The regularization of the amino acid sequence resulted in a 3-4 fold improvement of antimicrobial activity.[85] Synchrotron radiation CD measurements confirmed a higher degree of structural order, upon interaction with lipid vesicles.[85] Solid state $^{19}$F-NMR showed β-SB056-linear tendency to self-assemble into extended β-sheets characterized by low mobility with increasing the proportion of negatively charged lipids in the membrane model.[85] Conversely, SB056-linear showed a mostly monomeric behaviour up to the purely negative membrane model. Correspondingly, SB056-linear caused only slight perturbation, while β-SB056-linear induced massive disturbance in the lipid bilayer. Therefore, the correlation between the enhanced activity and the improved structural order was attributed to the amphipathic profile regularization.[85] It has to be stressed that the only difference between the two sequences is the position the tryptophan residue, being the net charge at neutral pH absolutely the same.

A step ahead in the knowledge of this new family of peptides was taken by solving the 3D structure of the two dendrimeric analogues in the presence of mixed micelles (70 mol% DPC and 30 mol% SDS, a zwitterionic and a negatively charged detergent, respectively). The proposed combination of liquid-state NMR experiments and MD simulations[35] allowed to obtain the first 3D structure of a dendrimeric peptide. This was a very important result, because in the literature, as far as I am aware, there are no clear reports about the actual conformation of dendrimeric peptides, with the exception of the work of Bai et al.[86] The case of β-SB056 and SB056 was particularly challenging, because the two peptide branches are identical, thus, in the 2D NMR spectra it is difficult to distinguish the contribution of intra- and inter-branch interactions.[35] On the basis of scalar J-couplings, chemical shift values and internuclear dipolar interactions, geometrical restraints were derived from the experiments. Three possible structure models were checked through all-atom MD simulations and, finally, only one model was found to be consistent with all the experimental observations.[35] Figure 1.5 shows some snapshots of the conformations obtained for both β-SB056 and SB056 at different stages along the overall process of structure refinement, namely, (i) in vacuum simulated annealing with geometrical restraints from experiments, (ii) all-atom MD in explicit solvent and micelle with geometrical restraints from experiments, and (iii) all-atom MD in explicit solvent and micelle after restraints removal.

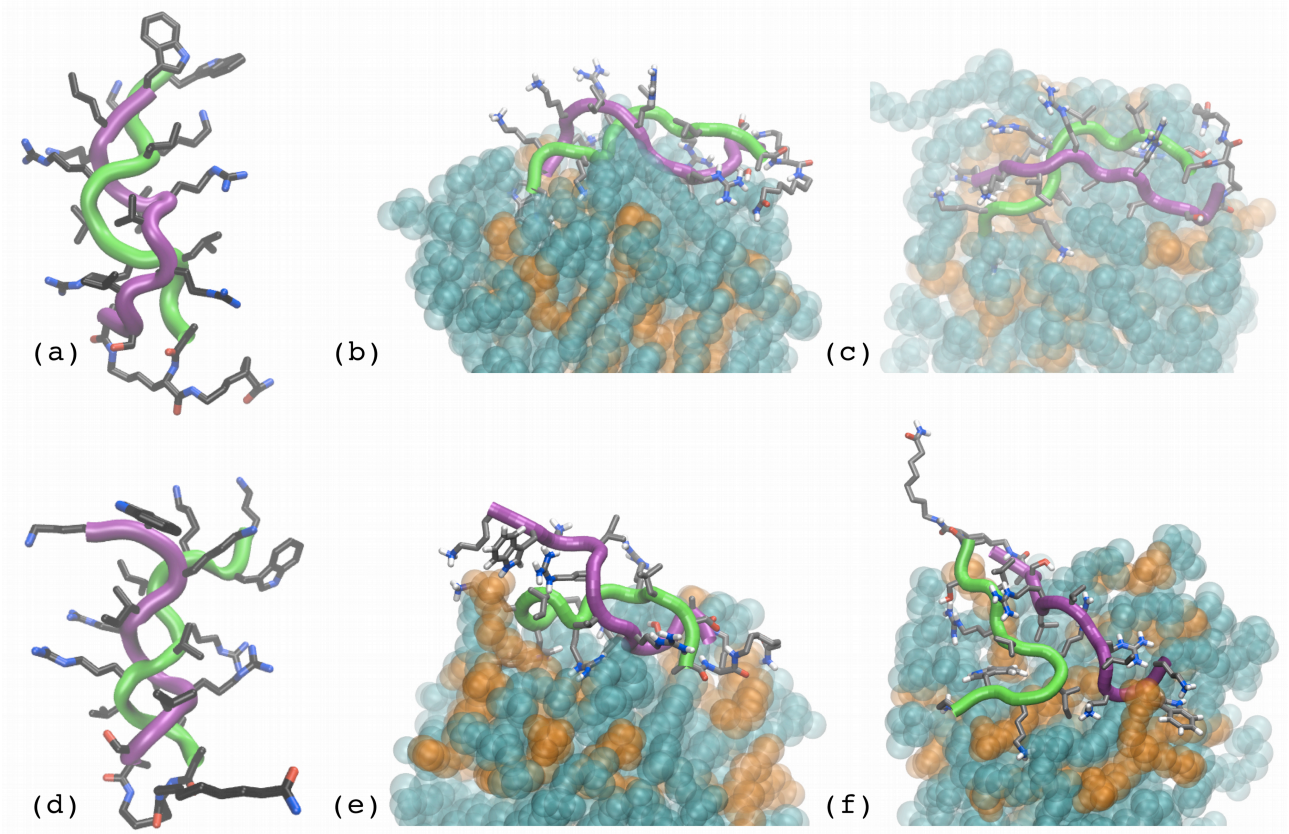


**Figure 1.5.** Structures obtained for (a-c) SB056 and (d-f) β-SB056. In a and d are reported the structures in vacuum obtained from a computer simulated annealing scheme, with distance restraints derived from the experimental NOEs. Subsequently, an equilibrium MD simulation was run using the same restraints and in the presence of water and detergent molecules. In figure b and e the last frame after 100 ns are reported. In figure c and f the last frame of a second 100 ns MD run performed without all restraints are shown. In green and purple are indicated the backbone of the α- and ε-branch, respectively. The atoms of the detergent are represented with the corresponding van der Waals spheres, with DPC and SDS indicated in cyan and orange, respectively. Figure reused from reference.[35]

In vacuum, the two branches had showed the clear tendency to coil right-hand one another, seeking for the maximum separation between the positively charged groups. During the first MD simulation, overall peptide conformation of the two peptides looked similar, both sharing a twisted pairing of the two peptide branches. However, β-SB056 showed a higher plasticity and, at the level of the N-termini, the tryptophan residues were less deeply inserted inside the micelle. Both peptides actually showed the tendency to untwist during the simulation, suggesting that the staring tightly twisted conformation was probably due to the "in-vacuum condition" applied during the very first stage of simulated annealing. Finally, when all the restraints were released in a second MD simulation, both peptides adopted a less twisted pairing of the two branches and moved deeper into the micelle. Interesting, while SB056 still showed a coiled conformation, β-SB056 was completely untwisted and characterized by a more regular β-hairpin structure.

It is worth mentioning that, through NMR experiments exploiting paramagnetic relaxation enhancement, the octanamide tail of both dendrimeric peptides resulted to be absolutely water exposed.[35] These findings made the hypothesized anchoring role of the tail questionable, thus opening the route to further modifications of the molecular architecture. The reason was probably the terminal polar amide group, making the whole tail not hydrophobic enough to help peptide interaction with the membrane model.

## 1.6 Aim of the work and thesis organization

The objective of my PhD work was the biophysical characterization of the SB056 peptide family. By using a battery of complementary experimental techniques, I attempted at taking steps further into the comprehension of the behaviour of this new dendrimeric peptides, both in solution and in the presence of suitable membrane models. Both spectroscopic and non-spectroscopic techniques were applied, aiming to identify and characterize the mechanism of action of these peculiar peptides. The structure-function relationship was the goal, in order to shed more light on the key physico-chemical parameters to tailor the membrane activity of the compounds. I think this would be the route to a possible application of the investigated peptides.

During the course of the studies previously performed by the research group, the collected results suggested (i) a higher structural order and activity for the sequence regularized analogue, β-SB056, and (ii) that possibly the octanamide tail could be substituted without affecting peptide performance. However, the investigations had never been performed with real lipid bilayers, so that such results needed to be confirmed and the biophysical characterization to be extended. My work was planned as two complementary parts. On the one hand, the comparison of SB056 and β-SB056 was extended in order to characterize their differences in more details. By having the same tail and net positive charge, their comparison was actually focused on the effects of amphipathic profile regularization. On the other hand, an experimental campaign on several β-SB056 analogues with highly hydrophobic tail of different length was undertaken, in order to focus on the role of the latter. In addition, during the very first period of my PhD, the basic comparison between the dendrimeric peptides and their linear counterpart was performed, aiming at highlighting possible additional advantages of the dendrimeric architecture.

The present thesis is organized in four chapters. Beside the *Introduction*, *Materials and methods*, *Results and discussion*, and *Summary and conclusions* follow.

The chapter *Materials and methods* reports the most important basic principles of the techniques applied in this PhD work together with experimental procedures and practical details.
Steady-state fluorescence spectroscopy has been widely used for different purposes, namely, (i) determination of peptides partition constant between the solution and the lipid phase, (ii) localization (depth) of tryptophan residues inside the lipid bilayer and (iii) evaluation of peptides ability to perturb lipid bilayer through vesicles leakage assay.
Infrared spectroscopy was applied for peptide conformational studies by using lipid vesicles as membrane system.
Measurements of surface pressure of lipid monolayers were performed to evaluate peptides surface excess.
UV-Vis absorption spectroscopy was employed to check possible variation in vesicles size induced by peptides, as expected by virtue of certain mechanisms like micellization, fusion or simple aggregation.
Finally, collection of some images was attempted by transmission electron microscopy.

The chapter *Results and discussion* presents the experimental findings obtained along 3 years work, comparing and discussing them in the light of the literature. When needed, simple models were also

employed to rationalize the results. The complete picture emerging from my work comprises pieces of information coming from different techniques. I tried to present the results in a logic order, aiming at constructing the picture step by step. The chapter is divided into two main sections. The first section, focuses on the *Effects of the amphipathic profile regularization*, by comparing SB056 and β-SB056 in their dendrimeric form with respect to different aspect pertaining to their structure and membrane interaction. The second section discusses the outcomes of the *Introduction of an anchoring lipid tail*, by following almost the same scheme adopted for the first section.

The chapter *Summary and conclusion* reports the main findings in a concise form, as the sum of the complementary application of different biophysical techniques. Several open points still remain and are highlighted. The conclusions stimulated the discussion on possible developments, so that an outlook is also presented with ideas and plans for the next future.

**References:**


1. Hancock, R. E. W. & Diamond, G. The role of cationic antimicrobial peptides in innate host defences. Trends Microbiol. 8, 402–410 (2000).
2. Giuliani, A. et al. Antimicrobial peptides: natural templates for synthetic membrane-active compounds. Cell. Mol. Life Sci. 65, 2450–2460 (2008).
3. Haney, E. F. & Hancock, R. E. W. Peptide design for antimicrobial and immunomodulatory applications. Pept. Sci. 100, 572–583 (2013).
4. A Nijnik & REW Hancock. Host defence peptides: antimicrobial and immunomodulatory activity and potential applications for tackling antibiotic-resistant infections. Merging Health Threats J. (2008). doi:10.3134/ehtj.09.001
5. Hancock, R. E. W. & Sahl, H.-G. Antimicrobial and host-defense peptides as new anti-infective therapeutic strategies. Nat. Biotechnol. 24, 1551–1557 (2006).
6. Yeung, A. T. Y., Gellatly, S. L. & Hancock, R. E. W. Multifunctional cationic host defence peptides and their clinical applications. Cell. Mol. Life Sci. 68, 2161 (2011).
7. Jenssen, H., Hamill, P. & Hancock, R. E. W. Peptide Antimicrobial Agents. Clin. Microbiol. Rev. 19, 491–511 (2006).
8. Choi, K.-Y., Chow, L. N. Y. & Mookherjee, N. Cationic Host Defence Peptides: Multifaceted Role in Immune Modulation and Inflammation. J. Innate Immun. 4, 361–370 (2012).
9. Bowdish, D. M. E., Davidson, D. J. & Hancock, R. E. W. A Re-evaluation of the Role of Host Defence Peptides in Mammalian Immunity. Curr. Protein Pept. Sci. 6, 35–51 (2005).
10. Andrea C. Rinaldi & Andrea Giuliani. Antimicrobial Peptides:methods and protocols. 618, (Methods in molecular biology).
11. Nguyen, L. T., Haney, E. F. & Vogel, H. J. The expanding scope of antimicrobial peptide structures and their modes of action. Trends Biotechnol. 29, 464–472 (2011).
12. Torcato, I. M., Castanho, M. A. & Henriques, S. T. The application of biophysical techniques to study antimicrobial peptides. J. Spectrosc. 27, 541–549 (2012).
13. Brogden, K. A. Antimicrobial peptides: pore formers or metabolic inhibitors in bacteria? Nat. Rev. Microbiol. 3, 238–250 (2005).
14. Teixeira, V., Feio, M. J. & Bastos, M. Role of lipids in the interaction of antimicrobial peptides with membranes. Prog. Lipid Res. 51, 149–177 (2012).
15. Giuliani, A. & Rinaldi, A. C. Beyond natural antimicrobial peptides: multimeric peptides and other peptidomimetic approaches. Cell. Mol. Life Sci. 68, 2255–2266 (2011).
16. Henzler Wildman, K. A., Lee, D.-K. & Ramamoorthy, A. Mechanism of Lipid Bilayer Disruption by the Human Antimicrobial Peptide, LL-37. Biochemistry 42, 6545–6558 (2003).

17. Hallock, K. J., Lee, D.-K., Omnaas, J., Mosberg, H. I. & Ramamoorthy, A. Membrane Composition Determines Pardaxin's Mechanism of Lipid Bilayer Disruption. Biophys. J. 83, 1004–1013 (2002).
18. Reddy, K. V. R., Yedery, R. D. & Aranha, C. Antimicrobial peptides: premises and promises. Int. J. Antimicrob. Agents 24, 536–547 (2004).
19. Fahrner, R. L. et al. Solution structure of protegrin-1, a broad-spectrum antimicrobial peptide from porcine leukocytes. Chem. Biol. 3, 543–550 (1996).
20. Matsuzaki, K. Magainins as paradigm for the mode of action of pore forming polypeptides. Biochim. Biophys. Acta BBA - Rev. Biomembr. 1376, 391–400 (1998).
21. Matsuzaki, K. Why and how are peptide–lipid interactions utilized for self-defense? Magainins and tachyplesins as archetypes. Biochim. Biophys. Acta BBA - Biomembr. 1462, 1–10 (1999).
22. Prenner, E. J., Lewis, R. N. A. H. & McElhaney, R. N. The interaction of the antimicrobial peptide gramicidin S with lipid bilayer model and biological membranes. Biochim. Biophys. Acta BBA - Biomembr. 1462, 201–221 (1999).
23. Bechinger, B. Structure and Functions of Channel-Forming Peptides: Magainins, Cecropins, Melittin and Alamethicin. J. Membr. Biol. 156, 197–211 (1997).
24. Shai, Y. Mode of action of membrane active antimicrobial peptides. Pept. Sci. 66, 236–248 (2002).
25. Sevcsik, E., Pabst, G., Jilek, A. & Lohner, K. How lipids influence the mode of action of membrane-active peptides. Biochim. Biophys. Acta BBA - Biomembr. 1768, 2586–2595 (2007).
26. Epand, R. F., Schmitt, M. A., Gellman, S. H. & Epand, R. M. Role of membrane lipids in the mechanism of bacterial species selective toxicity by two α/β-antimicrobial peptides. Biochim. Biophys. Acta BBA - Biomembr. 1758, 1343–1350 (2006).
27. Lee, I. H., Cho, Y. & Lehrer, R. I. Effects of pH and salinity on the antimicrobial properties of clavanins. Infect. Immun. 65, 2898–2903 (1997).
28. Organization, W. H. Antimicrobial resistance global report on surveillance : 2014 summary. (2014).
29. Mansour, S. C., Pena, O. M. & Hancock, R. E. W. Host defense peptides: front-line immunomodulators. Trends Immunol. 35, 443–450 (2014).
30. Yount, N. Y. & Yeaman, M. R. Peptide antimicrobials: cell wall as a bacterial target. Ann. N. Y. Acad. Sci. 1277, 127–138 (2013).
31. Zasloff, M. Magainins, a class of antimicrobial peptides from Xenopus skin: isolation, characterization of two active forms, and partial cDNA sequence of a precursor. Proc. Natl. Acad. Sci. 84, 5449–5453 (1987).
32. Park, C. B., Kim, H. S. & Kim, S. C. Mechanism of Action of the Antimicrobial Peptide Buforin II: Buforin II Kills Microorganisms by Penetrating the Cell Membrane and Inhibiting Cellular Functions. Biochem. Biophys. Res. Commun. 244, 253–257 (1998).
33. Simmaco, M. et al. Temporins, Antimicrobial Peptides from the European Red Frog Rana temporaria. Eur. J. Biochem. 242, 788–792 (1996).
34. Simmaco, M., Mignogna, G., Barra, D. & Bossa, F. Antimicrobial peptides from skin secretions of Rana esculenta. Molecular cloning of cDNAs encoding esculentin and brevinins and isolation of new active peptides. J. Biol. Chem. 269, 11956–11961 (1994).
35. Manzo, G. et al. The singular behavior of a β-type semi-synthetic two branches polypeptide. Three-dimensional structure and mode of action. Phys Chem Chem Phys (2016). doi:10.1039/C6CP05464A
36. Vaara, M. & Porro, M. Group of peptides that act synergistically with hydrophobic antibiotics against gram-negative enteric bacteria. Antimicrob. Agents Chemother. 40, 1801–1805 (1996).
37. Fritz, J. H. et al. The artificial antimicrobial peptide KLKLLLLLKLK induces predominantly a TH2-type immune response to co-injected antigens. Vaccine 22, 3274–3284 (2004).

38. Takahashi, D., Shukla, S. K., Prakash, O. & Zhang, G. Structural determinants of host defense peptides for antimicrobial activity and target cell selectivity. Biochimie 92, 1236–1241 (2010).
39. Serra, I. et al. Conformational analysis and cytotoxic activities of the frog skin host-defense peptide, hymenochirin-1Pa. Peptides 61, 114–121 (2014).
40. Dathe, M. & Wieprecht, T. Structural features of helical antimicrobial peptides: their potential to modulate activity on model membranes and biological cells. Biochim. Biophys. Acta BBA - Biomembr. 1462, 71–87 (1999).
41. Strandberg, E., Tremouilhac, P., Wadhwani, P. & Ulrich, A. S. Synergistic transmembrane insertion of the heterodimeric PGLa/magainin 2 complex studied by solid-state NMR. Biochim. Biophys. Acta BBA - Biomembr. 1788, 1667–1679 (2009).
42. Tremouilhac, P., Strandberg, E., Wadhwani, P. & Ulrich, A. S. Synergistic Transmembrane Alignment of the Antimicrobial Heterodimer PGLa/Magainin. J. Biol. Chem. 281, 32089–32094 (2006).
43. Strandberg, E., Zerweck, J., Wadhwani, P. & Ulrich, A. S. Synergistic Insertion of Antimicrobial Magainin-Family Peptides in Membranes Depends on the Lipid Spontaneous Curvature. Biophys. J. 104, L9–L11 (2013).
44. McLaurin, J., Yang, D.-S., Yip, C. M. & Fraser, P. E. Review: Modulating Factors in Amyloid-β Fibril Formation. J. Struct. Biol. 130, 259–270 (2000).
45. Lomakin, A., Chung, D. S., Benedek, G. B., Kirschner, D. A. & Teplow, D. B. On the nucleation and growth of amyloid beta-protein fibrils: detection of nuclei and quantitation of rate constants. Proc. Natl. Acad. Sci. 93, 1125–1129 (1996).
46. Wu, M., Maier, E., Benz, R. & Hancock, R. E. W. Mechanism of Interaction of Different Classes of Cationic Antimicrobial Peptides with Planar Bilayers and with the Cytoplasmic Membrane of Escherichia coli. Biochemistry 38, 7235–7242 (1999).
47. Hancock, R. E. W. & Lehrer, R. Cationic peptides: a new source of antibiotics. Trends Biotechnol. 16, 82–88 (1998).
48. Peters, B. M., Shirtliff, M. E. & Jabra-Rizk, M. A. Antimicrobial Peptides: Primeval Molecules or Future Drugs? PLOS Pathog 6, e1001067 (2010).
49. Doherty, T., Waring, A. J. & Hong, M. Dynamic Structure of Disulfide-Removed Linear Analogs of Tachyplesin-I in the Lipid Bilayer from Solid-State NMR. Biochemistry 47, 1105–1116 (2008).
50. Epand, R. M. & Epand, R. F. Bacterial membrane lipids in the action of antimicrobial agents. J. Pept. Sci. 17, 298–305 (2011).
51. Shai, Y. Mechanism of the binding, insertion and destabilization of phospholipid bilayer membranes by α-helical antimicrobial and cell non-selective membrane-lytic peptides. Biochim. Biophys. Acta BBA - Biomembr. 1462, 55–70 (1999).
52. Yeaman, M. R. & Yount, N. Y. Mechanisms of Antimicrobial Peptide Action and Resistance. Pharmacol. Rev. 55, 27–55 (2003).
53. Epand, R. M., Rotem, S., Mor, A., Berno, B. & Epand, R. F. Bacterial Membranes as Predictors of Antimicrobial Potency. J. Am. Chem. Soc. 130, 14346–14352 (2008).
54. Arouri, A., Dathe, M. & Blume, A. Peptide induced demixing in PG/PE lipid mixtures: A mechanism for the specificity of antimicrobial peptides towards bacterial membranes? Biochim. Biophys. Acta BBA - Biomembr. 1788, 650–659 (2009).
55. Silverman, J. A., Perlmutter, N. G. & Shapiro, H. M. Correlation of Daptomycin Bactericidal Activity and Membrane Depolarization in Staphylococcus aureus. Antimicrob. Agents Chemother. 47, 2538–2544 (2003).
56. Sahl, H.-G., Kordel, M. & Benz, R. Voltage-dependent depolarization of bacterial membranes and artificial lipid bilayers by the peptide antibiotic nisin. Arch. Microbiol. 149, 120–124 (1987).

57. Henriques, S. T. & Castanho, M. A. R. B. Consequences of Nonlytic Membrane Perturbation to the Translocation of the Cell Penetrating Peptide Pep-1 in Lipidic Vesicles. Biochemistry 43, 9716–9724 (2004).
58. Pécheur, E.-I., Martin, I., Ruysschaert, J.-M., Bienvenüe, A. & Hoekstra, D. Membrane Fusion Induced by 11-mer Anionic and Cationic Peptides: A Structure−Function Study. Biochemistry 37, 2361–2371 (1998).
59. Rappolt, M., Hickel, A., Bringezu, F. & Lohner, K. Mechanism of the Lamellar/Inverse Hexagonal Phase Transition Examined by High Resolution X-Ray Diffraction. Biophys. J. 84, 3111–3122 (2003).
60. Siegel, D. P., Green, W. J. & Talmon, Y. The mechanism of lamellar-to-inverted hexagonal phase transitions: a study using temperature-jump cryo-electron microscopy. Biophys. J. 66, 402–414 (1994).
61. Cladera, J., Martin, I., Ruysschaert, J.-M. & O'Shea, P. Characterization of the Sequence of Interactions of the Fusion Domain of the Simian Immunodeficiency Virus with Membranes ROLE OF THE MEMBRANE DIPOLE POTENTIAL. J. Biol. Chem. 274, 29951–29959 (1999).
62. Melo, M. N. & Castanho, M. A. R. B. Omiganan interaction with bacterial membranes and cell wall models. Assigning a biological role to saturation. Biochim. Biophys. Acta BBA - Biomembr. 1768, 1277–1290 (2007).
63. Hamill, P., Brown, K., Jenssen, H. & Hancock, R. E. Novel anti-infectives: is host defence the answer? Curr. Opin. Biotechnol. 19, 628–636 (2008).
64. Scorciapino, M. A. & Rinaldi, A. C. Antimicrobial Peptidomimetics: Reinterpreting Nature to Deliver Innovative Therapeutics. Front. Immunol. 3, (2012).
65. Violette, A. et al. Mimicking Helical Antibacterial Peptides with Nonpeptidic Folding Oligomers. Chem. Biol. 13, 531–538 (2006).
66. Claudon, P. et al. Consequences of Isostructural Main-Chain Modifications for the Design of Antimicrobial Foldamers: Helical Mimics of Host-Defense Peptides Based on a Heterogeneous Amide/Urea Backbone. Angew. Chem. Int. Ed. 49, 333–336 (2010).
67. Padhee, S. et al. Non-hemolytic α-AApeptides as antimicrobial peptidomimetics. Chem. Commun. 47, 9729–9731 (2011).
68. Niu, Y. et al. Lipo-γ-AApeptides as a New Class of Potent and Broad-Spectrum Antimicrobial Agents. J. Med. Chem. 55, 4003–4009 (2012).
69. Bracci, L. et al. Synthetic Peptides in the Form of Dendrimers Become Resistant to Protease Activity. J. Biol. Chem. 278, 46590–46595 (2003).
70. Bruschi, M. et al. Synthesis, characterization, antimicrobial activity and LPS-interaction properties of SB041, a novel dendrimeric peptide with antimicrobial properties. Peptides 31, 1459–1467 (2010).
71. Tam, J. P. Synthetic peptide vaccine design: synthesis and properties of a high-density multiple antigenic peptide system. Proc. Natl. Acad. Sci. 85, 5409–5413 (1988).
72. Jw, K. et al. Homogeneous Catalysts Based on Silane Dendrimers Functionalized with Arylnickel(II) Complexes. Nature 372, 659–663 (1994).
73. Douat-Casassus, C., Darbre, T. & Reymond, J.-L. Selective Catalysis with Peptide Dendrimers. J. Am. Chem. Soc. 126, 7817–7826 (2004).
74. Lagnoux, D., Delort, E., Douat-Casassus, C., Esposito, A. & Reymond, J.-L. Synthesis and Esterolytic Activity of Catalytic Peptide Dendrimers. Chem. – Eur. J. 10, 1215–1226 (2004).
75. Luganini, A. et al. Inhibition of Herpes Simplex Virus Type 1 and Type 2 Infections by Peptide-Derivatized Dendrimers. Antimicrob. Agents Chemother. 55, 3231–3239 (2011).
76. Falciani, C. et al. Design and In vitro Evaluation of Branched Peptide Conjugates: Turning Nonspecific Cytotoxic Drugs into Tumor-Selective Agents. ChemMedChem 5, 567–574 (2010).

77. Pini, A. et al. Antimicrobial Activity of Novel Dendrimeric Peptides Obtained by Phage Display Selection and Rational Modification. Antimicrob. Agents Chemother. 49, 2665–2672 (2005).
78. Stach, M. et al. Combining Topology and Sequence Design for the Discovery of Potent Antimicrobial Peptide Dendrimers against Multidrug-Resistant Pseudomonas aeruginosa. Angew. Chem. Int. Ed. 53, 12827–12831 (2014).
79. Lind, T. K., Polcyn, P., Zielinska, P., Cárdenas, M. & Urbanczyk-Lipkowska, Z. On the Antimicrobial Activity of Various Peptide-Based Dendrimers of Similar Architecture. Molecules 20, 738–753 (2015).
80. Scorciapino, M. A. et al. A novel dendrimeric peptide with antimicrobial properties: structure-function analysis of SB056. Biophys. J. 102, 1039–1048 (2012).
81. Blazyk, J. et al. A Novel Linear Amphipathic β-Sheet Cationic Antimicrobial Peptide with Enhanced Selectivity for Bacterial Lipids. J. Biol. Chem. 276, 27899–27906 (2001).
82. Wadhwani, P. et al. Stereochemical effects on the aggregation and biological properties of the fibril-forming peptide [KIGAKI] 3 in membranes. Phys. Chem. Chem. Phys. 15, 8962–8971 (2013).
83. Wadhwani, P. et al. Self-Assembly of Flexible β-Strands into Immobile Amyloid-Like β-Sheets in Membranes As Revealed by Solid-State 19F NMR. J. Am. Chem. Soc. 134, 6512–6515 (2012).
84. Meier, M. & Seelig, J. Length Dependence of the Coil  β-Sheet Transition in a Membrane Environment. J. Am. Chem. Soc. 130, 1017–1024 (2008).
85. Manzo, G. et al. Enhanced Amphiphilic Profile of a Short β-Stranded Peptide Improves Its Antimicrobial Activity. PLOS ONE 10, e0116379 (2015).
86. Bai, Y. et al. Progressive Structuring of a Branched Antimicrobial Peptide on the Path to the Inner Membrane Target. J. Biol. Chem. 287, 26606–26617 (2012).

# 2 Materials and Methods

## 2.1 Materials

***Peptides***. All the peptides studied in the present PhD work were purchased from Peptide Protein Research Ltd. (Fareham, U.K.) with a purity of 98%. They were provided as chloride salts and used without any further purification. Two similar peptide sequences were investigated, namely, SB056 [WKKIRVRLSA] and βSB056 [KWKIRVRLSA]. These were investigated both in the linear 10-mer form, and in the dendrimeric two-branches one. When in the linear form, the N-terminus was always free ($NH_3^+$ at neutral pH), while the C-terminus was amidated. The two peptides will be referred to as SB056-linear and β-SB056-linear, respectively. When in the dendrimeric form, a single lysine linker constituted the branching unit. The two peptide branches were bound to the α- and the ε-amino group, respectively. An 8-amino-octanamide tail was attached to the carboxyl group of the linker (figures 1.3 and 1.4, §1.5). The two N-termini were free ($NH_3^+$ at neutral pH). The two dendrimeric peptides will be referred to as SB056-dendrimeric and β-SB056-dendrimeric, respectively.

Experiments were also performed on a dendrimeric peptide identical to β-SB056-dendrimeric without the tail. In this case the C-terminus on the lysine linker was amidated. This analogue will be referred to as β-SB056-nt.

Different experimental campaigns were carried out on a series of β-SB056-dendrimeric analogues, where the octanamide tail was substituted with a fully apolar hydrocarbon chain. The idea was to study analogues endowed with a real lipophilic tail, avoiding the presence of a terminal amide group. To this aim, we contacted different peptide synthesis companies but all of them returned negative response. Finally, the Peptide Protein Research Ltd. proposed a modified linker, i.e. two covalently bound lysine residues through a standard peptide bond. The N-terminal lysine was used as our conventional peptide linker to join the two 10-mer branches in the usual dendrimeric architecture. The C-terminal lysine had the carboxyl group amidated, while the ε-amino group was targeted to covalently attach different fatty acid, namely, octanoic (8:0), myristic (14:0) and stearic (18:0). All of them were devoid of unsaturated bonds. These analogues will be referred to as β-SB056-t8, β-SB056-t14 and β-SB056-t18, respectively (figure 2.1).

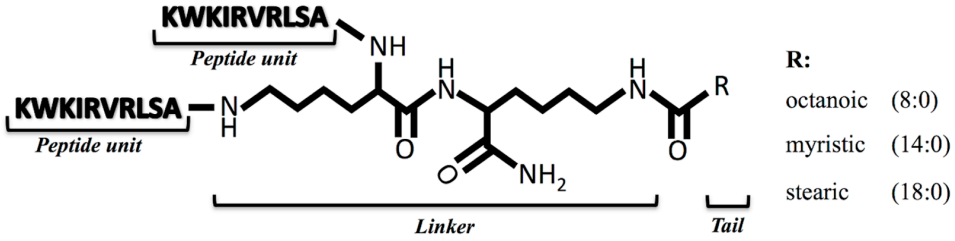


**Figure 2.1.** Schematic representation of the analogues of β-SB056 with lipophilic tail of different length.

Finally, a model β-sheet peptide was selected from the literature. The peptide $[KIGAKI]_3$, HCl salt, 95% purity, free N-terminus, amidated C-terminus was kindly provided by Prof. Anne S. Ulrich and Dr. Parvesh Wadhwani from the Karlsruhe Institute of Technology, who are greatly acknowledged. This model peptide will be simply referred to as KIGAKI. For further details and information, including synthesis and purification protocol, see the reference.[1,2]

***Other chemicals***. Unlabeled lipids were provided by Avanti Polar Lipids (Alabaster, AL, USA). In particular, 1-palmitoyl-2-oleyl-*sn*-glycero-3-phosphocholine (POPC) and 1-palmitoyl-2-oleyl-*sn*-glycero-3-phosphoglycerol (POPG) (both with a purity grade of >99%). All the other chemicals were purchased from Sigma-Aldrich (St. Louis, MO, USA), unless differently indicated. A complete list follows (with used names/abbreviations).

5-doxyl-stearic acid, (5NS); 16-doxyl-stearic acid, (16NS); 4-(1,1,3,3-tetramethylbutyl)phenyl-polyethylene glycol, electrophoresis purity (Triton X-100); Acrylamide, ≥ 99%; Bis[N,N-di(carboxymethyl)aminomethyl]fluorescein disodium salt, 75% (calcein); Chloroform, ≥ 99.8% ($CHCl_3$); Cholesterol, ≥ 99% ; Hydrochloric acid 1M, 37% (HCl); Methanol, ≥ 99.8% ($CH_3OH$); Perdeuterated water, 99%D ($D_2O$); Potassium dibasic phosphate, ≥ 98% ($K_2HPO_4$); Potassium monobasic phosphate, ≥ 99% ($KH_2PO_4$); Sodium chloride, 99% (NaCl); Sodium hydroxide 0.1M, volumetric (NaOH).

***Buffers***. Phosphate buffer (PB) was prepared by dissolving proper amount of $KH_2PO_4$ and $K_2HPO_4$ in deionized water at a final phosphates concentration of 10 mM. The pH was finally adjusted to 7.4 (pH meter reading) with small aliquots of HCl or NaOH 0.1 M. The PB was filtered through 2 μm filter before use. Phosphate buffer saline (PBS) was prepared with additional 150 mM NaCl.

## 2.2 Membrane models

Peptide-membrane interaction is the fundamental aspect of any peptide's mode of action. To work with real cell membranes is experimentally prohibitive due to their inherent complexity that would render impossible to understand which of the component actually determines or affect the peptide behavior. When performing biophysical investigations it is always necessary to use suitable models that mimic the membrane of interest. In the case of membrane active peptides, the target is often the non-specific lipid bilayer. Of course, the more suitable model has to be chosen by taking into account advantages and limitations of each of the techniques employed.[3,4]

***Lipid vesicles (or liposomes).*** Liposomes are spherical vesicles consisting of a lipid double-layer enclosing a water core. Depending on the size and the number of lamellas, i.e. the number of concentric lipid bilayers, these are usually classified into: multilamellar large vesicles (MLV), large unilamellar vesicles (LUV), and small unilamellar vesicles (SUV). In this work, LUVs have been always employed whenever lipid vesicles were the best option, with an average diameter of about 100 nm. LUVs were prepared through the extrusion method (see below), with the zwitterionic POPC and the anionic POPG

as comprising lipids. Different proportions of the two lipids were used in order to obtain vesicles with variable net negative charge, so to mimic different bacterial plasma membranes.[5] These two lipids were chosen for their relative low transition temperature (271K), making it possible to perform the extrusion easily at room temperature, well above transition one.[6] This is mandatory to obtain an homogeneous LUVs dispersion. In addition, they are reported to be ideally miscible,[7] which is fundamental to obtain vesicle of homogeneous composition. In spite of PG lipids are, in general, less abundant than PE (phosphatidylethanolamine) in bacteria,[5] POPE is not expected to be as highly miscibile as POPG with the POPC, and, importantly, its transition temperature is as high as 298 K.[6]

*Experimental details*. Proper amounts of POPC and POPG were dissolved in $CHCl_3/CH_3OH$ 1/1 V/V in order to obtain a homogeneous mixture. A gentle stream of nitrogen was used to remove the organic solvent and the obtained lipid film was placed under vacuum pumping overnight, in order to remove any residual. Next, the lipid dry film was hydrated with the buffer of choice and vortexed 5 x 1 minute. The obtained MLV suspension (10-20 mM total lipid concentration) was subjected to 5 freeze-thaw cycles between liquid nitrogen and 313K water bath, in order to improve homogeneity of the final suspension both in terms of size and lamellarity. After that, LUVs were obtained by the extrusion method, i.e. by passing the MLVs suspension 11 times through two different polycarbonate filters (Whatman Inc., Piscataway, NJ) with 400 and 100 nm pore size, respectively, using the Avanti mini-extruder® (Avanti Polar Lipids). Final lipid concentration was determined through NMR by lyophilizing a portion of the concentrated LUV stock, solubilizing the lipids in deuterochloroform and comparing the area of the signal due to the terminal methyl groups with those acquired on a reference sample. Size distribution was checked with dynamic light scattering.

In the case of calcein release assay, two different stocks of LUVs are required, namely, a standard one prepared as explained above, and another one with calcein loaded LUVs prepared as described hereinafter. The lipid dry film was prepared as mentioned, but a 60 mM calcein solution with final pH 7.4 was used for the rehydration instead of the buffer. The phases of vortex, freeze-thaw cycles and extrusion were performed as described above. Finally, unencapsulated calcein was removed through gel filtration. The latter was performed through a 30x1 cm column filled with Sephadex G-50 fine in a cold room at 277K.

***Lipid monolayers.*** This membrane model is a monolayer of lipid molecules packed and oriented at air/water interface. Lipid monolayers are spontaneously formed at the surface of a water or buffer drop simply by spreading a proper amount of lipids on top with a microsyringe. This useful self-assembly is due to their amphipathic nature, on the basis of which lipid tails will tend to orient towards the air to avoid contacts with the water molecules, where the polar head groups will be favorably hydrated on the other hand. Lipid monolayers were used in the present work as membrane models for surface pressure measurements (see below), by employing the same lipids chosen for preparing the LUVs.

*Experimental details*. Proper amounts of POPC and POPG were dissolved in $CHCl_3/CH_3OH$ 1/1 V/V in order to obtain a homogeneous mixture. The total lipid concentration was in the range $2 \cdot 10^{-6}$ - $5 \cdot 10^{-7}$

M. Proper volumes of the stock solution were spread at the air/buffer interface with Hamilton® microsyringes on top of 500 μL drop deposited in circular glass wells of 19 mm diameter.

## 2.3 Methods

### 2.3.1 Fluorescence spectroscopy

Fluorescence spectroscopy in the UV-vis range of the electromagnetic spectrum is considered to be one of the most important techniques for biophysical and biochemical investigations because of its broad applicability, from biotechnology and enzymology, to medical diagnostic and genetic analysis.[8] Principles will be briefly reported hereinafter; further details can be found in the very comprehensive textbook by J. R. Lakowicz.[8]

Fluorescence emission occurs when a molecule in an electronic excited state returns to the ground state, producing a radiation with a frequency determined by the difference in energy between the two levels involved in such radiative relaxation. The fluorescent emission strongly depends upon molecule environment, which can affect various parameters, e.g.: the wavelength of the maximum emission, the quantum yield, thus, the intensity of the emission band, and the lifetime of the excited state. This gives fluorescence spectroscopy a very high sensitivity and versatility, explaining its undisputed popularity. The typical emission spectrum is a plot of emission intensity versus the wavelength of the emitted radiation, and depends, of course, on the electronic structure of the fluorophore being considered, but also on the solvent used to solubilize the sample and the presence of other potentially interacting species in the same solution.[8] Not every molecule is fluorescent, but there are many fluorescent probes that can be used in properly designed experiments, usually divided into two groups: intrinsic and extrinsic fluorophores. An intrinsic fluorophore is a fluorescent moiety, which is naturally present in the chemical species under investigation, like the aromatic amino acids in the case of proteins. On the other hand, an extrinsic fluorophore is chemically or enzymatically added to make the species under investigation fluorescent, like the classic example of rhodamine.[8] Among the standard aromatic amino acids, tryptophan is definitely the most widely used in fluorescence spectroscopy studies. First of all, it is characterized by a remarkably high quantum yield and superior molar absorptivity when compared to tyrosine and phenylalanine, making it the most sensible intrinsic fluorophore in apoproteins. In addition, because of its high polarizability, it is highly sensitive to the local environment, which results in many possible applications, such as binding of ligands, protein–protein association, protein folding/unfolding equilibrium, to cite a few.[8] For instance, Trp fluorescence can be used to determine the partition constant of a peptide between the bulk water and the lipid bilayer in a liposomes dispersion, because Trp emission is different when it is exposed to a polar environment or it is embedded in more hydrophobic one. Basically, this is due to dipolar interaction between the indolic group and the water molecules, which cause the electronic exited states to relax to lower energy before the fluorescent emission.[9]

Other important applications of fluorescence spectroscopy are related to the fluorescence quenching phenomena, which can be defined as those processes leading to a fluorescence decrease.[8] Fluorescence quenching can occur through different mechanisms, such as excited-state reactions and molecular rearrangements, energy transfer, ground state complex formation and collisional quenching,

but it generally depends on the specific fluorophore-quencher pair, basically on the extent of the overlap between the emission spectrum of the fluorophore and the excitation spectrum of the quencher, and on their distance.[8] Fluorescence quenching can be a very useful tool to investigate fluorophores accessibility to different quenchers and ultimately estimate fluorophore localization within the sample, like in location studies concerning proteins and membranes.[8] Under certain conditions, the fluorophore can provoke a decrease of itself intensity, a process usually referred to as self-quenching. This is typically observed, for instance, in highly concentrated solutions of the fluorophore, where exited molecules transfer the energy to their nearest neighbors leading to fluorescence self-quenching. On the other hand, if the same solution is diluted, "normal" fluorescence is recovered. These were the basis for the liposome leakage assay presented in this work.

*Experimental details.* In the present work, fluorescence spectroscopy was applied to characterize different aspects of peptides behavior, namely, lipid bilayer affinity, insertion depth and perturbation activity. Most of the work was performed at the University of Cagliari, where spectra were recorded with a LS55 Luminescence Spectrometer (Perkin-Elmer, Waltham, MA, USA) equipped with a thermostated cuvette holder and magnetic stirrer. The quenching experiments concerning Trp localization were performed at the University of Porto, Faculty of Science, Department of Chemistry and Biochemistry, during 6 months Erasmus scholarship under the supervision of Prof. A. P. Gameiro dos Santos. Spectra were recorded with Varian Cary Elipse spectrofluorometer equipped with a temperature controller and a Varian Peltier multicell holder.
Sample preparation, spectra acquisition details and procedure of data analysis pertaining to the different experiments carried out in this work will be presented hereinafter, separated into distinct subsections.

***Partition studies.*** The partition constant quantitatively describes the concentration ratio for the given species in two different immiscible solvents or phases. In the case of membrane active peptides, it is of particular interest to determine partition constant between the aqueous bulk solution and the lipid bilayer for the peptides under investigation. Affinity of different peptides for the same membrane model can be compared through partition constants, likewise the affinity of the same peptide for different membrane models or under different conditions like temperature, ionic strength, pH, and so on. Determination of the partition constant can be attained by both physical methods aimed at separating bound and free peptide fractions and spectroscopy studies.[10] Among spectroscopic techniques, fluorescence spectroscopy is widely employed, especially when Trp is present in the amino acid sequence like in the present case, as Trp represents a suitable intrinsic fluorescent probe. It is possible, indeed, to monitor both the shift of the emission maximum or the intensity of its fluorescence emission. It is well known that when the peptide binds a lipid bilayer, and the Trp, in turn, experiences a less hydrophilic environment, a decrease of emission wavelength and a concomitant increase of the quantum yield of Trp fluorescence will be typically observed.[8,11,12]

*Experimental details*. In the present work, Trp emission spectra were recorded at 300 K between 300 and 500 nm. Excitation wavelength was 295 nm, and both beam entry and exit slit width were set to 5 nm. LUVs prepared with different POPC/POPG molar ratio were used to dissolve the peptide at a final

concentration of 1.3 μM. Spectra were recorded at different values of lipid/peptide ([L]/[P]) molar ratio. Spectrum of the lipid vesicles was always acquired before peptide solubilization as the background to be subtracted from the corresponding spectrum acquired in the presence of the peptide. Results were expressed as the average value obtained from three replicates.

The position of Trp emission maximum as a function of [L]/[P] is a useful although only qualitative parameter to compare bilayer affinity for different peptides under different conditions. Data are obtained relatively easily with minimal data treatment. However, it is widely recognized that quantitative determination of the partition constant cannot be attained, because of the (often) non-linear dependence of the emission wavelength on the ratio of bound/unbound peptide molar concentrations.[10,13] Quantitative determination of the partition constant can be obtained by applying a simple two-state model to the data of Trp emission intensity (I) obtained by integration.[9,14] The partition model function reported hereinafter was fitted to the experimental data as a function of total lipid concentration [L]:

$$\frac{I - I_W}{I_W} = \frac{K'_p \gamma_L [L] \alpha}{K'_p \gamma_L [L] + 1} \tag{1}$$

where, Iw is Trp fluorescence intensity recorded in "water" at the very beginning of the titration, when peptide is solubilized in the absence of lipid vesicles; $K'_p$ is the apparent partition constant that includes the molar volume of lipids and water (see equation 2) [9,13]; $\gamma_L$ is the lipid molar volume (0.762 $M^{-1}$ was used for both POPC and POPG);[15] and $\alpha$ is the horizontal asymptote of the hyperbolic curve described by equation 1, which is defined as $(I_\infty - I_W)/I_W$, where $I_\infty$ is the Trp emission intensity at infinite [L].

$$K'_p = K_p \frac{\gamma_W}{\gamma_L} \approx \frac{n_{S,L} / V_L}{n_{S,W} / V_W} \tag{2}$$

where, $K_p$ is the thermodynamic partition constant, $\gamma_W$ is the water molar volume; $n_{S,L}$ are the moles of solute in the lipid phase; $n_{S,W}$ are the moles of solute in the water phase; $V_L$ and $V_W$ are the volume of lipid and water phase, respectively. Thus, $K'_p$ represents the ratio of solute molar concentration in the two phases. Trp fluorescence intensity is expected to vary hyperbolically as a function of total lipid concentration if the two-state model presented here is valid, otherwise this data treatment is simply not applicable and more sophisticated models should be taken into consideration.[10,16,17]

***Tryptophan localization.*** Fluorescence quenching can be used to estimate peptides average localization in a vesicles dispersion. In particular, Trp accessibility to properly selected quenchers can provide

important information on the degree of peptides internalization inside the lipid bilayers.[8] When Trp residues are buried inside the hydrophobic region of vesicles' lipid bilayer, it will be less exposed to the surrounding water molecules, and therefore less accessible to an hydrophilic quencher. Quenchers like acrylamide and iodide ions will be less effective in reducing Trp fluorescence intensity.[13] On the other hand, in order to estimate peptide degree of penetration inside the lipid bilayer, i.e. its transverse location, in depth-dependent fluorescence quenching experiments can be performed by using spin-labeled fatty acids or phospholipids. Series of such hydrophobic quenchers are available on the market, characterized by the quenching group in different positions along their hydrocarbon chain.[13]

*Experimental details.* In the present work, measurements were performed at 300K with both beam entry and exit slit width set to 5 nm. Excitation and emission wavelength were 295 nm and 350 nm, respectively. LUVs were prepared using different POPC/POPG molar ratio, in ordered to obtain vesicles with different net negative charge. Two different [P]/[L] ratios were investigated, 0.003 and 0.06, in order to monitor the possible effects of an increased peptide local concentration in/on the vesicles bilayer. Results were expressed as the average of three independent measurements.

Experiments of quenching by acrylamide were carried out by measuring the decrease of Trp intensity in a buffered peptide solution (4μM) either in the presence or in the absence of the LUVs, after the addition of successive aliquots of acrylamide from a 3 M stock solution. After each addition, Trp emission was monitored for about 10 minutes, and the spectrum was recorded only after steady state was reached. As far as the lipophilic quenchers are concerned, experiments were performed by using two different probes, 5-nitroxyl (5NS) and 16-nitroxyl (16NS) stearic acid free radical, which are stearic acids with the doxyl quenching group at the level of the 5$^{th}$ and 16$^{th}$ carbon atom, respectively. 5NS is useful to probe the interface between the head groups and acyl chains region of the bilayer, whereas 16NS is more deeply buried within the latter.[18,19] Trp emission intensity was measured in a buffered peptide solution (4μM) in the presence of LUVs, after addition of successive aliquots of either 5NS or 16 NS from 0.002-0.03 M ethanol stock solutions. It is important to keep final ethanol concentration below 2%V/V to avoid vesicles disruption. After each addition, Trp emission was monitored for about 20 minutes, and the spectrum was recorded only after steady state was reached. Lipid probes have their own characteristic partition constant ($K'_p$(5NS)=89000 and $K'_p$(16NS)=9730, in the liquid-crystalline phase)[20] between water and lipid phase, which have to be taken into account to calculate their actual concentration in the lipid phase $[Q]_L$:[21]

$$[Q]_L \approx \frac{K'_p [Q]_T}{1 + K'_p \gamma_L [L]} \qquad \gamma_L [L] >> 1 \qquad (3)$$

where, $K'_p$ is the apparent partition constant of the quencher (see previous subsection); $[Q]_T$ is the total quencher concentration; $\gamma_L$ is the lipids molar volume; [L] is the lipid molar concentration.

For all measurements, actual quencher concentration was calculated by taking progressive dilution due to addition of the aliquots into account. The sum of the absorbance of both the fluorophore and the quencher was measured at 295 nm ($\lambda_{exc}$) over the whole range explored (up to 0.600 M) and it was always found below 0.1 a.u., therefore no correction for the inner filter effect was carried out.[18]

Results have been analyzed according to the Stern-Volmer equation, which correlates fluorescence quenching to the concentration of quencher $[Q]_L$:[13,18,19,22]

$$\frac{I_0}{I} = 1 + K_q[Q] \tag{4}$$

where, $I_0$ is the fluorescent intensity in the absence of the quencher recorded at the beginning of the titration; I is the fluorescent intensity of the sample in the presence of the quencher; $K_q$ is the so-called Stern-Volmer constant; $[Q]_L$ is the quencher concentration in the lipid phase.

The Stern-Volmer constant provides information of the accessibility of the fluorophore to the quenching species. The change in the Trp intensity ($I_0/I$) caused by the quencher is expected to be linearly dependent on [Q]. In our case, at high quencher concentrations, a positive deviation from the linearity was observed. This phenomena is known and often encountered when the extent of quenching is great.[8] In literature, such positive deviation from the Stern-Volmer equation is called "sphere of action", and generally it causes an increased in the probability of quenching, with the final result that the extent of quenching is higher in the absence this effect.[8]

***Vesicles leakage assay.*** The membrane cell is widely considered the main target of AMPs,[23] and fluorescent spectroscopy is a suitable technique to investigate damaging of the lipid bilayer, or alteration of its permeability, caused by peptides. A fluorescent dye is encapsulated inside LUVs at a concentration high enough for its emission to be self-quenched. One of the most commonly used dyes is calcein. If the peptide interacts with vesicles' bilayer and induces the formation of pores, breaks or, generally specking, an alteration of the bilayer permeability, the fluorescent dye will be released by the perturbed vesicles and diluted into the bulk solution. In turn, dye fluorescence will not be self-quenched any more and its signal will be recovered,[24] allowing to monitor both release extent and kinetics, ultimately providing fundamental information about peptide activity.

*Experimental details.* In the present work, measurements were carried out at 300 K, with both beam entry and exit slit width set to 5 nm. Few microliters of a diluted dispersion of calcein loaded LUVs was added to a dispersion of empty LUVs with the same composition at 40 μM total lipids concentration (final volume 1200 μL; final lipid concentration from the calcein loaded vesicles was absolutely negligible). Excitation and emission wavelength were 490 and 517 nm, respectively. LUVs prepared with different POPC/POPG molar ratio were tested, and experiments were carried out at different [P]/[L] values. Calcein emission signal from intact LUVs ($I_0$) was monitored over time before peptide addition in order to check system stability and to verify that vesicles did not release their calcein content spontaneously. After peptide solubilization, calcein intensity increased and the signal was monitored for about 15-20 minutes, up to a final steady-state fluorescence emission ($I_p$). Finally, in order to determine the fluorescence intensity corresponding to complete calcein release from all the vesicles ($I_t$), total disruption of the vesicles was attained by adding 10 μL of a 10%w/w solution of Triton X-100. Calcein release was reported as the percentage calculated as follows:

$$\%rel. = \frac{I_p - I_0}{I_t - I_0} \times 100 \quad (5)$$

***Numerical model for calcein release.*** The vesicles leakage experimental data were reported as %rel. (equation 5) as a function of [P]/[L] and analyzed by using an all-or-none release model. An iterative Monte Carlo minimization scheme was applied with the aim of estimating the minimum number of peptide molecules required to cause calcein release from the targeted vesicle.

The vesicles leakage model proposed was formulated on the basis of a general all-or-none release model, by taking inspiration from a pioneering work on the peptide melittin.[25] By definition, an all-or-none model implies that calcein is released by each vesicle at once, such that vesicles are considered to be either loaded or not, while intermediate loadings are supposed to be transient and scarcely populated.[26] In our model, vesicles release their whole calcein content only when a minimum number of peptide molecules are present in the bilayer, i.e. the bound peptide threshold.[27]

The molar fraction of vesicles bound peptides ($\chi_{pl}$) was calculated through equation 6:

$$\chi_{pl} = \frac{K'_p \gamma_l [L]}{K'_p \gamma_l [L] + 1} \quad (6)$$

where, $K'_p$ is the apparent partition constant that includes the molar volume of lipids and water (see equation 2); $\gamma_l$ is the lipids molar volume; [L] is the total lipid molar concentration.

From equation 6, the average number of vesicles bound peptide molecules $nP_l$ can be easily calculated for each experimental point.[28] The number of vesicles in solution can be estimated through their average diameter. On the basis of the polycarbonate filter used during vesicle extrusion (see section Lipid vesicles (or liposomes)), LUVs should have a diameter of about 100 nm. Dynamic light scattering measurements showed an average diameter of ~120 nm despite the specific POPC/POPG molar ratio. Since the latter can be taken as the actual hydrodynamic diameter, we selected the intermediate value of 110 nm to calculate the surface of the external leaflet, by considering our vesicles as perfect spheres. The surface density of lipid molecules was determined from surface pressure measurements of lipid monlayers in the saturation phase (see below). The resulted value of 1.3 $nm^{-2}$ was in agreement with data reported in the literature.[29,30] Finally, the number of lipid molecules per vesicles, the so-called vesicles aggregation number, and, in turn, the number of vesicles (*nv*) could be calculated for each experimental data point.[28]

The average number of bound peptide molecules per vesicle ($nP_l/nv$) was calculated for each data point, and coverage probability was described by a Gaussian distribution function. The integral of the distribution for $nP_l/nv \geq 0$ was then normalized to 1. For each membrane composition, the above mentioned bound peptide threshold (*th*) was set, while the calculated percentage of release (*%rel.*) was obtained from the integral of the coverage distribution for $nP_l/nv \geq th$. In order to minimize the sum of

square difference between the experimental and calculated data points, a Monte Carlo scheme was implemented. The bound peptide threshold and the standard deviation of the coverage distribution were used as fitting parameters for the three membrane compositions investigated (25, 50 and 75%mol. of POPG), thus, a total of six parameters were used for minimization. At each iteration, one parameter was randomly selected and changed in the range between -10% and +10%. Only iterations corresponding to a decrease in the sum of square difference between the experimental and calculated data points were accepted, rejected otherwise. For each peptide, all the data sets corresponding to different membrane compositions were fitted simultaneously.

### 2.3.2 Infrared spectroscopy

Fourier transform infrared spectroscopy (FTIR) is a fundamental technique for structure determination and it has many applications also for biological systems. Investigation of protein structure, protein folding/unfolding, orientation and conformation of membrane-associated protein, peptides and lipids represents some important examples.[31–34] In addition, FTIR offers the advantage of studying the protein/peptide in a wide range of conditions, from aqueous solutions to organic solvents, and to detected small conformational and structural changes in physiological conditions, even in the presence of detergents and lipids, using a relatively inexpensive technique.[33]

In protein and peptide studies, the most common application concerns conformational studies through the analysis of the most intense vibrational band arising from polypeptides, i.e. the amide I. This is centered near 1650 $cm^{-1}$ and is particularly sensitive to secondary structure of the polypeptide, while it is rather insensitive to the specific nature of the amino acids side chain.[33,35] The amide I band is actually due to different vibrational modes of the polypeptide backbone. The main contribution is due to C=O stretching vibration, but also to the out-of-phase stretching of the CN bond, the CCN bond angle deformation and the NH in-plane bend contribute significantly.[31] In particular, the latter is responsible for the slight but significant sensitivity of amide I vibration to sample deuteration. Numerous studies were devoted to the correlation between polypeptide secondary structure and amide I band shape and frequency. In the literature it is possible to find many reference tables.[31–33] Typically, α-helix and random coiled structures exhibit the maximum in the range 1640-1660 $cm^{-1}$, extended loops and β-turns are found at wavenumbers between 1660 and 1680 $cm^{-1}$, while β-sheets are characterized by two separate components, the main one in the range 1615-1640 and a less intense one in the range 1675-1695 $cm^{-1}$.

The inherent solvent of biological samples represents one of the main drawbacks of FTIR in the field of biophysics. Water gives rise to very strong bands, namely, both the symmetric and anti-symmetric OH stretching at 3280 and 3490 $cm^{-1}$,[32] respectively, and HOH bending at 1645 $cm^{-1}$. These dominate the FTIR spectrum even of the most concentrated samples and despite cells with very short pathlength are used, making spectral smoothing and background removal absolutely necessary. In addition, in the case of polypeptides, water bending overlap with the amide I band, such that retrieving the latter after background subtraction is difficult and not always devoid of artifacts.[31–33] For these reasons, $D_2O$ is usually employed in order to shift solvent bands to less interesting spectral regions. Nevertheless, signal/noise (S/N) ratio is often low anyway and, depending on sample solubility,

increasing the concentration might be not the best option. In the case of short peptides the situation is even more challenging, as the number of peptide bonds per mole can be very low when compared to proteins. Moreover, when peptides have to be studied in the presence of lipid vesicles or, generally speaking, lipid bilayers, a relatively high [L]/[P] ratio should be chosen to avoid possible bilayer overcrowding, which will lead, in turn, to have also remarkably high lipid bands to subtract. The C=O stretching can be particularly problematic, as this is typically found at 1730 $cm^{-1}$, i.e. very close to the peptide amide I band.

Attenuated total reflection mode for FTIR (ATR-FTIR) is particularly suited when facing with the strong absorption from the $H_2O$ or $D_2O$ solvent.[33] Basically, ATR is based upon the use of a high refractive crystal, e.g. diamond or germanium, on top of which a few microliters of the sample are deposited. The infrared beam travels through the crystal and points the crystal/sample interface with a specific incidence angle. Due to a refraction index much larger than that of the sample, the infrared radiation is totally reflected at the interface. An evanescent wave is created upon reflection, which is characterized by the same frequency of the incident infrared beam, but the amplitude of the electric field decays exponentially by moving away from the interface. If the sample absorbs part of the evanescent wave, the reflected beam will finally reach the detector carrying that information, so that the corresponding infrared spectrum can be obtained. The penetration depth of the evanescent wave is on the order of the wavelength, which means an optical thickness of few micrometers, i.e. small enough for measurements of aqueous solutions.[31] Further significant improvement in S/N can be obtained, of course, by preparing a dry film of the sample on top of the crystal. When starting from an aqueous solution, the "disturbing" solvent will be eliminated upon evaporation and the nominal sample concentration will be increased. However, it is advisable to rehydrate the film, such that a certain degree of hydration will guarantee a more physiological condition, but still a greatly improved S/N when compared to the starting fully hydrated sample.

*Experimental details.* In this work, all spectra were acquired with a Bruker Vector-22 equipped with a diamond single-reflection ATR accessory (Platinum ATR module) and a liquid nitrogen cooled MCT detector. The software OPUS (Bruker, V6.5) was used both for spectra acquisition and data analysis.

Peptides were studied in PBS solution prepared with D2O at different concentrations, namely, 0.4, 1.0 and 2.0 mM, both in the absence and presence of LUVs. Total lipid concentration was always equal to 20 mM, such that different [L]/[P] ratios were explored, namely, 50, 20 and 10. LUVs were prepared with two different compositions: a low negative charge formulation with 25%mol. POPG (and 75%mol. POPC) and a high negative charge formulation with 75%mol. POPG (and 25%mol. POPC). Spectra were acquired from 10 μL of each sample deposited on the ATR crystal. Such fully hydrated samples (FH) were acquired in the 3500-600 $cm^{-1}$ spectral range, with 4 $cm^{-1}$ resolution, automatic atmosphere compensation and 32 scans. Background was automatically removed. For the sake of clarity, it is important to stress here that term "background" is used to indicate the spectrum of the clean ATR crystal, which was acquired under the same conditions and with the same parameters as the sample immediately before deposition. In order to minimize $^2H/^1H$ exchange from atmospheric humidity, a small Petri dish was used to cover the sample on the ATR module, after having deposited several drops of $D_2O$ around the crystal (figure 2.2). In the case of peptide samples in the absence of

vesicles, the spectrum of PBS was acquired as the "blank" to be subtracted during spectra post-processing. In the case of vesicles containing samples, the spectrum of the corresponding LUVs dispersion was acquired as the blank.

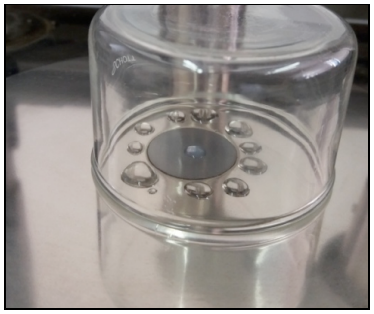

**Figure 2.2.** The typical experimental setting used for the rehydration of the dry film.

Beside acquisition of FH samples, the same were acquired as rehydrated film. 10 μL of the sample were deposited on the crystal and then dried with a gentle stream of nitrogen until solvent bands residuals were about ten times less intense than the amide I (about 5 minutes). A small Petri dish was used to cover the "dry" film on the ATR module, after having deposited several drops of $D_2O$ around the crystal (figure 2.2). The film tended to adsorb the $D_2O$ vapor underneath the Petri dish and this spontaneous rehydration was monitored by real time spectrum preview. After one minute, the maximum of $D_2O$ stretching band was between 1 and 2 times the amide I, and spectrum acquisition was started for such a rehydrated film (RF). Acquisition parameters were the same as in the case of FH samples but 16 scans were acquired for the RF ones. In the case of vesicles containing samples, the spectrum of the corresponding rehydrated LUVs film was acquired as the blank to be subtracted during spectra post-processing.

Post processing consisted of three steps: (i) baseline correction, (ii) blank spectrum subtraction and (iii) line smoothing. Full spectrum baseline correction was applied by using a 3$^{rd}$ order polynomial function. Blank subtraction was performed iteratively within the OPUS software. In practice, the blank spectrum was multiplied by an adjustable pre-factor and the resulting subtracted spectrum of the sample continuously updated. The optimal pre-factor was chosen as the one giving an almost flat 2000-2100 cm$^{-1}$ spectral region. This particular region is devoid of bands from both lipids and peptides and, thus, can be taken as a reference for checking correctness of blank subtraction.[32] Line smoothing was performed on the final corrected spectrum with a Savitzky-Golay function, using windows of 25 points. Finally, the amide I band was isolated from the full spectrum and a component deconvolution was performed with the free software Gnuplot (VS 4.6)[36] by using the sum of Gaussian functions. The minimum number of components was introduced in the least-square fitting procedure as determined through the analysis of the spectrum second derivative[32,33] implemented in OPUS. Each Gaussian function introduced represented a distinct component contributing to the full amide I band. Each Gaussian function presented three independent fitting parameters:

$$f(x) = ae^{-(x-b)^2/c^2} \tag{7}$$

where, *a* is the height; *b* is the position; *c* is the square root of the variance.

### 2.3.3 Surface pressure measurements

The action of many antimicrobial peptides involves their interaction with membrane lipid bilayer.[37] Lipid monolayers formed spontaneously at the air/water interface are widely considered easy to prepare and a suitable tool to investigate the peptide affinity and perturbation capability with varying lipid composition and environment conditions like pH, temperature, ionic strength and so on.[29] Surface pressure measurement of the lipid monolayer after peptide addition in the aqueous subphase provides important information about peptide tendency to accumulate at the interface and possible ability to insert between the lipid molecule, ultimately causing a stress on the monolayer and determining an increase of its equilibrium surface pressure.[38]

Lipids are amphipathic molecules and they act as surfactants by spontaneously accumulating at the interface between a polar and a non-polar environment, like the water/air interface, directing their polar head groups toward the polar side and the non-polar tails on the other. Lipids typically form a monolayer at such interface, which is characterized by the surface pressure ($\pi$) defined by the following equation:

$$\pi = \gamma_{solvent} - \gamma_{solution} \tag{8}$$

where, $\gamma$ is the surface tension.

*Experimental details.* Surface pressure of lipid monolayers was measured using the high precision tensiometer Kibron "DeltaPi" (software DeltaGraph VS 2.15, resolution of 0.01 mN/m).

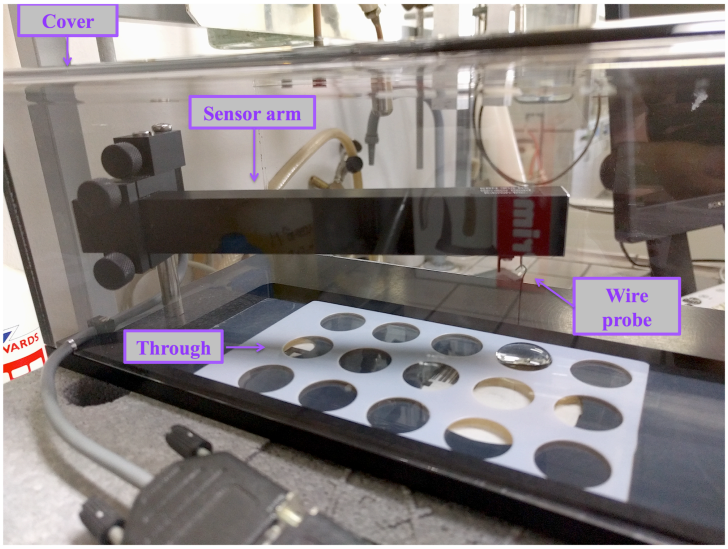


**Figure 2.3.** Tensiometer Kibron "DeltaPi".[39] The most important components

are labeled.

This is an electrobalance that exploits the Wilhelmy method.[29] This methods is one of the most used for the surface pressure determination of plane and liquid interfaces.[29] Briefly, let us consider a thin plate with *w* as width and *t* as thickness ($t << w$), which is not completely immersed in a liquid phase and connected to an electrobalance.[29] The forces that act on the plate are: its weight (P) and the surface tension, pointing downwards, and the Archimede buoyancy A, pointing upwards:[29]

$$F = P + 2\gamma(w + t)\cos\vartheta - A \tag{9}$$

where θ is the contact angle formed between the liquid and the solid plate. Due to the high wettability of the plate, θ=0, therefore:

$$\pi = \frac{-\Delta F}{2w} \tag{10}$$

If P and A are kept constant, after some simplifications the equation 10 can be rewritten as follow:

$$\Delta F = 2w(\gamma_{solution} - \gamma_{water}) = -2w\pi \tag{11}$$

Finally the surface pressure can be obtained as reported below:

$$\pi = \frac{-\Delta F}{2w} \tag{12}$$

All measurements were performed in a room with a constant temperature of 300±1K. All the results reported in the chapter 3 are the average of three independent measurements. The electrobalance was always calibrated with respect to deionized water, by setting the reference surface tension to 71.67 mN/m.[40]

This part of the present study was divided into two parts, whose specific details concerning sample preparation and data analysis are reported hereinafter in the two corresponding subsections. The first part consisted in the determination of isotherms for the different monolayers employed in the second part, in order to collect fundamental information about the different lipid systems at equilibrium before the addition of any peptides. The second part was focused on the peptides action by measuring the perturbation induced to the selected lipid monolayers.

***Lipid monolayers characterization.*** A lipid monolayer is spontaneously formed at the air/water interface but lipid packing, orientation with respect to the interface normal, lateral mobility, and so on, depend on the surface excess (Γ), which is basically the surface concentration (moles/area) of the surfactant.[29] The surface pressure of the interface increases with increasing Γ, and the π-Γ isotherm provides fundamental information on the monolayer phase and, thus, the degree of lipid packing.[41] It was thus particularly important to reconstruct such isotherm for each lipid mixture to be used in

forming the monolayers, in order to determine the best experimental conditions to subsequently study peptide induce perturbation.

*Experimental details.* Before each measurement, the reference zero pressure was set by measuring the surface pressure of 500 μL PBS deposited in a circular glass trough (19 mm diameter) in the absence of lipid molecules. Lipid monolayers were then prepared by spreading increasing amount of the given lipid mixture with a Hamilton microsyringe from a stock solution of the lipids ($1.8 \cdot 10^{-5}$ M total lipid concentration dispersed in CHCl3/CH3OH 1/1 V/V) on top of the PBS drop. All measurements were thus performed at constant-area. After organic solvent evaporation, the surface pressure reading became constant over time and was taken as the $\pi(\Gamma)$. Three independent replicas of the $\pi$-$\Gamma$ isotherm were reconstructed for each lipid mixture. Different mixtures of POPC/POPG were studied, namely, with POPG %mol. equal to 0, 25, 50, 75 and 100. Different linear regimes were fitted by least-squares minimization. Results of angular coefficients and y-axis intercepts have been reported as the corresponding average value and standard deviation.

***Peptide-monolayer interaction.*** After forming a lipid monolayer with selected composition and initial surface pressure ($\pi_i$), a known amount of the peptide under investigation can be injected in the aqueous subphase. Peptide molecules tendency to interact and eventually intercalate between the lipid molecules is revealed as surface pressure increase. The process is monitored over time (typically for 15-30 minutes) until stationary final pressure ($\pi_f$) is reached.

*Experimental details.* On the basis of the $\pi$-$\Gamma$ isotherm obtained for the different lipid monolayers (see previous subsection), either 25%mol. or 75%mol. POPG monolayers were prepared on 500 μL PBS deposited in a circular glass trough (19 mm diameter), at an initial surface pressure $\pi_i = 25 \pm 2$ mN/m, which corresponded to the monolayer liquid-condensed (L-C) phase. Before each measurement, the reference zero pressure was set by measuring the surface pressure of the 500 μL PBS in the absence of lipid molecules. The peptide under investigation was injected underneath the lipid monolayer in the aqueous subphase with a Hamilton microsyringe. Starting from PBS stock solution with 50 μM peptide concentration, injected aliquots were smaller than 15 μL, giving a final concentration of the peptide in the monolayer subphase in the range 0.5-3.0 μM. Preliminary tests performed by injecting the same volume of PBS (without peptide) showed negligible surface pressure variation (≈ 0.01 mN/m) due to volume increase. After peptide injection, monolayer surface pressure was monitored over time until the final stationary $\pi_f$ for each different concentration. The surface pressure variation ($\Delta\pi$) can be expressed as follows:

$$\Delta\pi = \pi_f - \pi_i = (\gamma_{reference} - \gamma_f) - (\gamma_{reference} - \gamma_i) = \gamma_i - \gamma_f \tag{13}$$

where, $\gamma_{reference}$ is determined by the calibration and the zero pressure setup. It is equal to the water value but then eliminated in the expression for $\Delta\pi$. Therefore, by changing the sign of the experimental $\Delta\pi$ we get the variation of the monolayer surface tension due to the peptide, which is in equilibrium

between the lipid monolayer and the aqueous subphase. For each peptide and each of the two lipid monolayer compositions, -Δπ was thus determined as a function of peptide concentration (at constant temperature, monolayer area and initial pressure). Results have been analyzed by the Gibbs equation:

$$d\gamma = -\Gamma RTd\ln C \tag{14}$$

where, Γ is the surface excess, R is the universal gas constant, T the absolute temperature and C is the molar concentration. Rearranging equation 14:

$$\Gamma = -\frac{1}{RT}\left(\frac{d\gamma}{d\ln C}\right)_T \tag{15}$$

Thus, peptide surface excess can be obtained from the angular coefficient of the straight line obtained through the least-square curve fitting of the experimental -Δπ as a function of ln[P]. Surface excess is finally obtained in mmol/m$^2$ and then straightforwardly converted into Å$^2$/molecule.

2.3.4 Other techniques

***Microbiological assays.*** The antimicrobial activity of both SB056 and β-SB056 was investigated through the determination of the minimal inhibitory concentration (MIC), minimal bactericidal concentration (MBC), evaluation of biofilm inhibition, and haemolytic activity.[42] This part of the study was performed by our collaborators in Rome (group of Prof. M. L. Mangoni, Dept. Biochemical Sciences "A. Rossi Fanelli", Pasteur Institute- Cenci Bolognetti Foundation, Sapienza University of Rome, Italy) and Pisa (group of Prof. G. Batoni, Dept. of Translational Research and New Technologies in Medicine and Surgery, University of Pisa, Italy). Procedures will be summarized briefly hereinafter for the sake of completion, but further details can be found in the quoted references.

*MIC determination and killing curves.* For all peptides, antimicrobial assays were performed against both *Escherichia coli* (ATCC 25922) and *Staphylococcus aureus* (ATCC 25923) using the microbroth dilution method in sterile 96-well plates as reported in details elsewhere.[42–44] Briefly, bacteria were grown in Luria-Bertani medium at 37 °C. Then, bacterial suspension was diluted in Mueller-Hinton broth at a final cell density of $2\cdot10^6$ colony-forming units (CFU)/mL. Aliquots of 50 μL were added to 50 μL of the broth either supplemented or not with 150 mM NaCl and containing the peptide at different concentrations. MIC was defined as the peptide concentration that caused 100% of microbial growth inhibition.[42,45] The bactericidal activity and killing kinetics curves were determined as reported in details elsewhere.[42,46] Briefly, 50 μL of the bacterial suspension ($2\cdot10^6$ CFU/mL) was added to wells of microtiter plate, each containing 50 μL broth supplemented with peptide at different concentration. The plate was incubated at 37°C. At different time intervals, 5 μL aliquots were withdrawn, properly diluted and then spread onto Luria-Bertani agar plates for counting after overnight incubation at 37°C. The minimal bactericidal concentration (MBC) was calculated as the minimal concentration of peptide causing a reduction in the number of viable cells ≥3 log10 within 90 min.[42,47]

*Biofilm inhibition assay.* Antibiofilm activity was tested against *Staphylococcus epidermidis* (ATCC 35984) and *Pseudomonas aeruginosa* (ATCC 27853). MIC values were previously determined against planktonic cells under the same experimental conditions used for the biofilm inhibition assay as reported in details elsewhere.[42] Biofilm biomass was assessed by crystal violet (CV) staining, as described in the reference.[48]

*Hemolytic activity.* Hemolytic activity was determined by using fresh human erythrocytes from healthy donors.[42] The release of hemoglobin was monitored through measurements of absorbance at 415 nm.[42] The control for zero hemolysis (blank) was a sample of erythrocytes suspended in 0.9% NaCl solution. Hypotonically lysed erythrocytes were used as a reference for 100% hemolysis. Hemolysis was finally reported as a percentage calculated as follows:

$$\%hemolysis = [(Abs_{sample} - Abs_{blank}) / (Abs_{total\_lysis} - Abs_{blank})] \times 100 \quad (16)$$

***Optical density measurements.*** Possible vesicles size increase as due to either aggregation or fusion was assessed through optical density measurements.[49] The latter increases with increasing vesicles size, thus, such measurements can also be applied to investigate micellization, which would lead to optical density decrease.[50,51] Absorbance at 400 nm was measured at 300 K with a Varian Cary-50 UV-visible spectrophotometer. Different samples (at different [P]/[L] and vesicles composition, final volume 1.2 mL) were prepared as for calcein leakage assay (§2.3.1). Optical density was monitored over time for each sample (20 min.). Wavelength of 400 nm was chosen for the greater sensitivity (but lower linearity as a function of size) when compared to measurements at 600 nm.[49] Zero absorbance was set with PBS. In order to test method performance, a small aliquot (10 µL) of either a solution of Triton X-100 10% V/V or $Ca^{2+}$ 10 mM in PBS was added to a suspension of LUVs. Addition of the detergent lead to vesicles disruption, while the presence of divalent cations caused aggregation due to net charge neutralization. Evident decrease or increase in the optical density was observed, respectively.

***Dynamic Light Scattering (DLS).*** The same samples analyzed with UV-vis spectroscopy for size estimation, were also investigated with DLS for a quantitative determination. LUVs size distribution was determined with Zetasizer nano-ZS (Malvern instruments, UK) with a 4 mW He-Ne laser operating at wavelength of 633 nm and an angle of 173°. All the measurements were performed at 300K. At least three measurements were carried out for each sample in disposable cuvettes (volume 1.2 mL). Refractive index of 1.381[52] and water viscosity were taken into account by the instrument software manager.

**Transmission electron microscopy.** Transmission electron microscopy images were collected by Prof. C. Cannas and Dr. A. Ardu, Department of Chemical and Geological Science, University of Cagliari. LUVs, after incubation with the peptides were dropped on a carbon-coated copper grid and observed in Bright-Field mode with a JEOL 200CX, operating at 200 kV. LUVs with different POPC/POPG molar ratio were used. Peptides were incubated with the selected LUVs suspension at a [L]/[P] of 100:1. At

room temperature, 10 µL were dropped on the sample grid (carbon-coated side up) for 2 minutes, then removing the excess solution with filter paper. After that, 10 µL of the staining solution (1% V/V phosphotungstic acid in deionized water, pH 7.4) was dropped in the same way, and removed after 1 min with filter paper. Samples were finally kept in a desicator at room temperature and atmospheric pressure overnight before observation.

**References:**


1. Wadhwani, P. *et al.* Self-Assembly of Flexible β-Strands into Immobile Amyloid-Like β-Sheets in Membranes As Revealed by Solid-State 19F NMR. *J. Am. Chem. Soc.* 134, 6512–6515 (2012).
2. Wadhwani, P. *et al.* Membrane-Active Peptides and the Clustering of Anionic Lipids. *Biophys. J.* 103, 265–274 (2012).
3. Johnsson, M. & Edwards, K. Liposomes, Disks, and Spherical Micelles: Aggregate Structure in Mixtures of Gel Phase Phosphatidylcholines and Poly(Ethylene Glycol)-Phospholipids. *Biophys. J.* 85, 3839–3847 (2003).
4. Seddon, A. M., Curnow, P. & Booth, P. J. Membrane proteins, lipids and detergents: not just a soap opera. *Biochim. Biophys. Acta BBA - Biomembr.* 1666, 105–117 (2004).
5. Shaw, N. Bacterial Glycolipids. *Bacteriol. Rev.* 34, 365–377 (1970).
6. Phospholipids | Avanti Polar Lipids.
7. Miscibility of Phospholipid Binary Mixtures | Avanti Polar Lipids https://avantilipids.com/tech-support/physical-properties/miscibility/.
8. Lakowicz, J. R. *Principles of Fluorescence Spectroscopy*. (Springer Science & Business Media, 2013).
9. Matos, P. M., Franquelim, H. G., Castanho, M. A. R. B. & Santos, N. C. Quantitative assessment of peptide–lipid interactions.: Ubiquitous fluorescence methodologies. *Biochim. Biophys. Acta BBA - Biomembr.* 1798, 1999–2012 (2010).
10. White, S. H., William C. Wimley, Alexey S. Ladokhin & Kalina Hristova. Protein folding in membranes: determining energetics of peptide-bilayer interactions. *Methods Enzymol.* 295, 62–87 (1998).
11. Zhao, H. & Kinnunen, P. K. J. Binding of the Antimicrobial Peptide Temporin L to Liposomes Assessed by Trp Fluorescence. *J. Biol. Chem.* 277, 25170–25177 (2002).
12. Christiaens, B. *et al.* Tryptophan fluorescence study of the interaction of penetratin peptides with model membranes. *Eur. J. Biochem.* 269, 2918–2926 (2002).
13. Loura, L. M. S., de Almeida, R. F. M., Coutinho, A. & Prieto, M. Interaction of peptides with binary phospholipid membranes: application of fluorescence methodologies. *Chem. Phys. Lipids* 122, 77–96 (2003).
14. Santos, N. C., Prieto, M. & Castanho, M. A. R. B. Quantifying molecular partition into model systems of biomembranes: an emphasis on optical spectroscopic methods. *Biochim. Biophys. Acta BBA - Biomembr.* 1612, 123–135 (2003).
15. Santos, N. C., Prieto, M. & Castanho, M. A. R. B. Interaction of the Major Epitope Region of HIV Protein gp41 with Membrane Model Systems. A Fluorescence Spectroscopy Study. *Biochemistry* 37, 8674–8682 (1998).
16. Melo, M. N. & Castanho, M. A. R. B. Omiganan interaction with bacterial membranes and cell wall models. Assigning a biological role to saturation. *Biochim. Biophys. Acta BBA - Biomembr.* 1768, 1277–1290 (2007).

17. Rodrigues, M. *et al.* Molecular characterization of the interaction of crotamine-derived nucleolar targeting peptides with lipid membranes. *Biochim. Biophys. Acta BBA - Biomembr.* 1818, 2707–2717 (2012).
18. Franquelim, H. G., Loura, L. M. S., Santos, N. C. & Castanho, M. A. R. B. Sifuvirtide Screens Rigid Membrane Surfaces. Establishment of a Correlation between Efficacy and Membrane Domain Selectivity among HIV Fusion Inhibitor Peptides. *J. Am. Chem. Soc.* 130, 6215–6223 (2008).
19. Moreno, M. R., Pérez-Berná, A. J., Guillén, J. & Villalaín, J. Biophysical characterization and membrane interaction of the most membranotropic region of the HIV-1 gp41 endodomain. *Biochim. Biophys. Acta BBA - Biomembr.* 1778, 1298–1307 (2008).
20. Wardlaw, J. R., Sawyer, W. H. & Ghiggino, K. P. Vertical fluctuations of phospholipid acyl chains in bilayers. *FEBS Lett.* 223, 20–24 (1987).
21. Stauffer, F. *et al.* Interaction between dengue virus fusion peptide and lipid bilayers depends on peptide clustering. *Mol. Membr. Biol.* 25, 128–138 (2008).
22. Mateo, C. R., Prieto, M., Micol, V., Shapiro, S. & Villalaín, J. A fluorescence study of the interaction and location of (+)-totarol, a diterpenoid bioactive molecule, in model membranes. *Biochim. Biophys. Acta BBA - Biomembr.* 1509, 167–175 (2000).
23. Wu, M., Maier, E., Benz, R. & Hancock, R. E. W. Mechanism of Interaction of Different Classes of Cationic Antimicrobial Peptides with Planar Bilayers and with the Cytoplasmic Membrane of Escherichia coli. *Biochemistry* 38, 7235–7242 (1999).
24. Andrea C. Rinaldi & Andrea Giuliani. *Antimicrobial Peptides:methods and protocols*. 618, (Methods in molecular biology).
25. Benachir, T. & Lafleur, M. Study of vesicle leakage induced by melittin. *Biochim. Biophys. Acta BBA - Biomembr.* 1235, 452–460 (1995).
26. Gregory, S. M., Cavenaugh, A., Journigan, V., Pokorny, A. & Almeida, P. F. F. A Quantitative Model for the All-or-None Permeabilization of Phospholipid Vesicles by the Antimicrobial Peptide Cecropin A. *Biophys. J.* 94, 1667–1680 (2008).
27. Manzo, G. *et al.* The singular behavior of a β-type semi-synthetic two branches polypeptide. Three-dimensional structure and mode of action. *Phys Chem Chem Phys* (2016). doi:10.1039/C6CP05464A
28. Manzo, G. *et al.* The singular behavior of a β-type semi-synthetic two branched polypeptide: three-dimensional structure and mode of action. *Phys. Chem. Chem. Phys.* (2016). doi:10.1039/C6CP05464A
29. Maget-Dana, R. The monolayer technique: a potent tool for studying the interfacial properties of antimicrobial and membrane-lytic peptides and their interactions with lipid membranes. *Biochim. Biophys. Acta BBA - Biomembr.* 1462, 109–140 (1999).
30. Melo, M. N. *et al.* Prediction of Antibacterial Activity from Physicochemical Properties of Antimicrobial Peptides. *PLOS ONE* 6, e28549 (2011).
31. Barth, A. Infrared spectroscopy of proteins. *Biochim. Biophys. Acta BBA - Bioenerg.* 1767, 1073–1101 (2007).
32. Tamm, L. K. & Tatulian, S. A. Infrared spectroscopy of proteins and peptides in lipid bilayers. *Q. Rev. Biophys.* 30, 365–429 (1997).
33. Haris, P. I. & Chapman, D. The conformational analysis of peptides using fourier transform IR spectroscopy. *Biopolymers* 37, 251–263 (1995).
34. Jackson, M. & Mantsch, H. H. The Use and Misuse of FTIR Spectroscopy in the Determination of Protein Structure. *Crit. Rev. Biochem. Mol. Biol.* 30, 95–120 (1995).
35. Hiramatsu, H. & Kitagawa, T. FT-IR approaches on amyloid fibril structure. *Biochim. Biophys. Acta BBA - Proteins Proteomics* 1753, 100–107 (2005).

36. gnuplot homepage. Available at: http://gnuplot.sourceforge.net/.
37. Straus, S. K. & Hancock, R. E. W. Mode of action of the new antibiotic for Gram-positive pathogens daptomycin: Comparison with cationic antimicrobial peptides and lipopeptides. *Biochim. Biophys. Acta BBA - Biomembr.* 1758, 1215–1223 (2006).
38. Zhang, L., Rozek, A. & Hancock, R. E. W. Interaction of Cationic Antimicrobial Peptides with Model Membranes. *J. Biol. Chem.* 276, 35714–35722 (2001).
39. DeltaPi - Kibron. Available at: http://www.kibron.com/products/langmuir-tensiometers/deltapi. (Accessed: 2nd November 2016)
40. Haynes, W. M. *CRC Handbook of Chemistry and Physics, 93rd Edition*. (CRC Press, 2016).
41. MacDonald, R. C. & Simon, S. A. Lipid monolayer states and their relationships to bilayers. *Proc. Natl. Acad. Sci.* 84, 4089–4093 (1987).
42. Batoni, G. *et al.* Rational modification of a dendrimeric peptide with antimicrobial activity: consequences on membrane-binding and biological properties. *Amino Acids* 48, 887–900 (2015).
43. Marcellini, L. *et al.* Esculentin-1b(1–18) – a membrane-active antimicrobial peptide that synergizes with antibiotics and modifies the expression level of a limited number of proteins in Escherichia coli. *FEBS J.* 276, 5647–5664 (2009).
44. Coccia, C. *et al.* Membrane interaction and antibacterial properties of two mildly cationic peptide diastereomers, bombinins H2 and H4, isolated from Bombina skin. *Eur. Biophys. J.* 40, 577–588 (2011).
45. Luca, V., Stringaro, A., Colone, M., Pini, A. & Mangoni, M. L. Esculentin(1-21), an amphibian skin membrane-active peptide with potent activity on both planktonic and biofilm cells of the bacterial pathogen Pseudomonas aeruginosa. *Cell. Mol. Life Sci.* 70, 2773–2786 (2013).
46. Mangoni, M. L., Fiocco, D., Mignogna, G., Barra, D. & Simmaco, M. Functional characterisation of the 1–18 fragment of esculentin-1b, an antimicrobial peptide from Rana esculenta. *Peptides* 24, 1771–1777 (2003).
47. Mangoni, M. L. *et al.* Comparative Analysis of the Bactericidal Activities of Amphibian Peptide Analogues against Multidrug-Resistant Nosocomial Bacterial Strains. *Antimicrob. Agents Chemother.* 52, 85–91 (2008).
48. Brancatisano, F. L. *et al.* Inhibitory effect of the human liver-derived antimicrobial peptide hepcidin 20 on biofilms of polysaccharide intercellular adhesin (PIA)-positive and PIA-negative strains of Staphylococcus epidermidis. *Biofouling* 30, 435–446 (2014).
49. Read, J. A. & Duncan, R. Biophysical and functional assays for viral membrane fusion peptides. *Methods* 55, 122–126 (2011).
50. Fujii, G., Horvath, S., Woodward, S., Eiserling, F. & Eisenberg, D. A molecular model for membrane fusion based on solution studies of an amphiphilic peptide from HIV gp41. *Protein Sci.* 1, 1454–1464 (1992).
51. Matsuzaki, K. Magainins as paradigm for the mode of action of pore forming polypeptides. *Biochim. Biophys. Acta BBA - Rev. Biomembr.* 1376, 391–400 (1998).
52. Matsuzaki, K. *et al.* Optical characterization of liposomes by right angle light scattering and turbidity measurement. *Biochim. Biophys. Acta BBA - Biomembr.* 1467, 219–226 (2000).

# 3 Results and Discussion

## 3.1 Effects of the amphipathic profile regularization

The amino acid sequence of the original peptide, SB056, was modified in order to attain a perfect alternation of hydrophobic and hydrophilic/charged residues. This was aimed at obtaining an analogue with an improved amphipathic profile and, in turn, a more regular β-type conformation upon adhesion to the target membrane. The final expectations were an improved peptide/membrane interaction and an enhanced perturbative activity, as it is typically observed for antimicrobial or, more generally speaking, membrane active peptides.[1] The new derivative was named β-SB056, whose modification with respect to the parent peptide simply consisted in the position exchange of the first two residues (Figure 3.1).

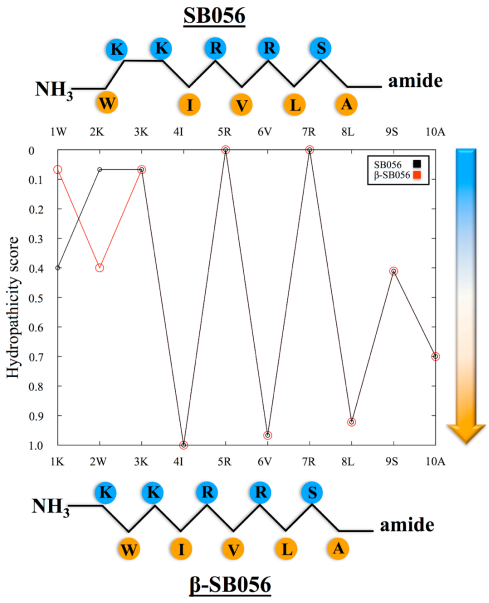


**Figure 3.1.** Hydropathicity plot of both SB056 and β-SB056. Hydrophilic and hydrophobic residues are represented in blue and orange, respectively. The scores were calculated using the method of Kyte and Doolittle[2] with a window of 3 residues and a weight of 30% at the window edges. Values are normalized between 0 and 1: the higher the value, the more hydrophobic the residue. Rearranged from the original reported in ref.[3]

However, most of the rules of thumb on membrane active peptides deduced so far are mainly based upon the numerous studies of helical peptides. Relatively few is known about the structure/function relationship of peptides with β conformations.[1] In addition, dimeric branched peptides, like the ones studied in this work, can exhibit peculiar aspects for which we have no references in the literature. First, a preliminary investigation on the biological activity by our collaborators of both the dendrimeric peptides and their linear counterparts will be presented, which was complemented by qualitative investigation of peptide affinity for differently charged lipid bilayers.[4] Then, the results from complementary biophysical techniques are orderly reported to present the detailed comparison undertaken by focusing on the dendrimeric form of SB056 and β-SB056, in order to clarify the effects of a more regular amphipathic profile for these branched peptides.

### 3.1.1 Linear vs. branched peptides

***Bilayer affinity.*** The dendrimeric architecture is responsible for resistance to proteases degradation, by virtue of steric hindrance that prevents entry into the enzyme active site.[5] This is certainly

desirable since proteases/peptideases severely limit the applicability of linear peptides in-vivo. However, another important drawbacks is represented by the relatively high physiological electrolytes concentration. Usually it is sufficient to dramatically reduce peptide affinity for the lipid membrane, which is purely electrostatics before actual adhesion and represents the very first step of any mechanism of action.[1] In addition, electrostatics is also fundamental for selectivity of cationic peptides. In the case of antimicrobial peptides, for instance, the relatively high content of negatively charged lipids in the bacterial membranes, when compared to the almost zwitterionic membrane of eukaryotic cells, should direct the action of peptides towards the former.

Peptide/membrane affinity can be evaluated by using steady-state fluorescence spectroscopy, and the investigation can be performed in various conditions, like in the presence or in the absence of electrolytes. In the case of the peptides investigated here, the presence of Trp offers the opportunity to use the latter as an intrinsic probe, thus avoiding the insertion of specific fluorophores that might potentially alter peptide's behaviour. When a peptide molecule binds to the surface of a lipid membrane, Trp side chain will tend to insert in the less hydrophilic environment offered by the lipids to avoid contacts with water molecules from the surrounding. This is typically accompanied by a decrease in the emission wavelength and an increase in the quantum yield of Trp emission. The so-called Trp blue shift has been used to asses peptide affinity for membrane mimicking models in numerous investigations.[6,7] Usually, the peptide is titrated with increasing amount of lipid vesicles and Trp emission wavelength ($\lambda$) is monitored. The higher the peptide affinity for the membrane model employed, the lower the [L]/[P] ratio at which the curve reaches saturation ($\Delta\lambda_{max}$). Results are reported in Figure 3.2 for both SB056 and β-SB056, both as dendrimeric and linear peptides. Trp blue shift was monitored in the presence of LUVs prepared with variable molar ratio between zwitterionic (POPC) and negatively charged (POPG) lipids. Experiments were carried out either in PBS buffer (10 mM phosphates + 150 mM NaCl; pH 7.4) and PB (10 mM phosphates; pH 7.4) in order to investigate the role of ionic strength.

In all the cases, peptide affinity increased with increasing the negative charge of vesicles, as expected for highly cationic peptides like the ones investigated (net charge +5 with only 10 residues for the linear analogues, +10 with 21 residues for the dendrimeric ones). It is worth noting how low was the affinity for vesicles prepared with only the zwitterionic POPC (0%PG), recalling one of the most important features for antimicrobial peptides, i.e. selectivity for negatively charged membranes. In the low ionic strength buffer (black curves, figure 3.2), dendrimeric peptides showed higher membrane affinity then their linear analogues, although the difference became less pronounced with increasing membrane charge. SB056 analogues showed a general lower affinity than their corresponding regularized β-derivatives. Differences are less pronounced among the two dendrimeric peptides, while it is particularly remarkable how sequence regularization led to such a significant increase of bilayer affinity in the case of the linear analogues. Indeed, β-SB056-linear showed a remarkable affinity even for the zwitterionic membrane model. These results cannot be explained by taking only electrostatics into consideration, since it has to be recall that formal net charge of the peptide was not modified by amphipathic profile regularization. This observation suggests that other features play a role in the overall peptide-membrane affinity. For instance, regularization of the sequence led to a more regular distribution of charge density along the sequence, but also inherently to a more regular hydrophobic side. It is reasonable to presume that while electrostatic interactions are responsible for recalling peptides from water solution to the vesicle surface, upon adhesion, the charge distribution and the amphipathic profile might control

peptide folding, possible oligomerization and, ultimately, stability of the membrane bound state. Possibly, an extremely regular amphipathicity like in the case of β-SB056-linear makes the bound state stable even in the absence of strong electrostatic interactions.

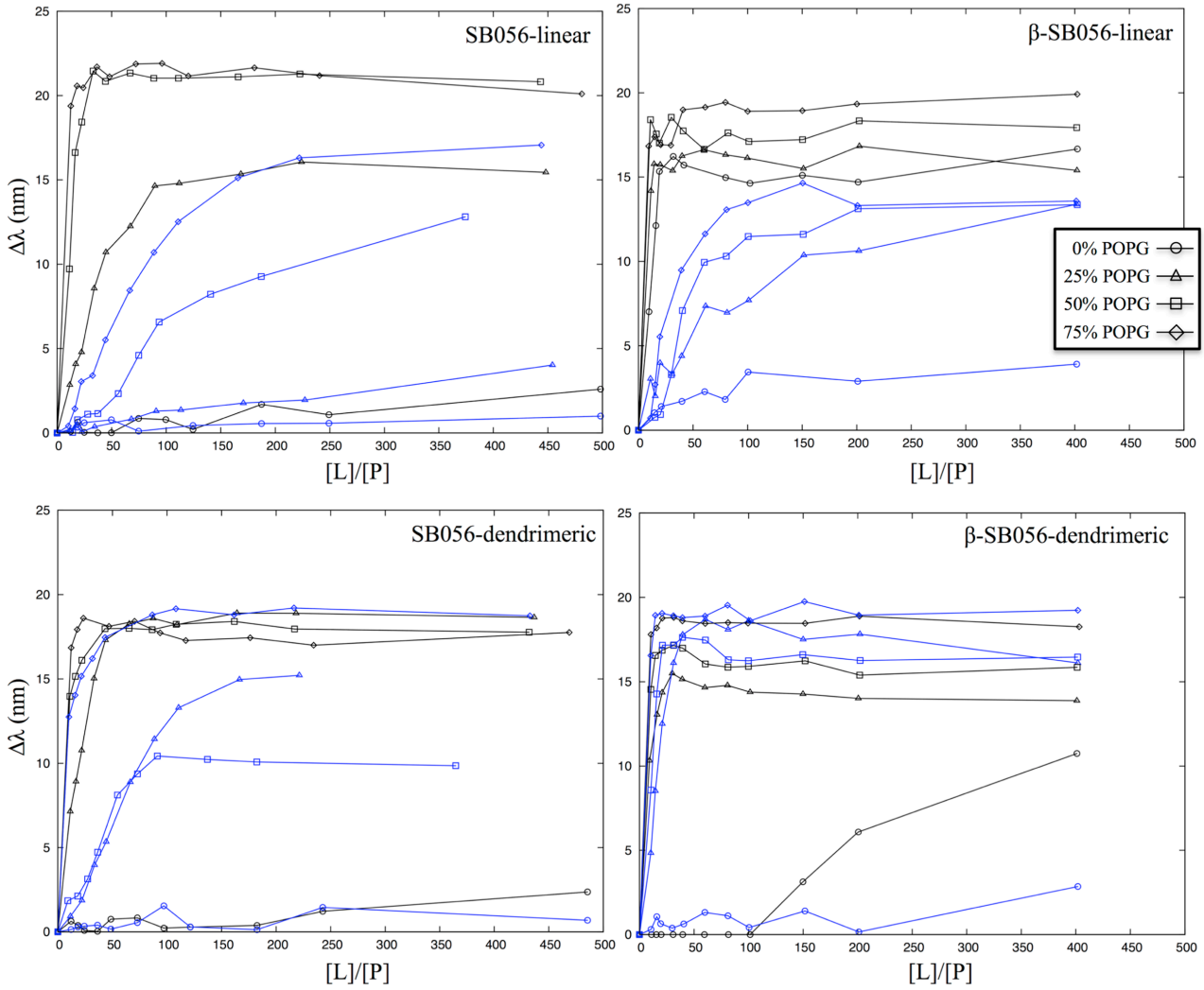


**Figure 3.2.** Peptide-membrane affinity for the four peptide analogues in the presence of differently negatively charged lipid vesicles (different mol% of phosphatidylglycerols). $\Delta\lambda_{max}$ of Trp residues is reported as a function of [L]/[P] ratio. Results obtained in PB and PBS are reported in black and blue, respectively. Image rearranged from the original one reported in ref.[4] Repeatability was 15% (maximum deviation observed over three replicates).

Results obtained in the more physiological PBS buffer (blue curves, figure 3.2) are even more interesting. They clearly show that, while the two linear peptides underwent a dramatic reduction in membrane affinity when ionic strength was increased, the two dendrimeric peptides were able to maintain a significant affinity. In particular, β-SB056-dendrimeric seemed to be almost insensitive to the presence of the electrolytes. Again, these observations cannot be explained only with the long range electrostatics shielding operated by the electrolytes in the medium, neither by invoking the double number of net positive charges of the dendrimeric peptide when compared to its linear analogue. If this was the case, why SB056-dendrimeric suffers from electrolytes addition despite having exactly the same net charge as β-SB056-dendrimeric? In addition, why electrolytes reduce affinity of β-SB056-linear for the purely zwitterionic vesicles? It appeared clear that amphipathic profile regularization favoured the bound state and that, apart from the quite obvious long range

electrostatics shielding effects, short range interactions shall be important for peptide folding, possible oligomerizzation and overall interaction with the lipid bilayer.

***Biological activity.*** The antimicrobial activity of both SB056 and β-SB056 was investigated through the determination of the minimal inhibitory concentration (MIC), minimal bactericidal concentration (MBC), evaluation of biofilm inhibition, and haemolytic activity.[4] This part of the study was performed by our collaborators in Rome (group of Prof. M. L. Mangoni) and Pisa (group of Prof. G. Batoni) and will be here concisely summarized. For the interested reader, full tables and graphics are reported in appendix.

MICs were determined against two representative strains of Gram-negative and Gram-positive bacteria, i.e., *Escherichia coli* (ATCC 25922) and *Staphylococcus aureus* (ATCC 25923), respectively. The assays were performed both in the standard Mueller-Hinton broth (MHB) and in the presence of 150 mM NaCl added to the same broth. Results were in good agreement with the relative affinity for the lipid vesicles through Trp blue shift (§ 3.1.1.1). SB056-linear was the least active peptide tested both against *E. coli* (MIC of 25 in MHB and 100 μM in MHB+NaCl)[4] and *S. aureus* (MIC >100 μM, both in MHB and in MHB+NaCl)[4]. In the standard broth, the activity of the other three peptides was comparable but differences emerged in the "saline" broth. In particular, both β-SB056-linear (MIC of 12.5 μM against *E. coli* and >100 μM for *S. aureus*)[4] and SB056-dendrimeric (MIC of 6.25 μM against *E. coli* and 25 μM for *S. aureus*)[4] showed reduced activity against both strains, while β-SB056-dendrimeric revealed an improved efficacy (MIC of 3.125 μM against *E. coli* and 6.25 μM for *S. aureus*)[4].

MBCs were determined for all of the peptides under investigation. MBC is defined as the minimal peptide concentration that produce a reduction in the number of viable cells $\geq 3$ $\log_{10}$ within 90 min.[8] Linear analogues displayed a bactericidal activity that started at peptide concentrations higher than MIC values, requiring two to four times the MIC to observe 3 $\log_{10}$ reduction in the total amount of living bacteria. Differently, dendrimeric peptides were able to kill 99.9% of bacteria at peptide concentration coincident to the MIC value, with the only exception of SB056 against *S. aureus* for which a two-fold increase in peptide concentration was needed. These results clearly indicate the superior potentiality of dendrimeric analogues, which exhibited a real bactericidal potency compared to the mostly bacteriostatic activity of the linear ones. Finally, the fundamental aspect of cytotoxicity was also investigated in terms of haemolytic activity.[4] The haemolytic activity of the fourth peptides was evaluated using fresh human erythrocytes from healthy donors.

Linear peptides were less haemolytic than dendrimeric peptides at all the concentrations tested, likely because of the double number of bioactive units per molecule, even though there was not a linear dependence. SB056-linear always displayed a smaller % of haemolysis than β-SB056-linear, but the haemolytic character was quite bland even at peptide concentration close to the corresponding MIC values (2% of haemolysis at 25μM for SB056-linear, 6% of haemolysis at 6.25 μM for β-SB056-linear)[4]. The comparison between the two dendrimeric peptides was particularly interesting. At low concentrations, β-SB056 was a little more toxic than SB056, while the latter became more toxic with increasing the concentration. Anyway, also in the case of dendrimeric peptides, the percentage of hemolysis was relative low, ranging between 5 and 20% at peptide concentrations close to the corresponding MIC values for both *E. coli* and *S. aureus*.[4]

Today, microbial adhesion and biofilm formation represent an increasing concern. Bacteria included in a biofilm do not have the same metabolism as the planktonic (i.e. drifting or floating in

the medium) cells and exhibit the same susceptibility to antibiotic agents hardly ever.[4,9] Biofilm resistance to conventional treatments is threatening different fields, such as food industry, both human and animal health-care.[9] The cases where resistant biofilms are found in medical implants are particularly serious, since more and more often the complete removal of the implant is the only option available.[4,10,11] In order to find a possible solution to biofilm resistance, many AMPs were tested and a dedicated database of biofilm-active antimicrobial peptides (BaAMPs, http://www.baamps.it) has been created.[12] Antibiofilm activity was investigated for the four peptides of the SB056 series investigated here,[4] against *Staphylococcus epidermidis* (ATCC 35984) and *Pseudomonas aeruginosa* (ATCC 27853). These particular strains were chosen for their frequent involvement in biofilm-associated infections and for their capacity of producing biofilms.[11] Interestingly, both against biofilm forming bacteria and pre-formed biofilm, the most potent peptide was β-SB056-linear, who was able to cause a reduction in biofilm biomass of approximately 98%.[4] This confirm the best performance obtained by a more regular amphipathic sequence but also how sometimes the best peptide against planktonic bacteria might be ineffective against biofilms, like in the case of β-SB056-dendrimeric.

From these preliminary investigations the advantages of dendrimeric over linear peptides emerged. Apart from known improved resistance to proteases, the branched peptides under investigation showed to maintain activity even in the presence of electrolytes at physiological concentrations. Correspondingly, branched peptides showed to maintain vesicles affinity as reported above (§3.1.1). As discussed, electrostatics alone cannot explain our observations, and the rest of section 3.1 is dedicated to the results from the biophysical techniques we applied in order to characterize the structure/function relationship and the mechanism of this novel class of branched polypeptides. The regularization of the amphipatic profile of these peptides resulted in an improved performance, both in the case of the dendrimeric peptides, against planktonic bacteria, and the linear ones, in the case of biofilms, indicating structural order as one of the important features for this class of peptides.

### 3.1.2 Dendrimeric peptides partition

As mentioned above, the rest of the section 3.1 is focused on the dendrimeric form of the two peptide analogues that will be thus simply referred to as SB056 and β-SB056. In the case of membrane active peptides, whatever mechanism of action is adopted, the very first step is always the electrostatic attraction from the solution bulk onto the target membrane. The ratio between the molar concentration of the peptide in the lipid and the aqueous environment at equilibrium, depends on the stability of the bound state with respect to the fully solvated state. Peptide partition in the conditions of interest (e.g.: lipid composition, temperature, ionic strength, etc.) is a fundamental information needed to perform any other biophysical studies on the same system, in order to know the actual amount of peptide bound/inserted in the given membrane.[13]

Fluorescence spectroscopy is one of the most used spectroscopic techniques for this purpose in the field of membrane active peptides. After peptide-membrane affinity was just qualitatively evaluated through Trp blue-shift (§3.1.1), a step further was taken with a more quantitative determination. The simplest two-states partition model function (equation 1, §2.3.1)[13–15] was fitted to the emission intensity of the Trp residues as a function of the total lipid concentration, from which the peptide partition constant $K_p$ was obtained (see Chapter 2 for details). In Figure 3.3,

results are shown for β-SB056 together with the resulting partition constant in the presence of vesicles with three different lipid compositions. In particular, the zwitterionic POPC and negatively charged POPG were used at different molar ratio.

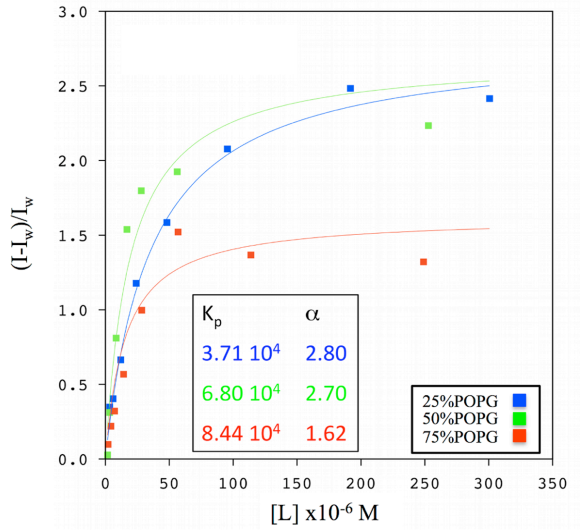


**Figure 3.3.** Partition curves obtained for β-SB056 in the presence of LUVs prepared with different molar ratio of POPC/POPG. Least-squares curve fitting by equation 1 (solid lines) led to the $K_p$ and α values reported in the inset. Repeatability was 15% (maximum deviation observed over three replicates).

All the three titrations resulted in a hyperbolic trend. At low lipid concentrations, Trp intensity is relatively low and close to the value observed in buffer before adding any vesicles. The more the vesicles are available for peptide partitioning, the higher is the molar fraction of peptide (actually, the Trp) in the more hydrophobic environment of the lipid bilayer. In the latter, conversely to what happens in the water environment, Trp exited state is less effectively relaxed by dipolar interactions and this is responsible for (the blue shift and) emission intensity increase. This behaviour is well described in the literature and, in the simplest model applied here, peptide is considered to be distributed between two states only, either water or lipid bilayer phase,[13,16] without taking possible aggregation or different localization in the bilayer into account.

When compared to the values reported in the literature for other peptides, like Omiganan ($1.46 \cdot 10^4$ in 100% POPG)[17], Pep-1 ($3.4 \cdot 10^4$ in 20% POPG)[18] and BP100 ($8.41 \cdot 10^4$ in POPC/POPG 2:1)[19], the partition constant obtained for β-SB056 are remarkably high for all the three membrane compositions investigated. This shows the really high peptide affinity for negatively charged bilayers, which clearly increases with the proportion of negatively charged lipids, as it can be expected for a highly cationic peptide.

For the sake of completion, the peculiar trend of the intensity data obtained in the case of 75% POPG has to be commented. After the usual increase of the emission intensity at low [L], intensity appeared to be levelled off above a certain lipid concentration. A similar behaviour was reported in the literature for other antimicrobial peptides like temporin L and some mutant analogues of nisin,[6,20] which tended to aggregate on top of vesicles with increasing the content of negatively charged lipids. Aggregation, indeed, can generate Trp fluorescence self-quenching as Trp residues on different polypeptide chains can be kept close each other and exchange energy through dipolar interaction. Trp quenching in relatively immobilized aggregates can also be due to flanking positively charged residues,[6] like lysine in the present case. In addition, also the negatively charged headgroups of POPG are able to quench Trp emission,[6] which is of particular importance, of course, in the case of 75%POPG with respect to the other compositions tested in the present study. Previous investigations performed by our research group on the linear analogues revealed the

formation of extended β-sheets on top of highly negatively charged vesicles by the β-SB056 analogue.[3] By analogy, the same can be thus hypothesized for the corresponding dendrimeric peptide.

Partition data for SB056 are shown in Figure 3.4. In this case we limited data acquisition to only two compositions, namely, with low (25%) and high (75%) content of negatively charged POPG. SB056 displayed a non-ideal peptide partition in the buffered vesicles dispersions used here. Curve fitting with equation 1 (§2.3.1) was not feasible and, thus, $K_p$ values could not be determined. For this reason we decided not to acquire the data at 50% POPG.

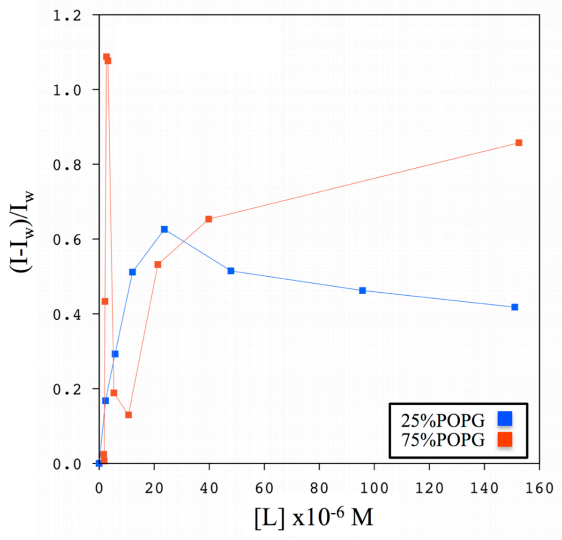


**Figure 3.4.** Partition curves obtained for SB056 in the presence of LUVs prepared with different molar ratio of POPC/POPG. The application of equation 1 was not possible for this peptide in both cases, as it had a non-ideal behaviour. Thus, determination of $K_p$ was not possible. Experimental data points are linked with a solid line just to facilitate their visualization. Repeatability was 15% (maximum deviation observed over three replicates).

First of all, overall fluorescence intensity recorded in both cases for SB056 was always lower than observed for β-SB056, regardless vesicles' composition. Despite an interaction between peptides and vesicles can be surely inferred, the difference of fluorescence at the end of the titration with respect to the water environment (the beginning of the titration) was remarkably low in the cases of SB056. In other words, it seems that Trp environment did not change as much as observed for β-SB056 upon addition of lipid vesicles. This point will be clarified better in the next sections.

The trend followed by data points is clearly different from the cases of β-SB056. As already mentioned, the absence of a hyperbolic trend indicated a non-ideal partitioning and did not allow proceeding with any curve fitting and, thus, partition constant determination. A careful inspection shows that, interestingly, the data obtained at only 25% of POPG have a trend similar to that obtained for β-SB056 as a content of POPG as high as 75% (figure 3.3), although intensity was always lower for SB056. Deviation from ideality became absolutely clear at 75% POPG. On the low [L] side, fluorescence intensity showed a marked sharp peak, seemingly recovering a sort regular trend on the high [L] side (figure 3.4).

A similar behaviour was already observed and reported in the literature by others authors.[17,21] Melo and Castanho reported the case of the cationic antimicrobial peptide omiganan.[17] In most of the cases, at low [L] and in the presence of negatively charged liposomes, they obtained partition curves similar to those reported here for SB056. The effect appeared to depend definitely on electrostatics, because the higher the negative charge of the vesicles, the more marked the deviation from the ideal hyperbolic trend. They proposed an explanation based on membrane saturation. Highly positive peptides can be predicted to have a very high $K_p$ for highly negatively charged bilayers. At low [L], this can give rise to overcrowding of the relatively few vesicles,

generating the anomalous increase in fluorescence intensity.[17] White et al. ascribed this enhancement of fluorescent emission to a cooperative binding phenomena, described as peptide self-association on the vesicles surface leading to the formation of peptide aggregates.[21,22] With increasing [L], a more familiar partition curve is progressively recovered, as a larger number of liposomes are available to accommodate peptide molecules.

These partition studies showed how profoundly different is the behaviour of the two dendrimeric peptide analogues investigated. Despite they just differ for the relative position of the first two residues, their interaction with differently charged bilayer is distinct. The more "regular" β-SB056 exhibited an ideal partition. The interaction with the lipid bilayer increase with increasing the content of negatively charged lipids as one would expect, up to a probable reduction in peptide mobility. On the other hand, SB056, despite bearing the same net positive charge, is intrinsically more disordered and present a certain degree of immobilization already at 25% POPG. The non-ideal partitioning at the highest 75% POPG can be explained with cooperative binding leading to severe aggregation on the bilayer surface.

### 3.1.3 Tryptophan insertion depth

Steady-state fluorescence can also be used to perform Trp fluorescence quenching experiments and gain information about its localization inside the lipid bilayer.[16] Partition studies provided only information about the tendency of the peptides to move from the bulk solution to the vesicles bilayers but any detail about actual depth of penetration was completely lacking. Experiments were performed both in buffer and in the presence of differently charged vesicles. Trp emission intensity was monitored after the addition of both hydrophilic and hydrophobic probes able to quench its emission. In practice, Trp emission is measured as a function of the quencher concentration and the quenching constant ($K_q$) is obtained from linear curve fitting, providing estimation for the quencher ability in the given conditions (see Chapter 2 for details).

First, Trp fluorescence quenching by the hydrophilic acrylamide was measured in PBS without adding vesicles to the solution. Results are reported in table 3.1.

**Table 3.1.** Quenching constants of Trp emission obtained for both SB056 and β-SB056 in PBS by using acrylamide as hydrophilic probe. The value of free Trp amino acid in Tris-HCl at 7.4 pH from the literature[23] is reported for comparison.

| **Peptide** | **$K_q$ ($M^{-1}$)** |
|---|---|
| *SB056* | 0.8 ± 0.1 |
| *β-SB056* | 2.7 ± 0.6 |
| *Free Trp* [23] | 15.8 |
| *Temporin L*[6] | 13.53 |
| *$(KW)_3$* [24] | 15 |

By comparing the $K_q$ values obtained for the two dendrimeric peptides with those for free Trp, Temporin L and $(KW)_3$, the tendency of both peptides to protect Trp residues from the quencher is clear. This can be achieved by the formation of aggregates in solution, where Trp, and probably also other hydrophobic residues, can avoid the contact with water by directing themselves towards the interior of the aggregate.[17] The lower $K_q$ found for SB056 than for β-SB056 suggests that aggregation tendency is higher for the former already in solution. This should be given by the

intrinsically less regular amphipathicity, being this one the only difference between the two analogues, and it is in agreement with the smaller difference between the start and end fluorescence along the partition titration (§3.1.2). When SB056 is in the solution, the environment of its Trp residues is already less hydrophilic than for β-SB056, so that the difference is less upon interacting with the lipid bilayer.

When vesicles were introduced, zero quenching constants were found in all the cases investigated: both peptides, any %POPG and [P]/[L] ratio. This means that Trp residues were not accessible to acrylamide at all, reflecting the high partition constant discussed above and indicating that most peptides (actually, the Trp residues) were "hidden" inside the bilayer. More information about the transverse location of peptide molecules could be obtained by using the spin-labelled phospholipids, 5-NS and 16-NS, described in the methods section. In these lipid probes, the doxyl quenching group is located in definite position along the acyl chain. The closer the Trp to the quenching group, the higher the $K_q$.[16] The 5-NS probe is typically used as a rather superficial one, since its quenching group is located at level of the 5$^{th}$ C atom along the acyl chain. Conversely, the 16-NS can probe deeper insertion into the membrane with the quencher group located at the 16$^{th}$ C atom.[25] However, the two peptides cannot be straightforwardly compared with respect to the $K_q$ obtained for each lipid probe. The different position of the Trp residues along the amino acid sequence, a different folding and/or aggregation state, the different partition, can differently contribute to the quenching efficiency of the probe and erroneously translated into a direct information about their relative depth of penetration inside the bilayer. In order to compare the two peptides, we used two probes indeed, finally comparing the ratio of the $K_q$ obtained with the two ($K_{16\text{-}NS}/K_{5\text{-}NS}$). By this approach, inherent differences should be eliminated, and the relative depth of the two peptides in the same conditions retrieved. Roughly, a value of $K_{16\text{-}NS}/K_{5\text{-}NS}$ close to 1 should be indicative of Trp residues located half a way through the hydrophobic portion of the external leaflet, i.e. half a way between the $C_5$ and $C_{16}$, which is in the region of the $C_{10}$. A value of $K_{16\text{-}NS}/K_{5\text{-}NS} < 1$ corresponds to a superficial localization, closer to the $C_5$. A value of $K_{16\text{-}NS}/K_{5\text{-}NS} > 1$ corresponds to a rather deep localization, closer to the $C_{16}$. In figure 3.5 a schematic representation is reported to graphically summarize the correlation between insertion depth of Trp and different $K_{16\text{-}NS}/K_{5\text{-}NS}$ values.

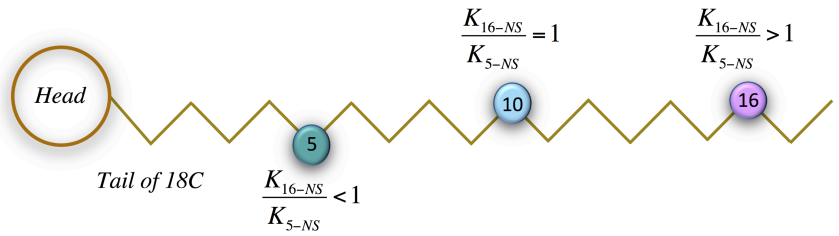


**Figure 3.5.** Schematic representation of a lipid molecule. The numbers along the acyl chain are used to highlight the position of $C_5$, $C_{10}$ and $C_{16}$, respectively. The rough correlation between Trp insertion depth and the $K_{16\text{-}NS}/K_{5\text{-}NS}$ is shown as discussed in the text.

Experiments were performed with two different vesicle compositions, namely 25% POPG and 75% POPG, to compare peptide insertion as a function of the content of negatively charged lipids in the bilayer. Moreover, experiments were performed at two different [P]/[L], in order to investigate possible differences due to amount of peptide bound to the vesicles. Results are presented in table 3.2, but figure 3.6 also illustrates the results for a more clear visualization.

**Table 3.2.** Ratio between quenching constants obtained by using 5-NS and 16-NS lipid probes. Results are shown for both SB056 and β-SB056 peptides in the presence of two different membrane compositions and at two [P]/[L] (low [P]/[L] = 0.003; high [P]/[L] = 0.06).

| Peptide | $K_{16\text{-NS}}/K_{5\text{-NS}}$ | | | |
|---|---|---|---|---|
| | *25%POPG* | | *75%POPG* | |
| | **Low** [P]/[L] | **High** [P]/[L] | **Low** [P]/[L] | **High** [P]/[L] |
| SB056 | 5.8 ± 0.9 | 3.2 ± 1.5 | 0.5 ± 0.2 | 0.5 ± 0.2 |
| β-SB056 | 2.4 ± 0.5 | 1.4 ± 0.4 | 2.6 ± 0.7 | 1.6 ± 0.3 |

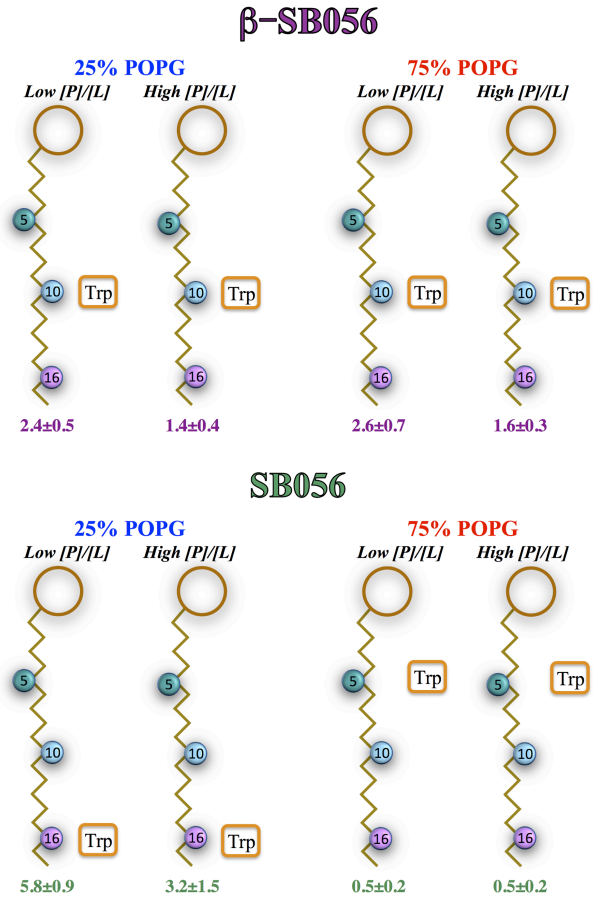


**Figure 3.6.** Schematic representation of the results obtained from Trp quenching experiments with the two lipid probes 5-NS and 16-NS. The same lipid model of figure 3.5 was used. Results are shown for both SB056 and β-SB056 peptides in the presence of two different membrane compositions and at two [P]/[L] (low [P]/[L] = 0.003; high [P]/[L] = 0.06). A label "Trp" is placed next to the $C_5$, $C_{10}$ or $C_{16}$ to indicate its insertion depth in the bilayer as inferred from the measured $K_{16\text{-NS}}/K_{5\text{-NS}}$.

In all the cases, a significantly lower $K_{16\text{-NS}}/K_{5\text{-NS}}$ was found upon increasing the [P]/[L]. The only exception was SB056 in the presence of vesicles with the high proportion of negatively charged lipids (75% POPG). A possible explanation for this general observation is that bilayer is progressively crowded with enhancing [P]/[L], increasing the fraction of aggregates in the membrane with respect to monomers. Whether such aggregates are ordered like in a regular β-sheet or amorphous, the ability to insert within the phospholipids appear to be less from the present data, causing the reduction in the average $K_{16\text{-NS}}/K_{5\text{-NS}}$ resulting from our measurements. SB056 in 75%POPG vesicles showed a very low value already at low [P]/[L] and, in turn, seemed not to be

affected by the increase of the latter. This suggests that 0.5 represents a sort of limit value in our experimental conditions and for the two peptides under investigation, indicative of the outmost localization of the Trp residues. In the case of SB056, this is probably due to the very high tendency for aggregation in high negatively charged vesicles as already suggested by the partition data (§3.1.2), such that further aggregation promoted by the [P]/[L] increase cannot be accompanied by a further reduction of $K_{16\text{-}NS}/K_{5\text{-}NS}$.

SB056 showed also the highest values of $K_{16\text{-}NS}/K_{5\text{-}NS}$ values, i.e. in the case of 25%POPG vesicles. Such high values, when compared to those obtained for β-SB056 in the same conditions, indicated that its Trp residues were able to insert deeper in the bilayer, probably really approaching $C_{16}$ position. Overall, SB056 changed behaviour dramatically as a function of negative lipid content in the vesicles. Conversely, β-SB056 showed a more regular behaviour, apparently not being affected by the electrostatics, in agreement with the almost ideal partition observed despite vesicles %POPG (§3.1.2). In particular, apart from the already mentioned decrease of $K_{16\text{-}NS}/K_{5\text{-}NS}$ with increasing [P]/[L], β-SB056 resulted to be always located (actually its Trp residues) half a way between $C_5$ and $C_{16}$. Thus, also from these quenching experiments, β-SB056 seems to be the "ordered" analogue, characterized by an intrinsically more regular amphipathic profile, which appeared to be reflected by a more regular behaviour both in terms of partition and insertion depth.
In order to confirm 0.5 as the $K_{16\text{-}NS}/K_{5\text{-}NS}$ value reflecting outermost Trp localization, the same measurements were performed for β-SB056 by using vesicles with a POPG/POPC molar ratio of 1:3, which corresponded to 25%POPG as far as the lipid composition was concerned, but also 30% mol/mol of cholesterol was added during vesicles preparation. Cholesterol has the ability to change lipid bilayer packing and permeability,[26,27] by filling the empty spaces naturally created within lipid molecules. In the present case, indeed, the bilayer moved from liquid-disordered to liquid-ordered phase, where lipid molecules have still a comparable lateral diffusivity but a higher order. In the case of vesicles made with POPC and POPG lipids, which have zero spontaneous curvature,[28] a higher later pressure applies in region of the acyl chains than in the region of polar headgroups. This, in turn, is expected to naturally generate "voids" between the latter, where peptide molecules or cholesterol can be accommodated quite easily. When cholesterol fills these spaces, bilayer packing increases and peptide molecules should insert less likely and should be localized more externally. Comparison between results obtained for β-SB056, 25%POPG, low [P]/[L], both with and without cholesterol is reported in figure 3.7.

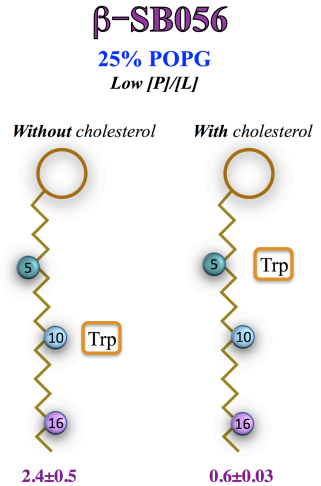


**Figure 3.7.** Comparison between the insertion depth of β-SB056 in the absence and presence of cholesterol in the vesicles. LUVs with 25%POPG were used at low [P]/[L] (i.e. 0.003). A label "Trp" is placed next to the $C_5$, $C_{10}$ or $C_{16}$ to indicate its insertion depth in the bilayer as inferred from the measured $K_{16\text{-}NS}/K_{\text{-}NS}$, which is shown together with the standard deviation.

In the presence of cholesterol a lower value for $K_{16\text{-}NS}/K_{5\text{-}NS}$ was obtained, as expected. In particular, the result was in remarkable agreement with the ones obtained for SB056 in the presence of 75%POPG vesicles (figure 3.6), confirming the above reported interpretation. Value of $K_{16\text{-}NS}/K_{5\text{-}NS}$ as low as ~0.5 correspond to Trp located in the outermost region of the bilayer. This result also indirectly confirm that Trp residues were always significantly more inserted in the case of β-SB056, and located even more deeper in the case of SB056 and 25%POPG. For the sake of clarity, it has to be recalled that the present localization study was performed exploiting Trp fluorescence emission. Therefore, the only direct information available is concerned with Trp insertion depth, while localization of the whole peptide can only be inferred by proceeding through hypotheses.

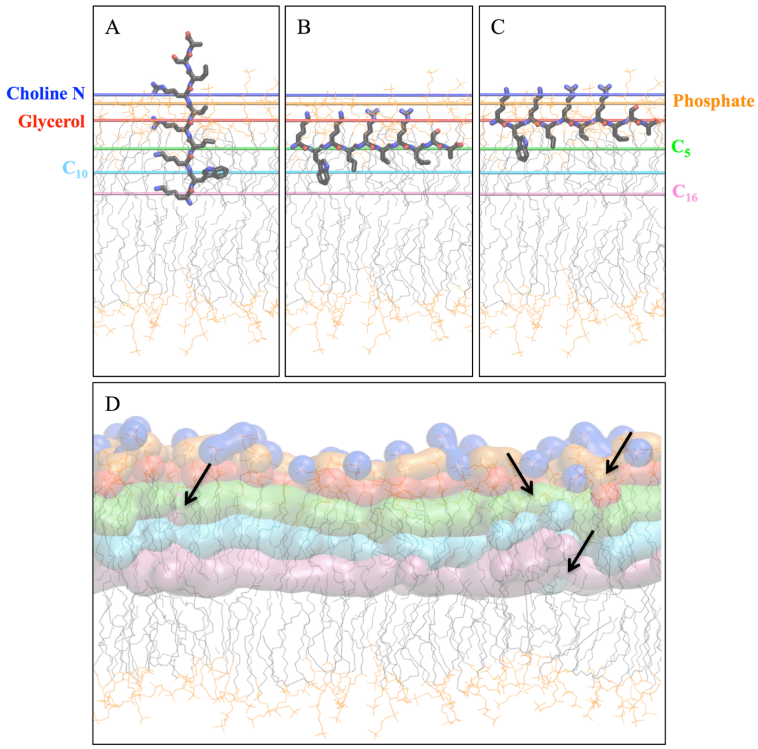


**Figure 3.8.** 3D model of different degree of insertion and orientation for one of the two branches of β-SB056 inside a POPC bilayer (pdb file of all-atom MD equilibrated bilayer was kindly provided by Prof. M. Ceccarelli). In (A-C), the differently coloured lines indicate the average position of the specified atoms or groups across the external leaflet. The same colours are used in (D), where the same atoms/groups are represented as Van der Waals surface. Arrows are used to show local deformations where the depth level between our reference atoms and groups significantly deviate from a simple sandwich model.

A very simple 3D model was built by taking a POPC lipid bilayer and one of the two branches of β-SB056 (figure 3.8). An intermediate value of about 1-2 was obtained for $K_{16\text{-}NS}/K_{5\text{-}NS}$ despite the content of POPG lipids and the [P]/[L] (table 3.2). On the basis of the simplistic assumptions made above, this should correspond to the Trp roughly located at the level of the $10^{th}$ C atom along the lipid acyl chains. In figure 3.8a, the center of mass of Trp indolic group was exactly placed at the level of C10 inside the outer leaflet, than the extreme condition of a completely extended polypeptide backbone oriented perpendicular to the membrane surface was considered. The N-terminus was placed inward on the basis of the results obtained by the research group with NMR experiments performed in the presence of detergent micelles, showing that the linker and the

aminooctanamide tail were completely exposed to the water environment.[29] I am aware that such a perfect vertical insertion is rather unlikely, for a monomeric peptide at least. Positively charged residues should be internalized into the more hydrophobic region of the bilayer and this would be highly thermodynamically unfavourable, unless some sort of oligomeric pore is hypothesized. Nevertheless, this simple model is useful to illustrate some interesting considerations. If we now think about the sequence of one of the SB056 branches placed in exactly the same position as in figure 3.8a, just the fact that Trp would be the first residue of the sequence would localize the center of mass of its indolic group at the level of the C16, like the N-terminal lysine in figure 3.8a. In other words, the higher values of $K_{16\text{-}NS}/K_{5\text{-}NS}$ obtained for SB056 in the presence of 25%POPG vesicles (table 3.2), straightforwardly lead to think that the latter insert deeper than β-SB056 in those conditions. Our simple model shows, conversely, that a higher $K_{16\text{-}NS}/K_{5\text{-}NS}$ might simply reflect the different Trp position along the amino acid sequence, if the peptide is sufficiently tilted in the membrane.

This concept is bolstered by figure 3.8b, when the other extreme orientation is inspected. Here Trp is still located at the level of $C_{10}$, but the backbone is oriented parallel to the bilayer surface. Such orientation is certainly more likely from a thermodynamic point of view, since all the positively charged residues are now embedded within the lipids polar headgroups and, thus, to hydration waters. However, if we now take the position exchange of the first two residues in order to compare the corresponding situation for SB056, it is easy to perceive that a remarkably comparable, if not the same, $K_{16\text{-}NS}/K_{5\text{-}NS}$ should have been found in this case, which is not in agreement with our experimental results. In addition, the position of the C-terminus in figure 3.8b is not compatible with the already mentioned water exposure found by the research group, when NMR was applied to study this peptide in the presence of detergent micelles.[29] Despite the membrane model employed for those experiments is remarkably different from the present one, one would aspect roughly the same behaviour, at least in terms of affinity for the more and less hydrophobic regions of the system.

In conclusion, the $K_{16\text{-}NS}/K_{5\text{-}NS}$ data in the presence of 25%POPG vesicles can be rationalized by a tilted orientation. At low [P]/[L], the mostly monomeric peptides tilt into the external leaflet, inserting the N-terminus down and leaving the linker and the tail mostly exposed to the water. In this orientation, the different $K_{16\text{-}NS}/K_{5\text{-}NS}$ observed for the two analogue peptides depends mostly on the different position of Trp along the sequences. Upon increasing the [P]/[L], more or less ordered aggregates are formed, whose insertion is more hindered by steric reasons and this is reflected by a lower $K_{16\text{-}NS}/K_{5\text{-}NS}$, still indicating a rather deep insertion of Trp residues anyway.

The same model is also valid for β-SB056 in the presence of 75%POPG vesicles, as the same results were obtained at both low and high [P]/[L]. On the other hand, SB056 changed behaviour dramatically as a function of vesicles negative charge. Measurements performed in the presence of cholesterol have shown that the rather low $K_{16\text{-}NS}/K_{5\text{-}NS}$ obtained are strongly indicative of a superficial localization of the peptide. This, together with the above discussed partition data (§3.1.2) bolsters the high tendency to aggregation of SB056, probably disordered, on highly negatively charged bilayers. Following our previous interpretation scheme for the different $K_{16\text{-}NS}/K_{5\text{-}NS}$ values, 0.5 should correspond to the Trp center of mass localized at the level of the 5$^{th}$ C atom along the lipid acyl chains. In figure 3.8c this situation is depicted, with the peptide backbone oriented parallel to the membrane surface. Interestingly, the backbone resulted to be perfectly accommodated between the lipid headgroups, localized at the level of glycerol moiety. Such a

localization would perfectly fit the general picture of an amphiphilic peptide bound to the surface of a lipid bilayer, with all the hydrophobic residues embedded between the lipid chains and the hydrophilic ones between the headgroups and partially exposed to the water molecules from the surrounding solution.

However, for the sake of clarity, it has to be stressed that the values obtained for $K_{16\text{-}NS}/K_{5\text{-}NS}$ should only be used as rough indication of Trp insertion depth. These have to be considered as a way to compare the relative depth of insertion in the different cases, rather than to be used to really quantify the localization inside the bilayer. The considerations made above are certainly useful and help to interpret the data as a first approximation. However, although the quenching group is the same in both the lipid probes we used, they may have a different quenching efficiency due to their localization in inherently different environments. As they are located at rather different depth inside the bilayer, their immediate surrounding is different both in terms of polarity of the nearby groups and density. In other words, our simplistic interpretation of the ratio $K_{16\text{-}NS}/K_{5\text{-}NS}$ may be slightly biased by small but significant differences in the performance of the two lipid quenchers.

Our simple 3D model considers the bilayer as an almost perfectly regular sandwich of different layers, without taking any possible deformation into account. Figure 3.8d, for instance, shows a POPC bilayer where different atoms or groups have been differently coloured and represented as the corresponding Van der Waals surface. Even in this simple example, extracted from an all-atom MD simulation performed in the absence of any peptide (kindly provided by Prof. M. Ceccarelli, Dept. Physics, University of Cagliari, Italy), the bilayer is not perfectly flat and somewhere lipids can significantly bend, generating local situations where the relative depth of the different groups and atoms we used as reference can be not that marked (see the black arrows in figure 3.8d). This can be even more important, of course, depending on the degree of local perturbation generated by the peptides themselves, but, on average, $K_{16\text{-}NS}/K_{5\text{-}NS}$ can still be used as a qualitative parameter to compare the different relative penetration in the various cases investigated. More importantly, we have to consider that the hydrophobic probes we used are actually free fatty acids, not glycerophospholipids. Due to the very small headgroup and its net negative charge, they likely insert less deep than a phospholipid. Indeed, 5-NS is typically taken as a rather superficial probe.[25]

Thus, summarizing our findings so far, β-SB056 showed a rather regular behaviour, in terms of both bilayer partitioning and penetration. Its behaviour does not change with vesicles negative charge. It appeared to insert up to the level of cholesterol in both the bilayer composition tested. By adopting a tilted orientation it insert the most hydrophobic residue, the tryptophan, down into the acyl-chains region of the bilayer ($K_{16\text{-}NS}/K_{5\text{-}NS} \approx 2.5$), but keeping the aminooctanamide tail exposed to the solvent. At low [P]/[L], peptide is expected to be mostly monomeric and makes use of the voids between the lipid headgroups to firmly adhere to the bilayer surface. When it possibly forms some extended aggregates at high [P]/[L], they should be characterized by a certain degree of structural order, as suggested by the almost ideal partition (§3.2.1) and by the only slight decrease of $K_{16\text{-}NS}/K_{5\text{-}NS}$ ($\approx 1.5$), meaning that aggregation does not exclude peptide penetration in this case. β-SB056 appeared to localized almost at the same depth despite the amount of negatively charged lipids in the vesicles and the [P]/[L].

The case of SB056, endowed with a less regular amphipathic profile, is clearly more heterogeneous, as shown by both partition data (§3.2.1) and the present quenching results. Its behaviour is profoundly affected by the electrostatics and tends to disordered cooperative aggregation with increasing the amount of negatively charged lipids in the vesicles. At low [P]/[L]

and low vesicles charge, the insertion depth and orientation are probably comparable to those concluded for β-SB056, making use of the voids between lipid headgroups. When vesicles negative charge is low the peptide seemed to aggregate but only to a moderate extent, such that peptide penetration is not prevented. The higher $K_{16\text{-}NS}/K_{5\text{-}NS}$ values (5.8 and 3.2 at low and high [P]/[L], respectively) are probably simply due to the fact that Trp are the very first residues in this case. However, with increasing vesicles negative charge, cooperative binding increases and leads to aggregation. These aggregates are probably highly disordered and bilayer penetration is prevented ($K_{16\text{-}NS}/K_{5\text{-}NS}$= 0.5) despite the [P]/[L].

### 3.1.4 Vesicles leakage

Fluorescent spectroscopy was also used to study bilayer-perturbing activity of the dendrimeric peptides SB056 and β-SB056. Briefly, a fluorescent dye, calcein, was encapsulated inside vesicles with variable composition (different POPC/POPG molar ratio) so that its fluorescent emission was self-quenched. Upon addition of peptide molecules to the vesicles dispersion, if these are able to perturb the lipid bilayer and impair its permeability, calcein is released and its emission recovered. This type of membrane leakage assay is quite common and widely reported in the literature to retrieve information about peptide membrane-perturbing activity from the kinetics of the fluorescent dye release.[30,31] Details are reported in the methods section. Figure 3.9 shows an example of the kinetics obtained.

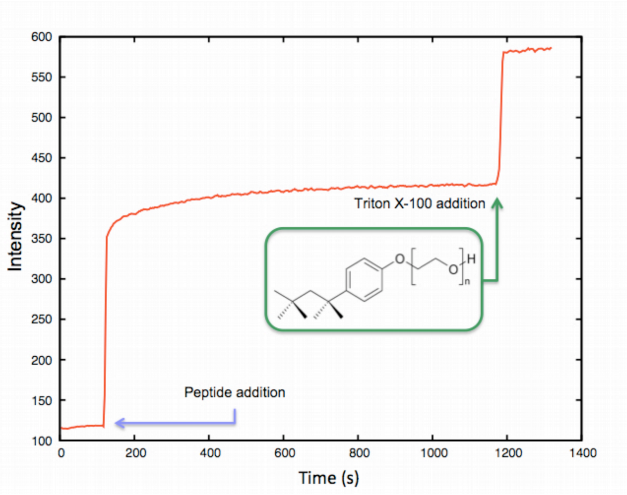


**Figure 3.9.** Example of calcein release curve. After peptide addition (β-SB056 in this case) rapid release of calcein was recorded, followed by equilibrium plateau. Addition of the detergent triton X-100 lead to complete release from all vesicles (100% release level).

Both SB056 and β-SB056 gave similar calcein release kinetics with all the vesicles compositions investigated and regardless of [P]/[L]. After peptide addition, calcein release was rather rapid without any lag phase, up to an equilibrium plateau reached quite fast. Only a single "jump" was observed and a stable equilibrium value was always observed, in contrast to a continuous increase in calcein fluorescence recovery. This observation suggests a very slow, if not absent, exchange of bound peptides among different vesicles.[30] The typically obtained curve (figure 3.9) is significantly different from those reported in the literature for peptides such as esculentin-1b and temporin-L,[30,32,33] whose mechanism of action is widely recognized to be that of pores formation. Conversely, the releases observed in the present work are more compatible with an all-or-none mechanism, on the basis of which peptide molecules induce the targeted vesicle to release all of its content at once, instead of a gradual release that depends on the number of pores or breaks formed from time to time.[34] Similar curves are reported, for instance, for the natural antimicrobial peptide melittin, for

which a model all-or-none was invoked to describe the calcein release kinetics, and a detergent-like mode of action was put forward.[35] For both the dendrimeric peptides under investigation, different vesicles compositions were investigated, and the percentage of calcein release was determined as a function of [P]/[L]. Then, by using the partition constants $K_p$ determined for β-SB056 (in the case of SB056 we simply hypothesized comparable values), the molar ratio between the bound peptide and the total lipid concentration ($[P_l]/[L]$) was calculated and used to report the results (figure 3.10).

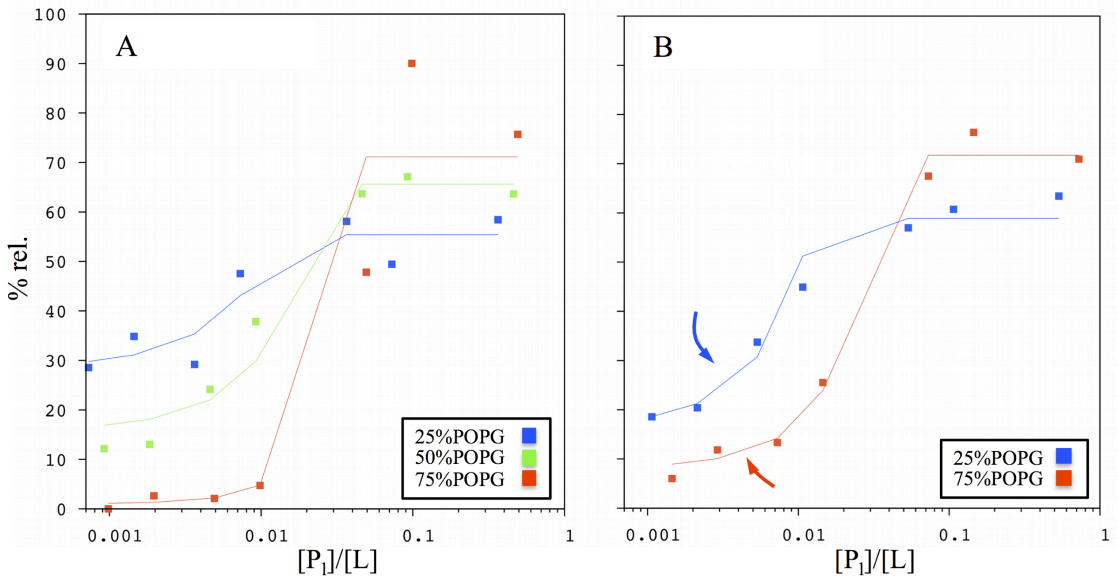


**Figure 3.10.** Calcein release (% rel.) measured for β-SB056 (a) and SB056 (b) is reported as a function of $[P_l]/[L]$, i.e. the ratio between the peptide bound to the vesicles and the total lipid concentration. Experimental data points are shown together with calculated data (lines), as obtained by applying a Monte Carlo least squares fitting procedure of the all-or-none release model described in the methods section. In (b), the blue and red arrows are used to highlight the differences between the curves obtained for SB056 in the presence of the 25% and 75% POPG vesicles when compared to the corresponding ones for β-SB056. Repeatability was 15% (maximum deviation observed over three replicates).

Calcein release data obtained for both the branched peptides share a peculiar trend as a function of vesicles negative charge, depending also on the [P]/[L] regime. At low $[P_l]/[L]$, the release level was rather low anyway, but the higher the amount of negatively charged lipids in the bilayer, the lower the release. On the other hand, the release level increased with the $[P_l]/[L]$ in all the cases but an inversion was observed, i.e. the higher the bilayer negative charge, the higher the release. The present case, again, resulted to be similar to melittin, at least on the low [P]/[L] side. In the case of melittin, indeed, progressive reduction of the release activity was reported as due to excessive amount of negatively charged lipids in the bilayer.[35] In the light of the increase of partition constant as function of the bilayer negative charge, an insufficient peptide affinity for the vesicles could not be invoked like in our case. In the case of melittin, the strong electrostatic interactions between the cationic peptide and the negatively charged lipids were proposed to prevent peptide redistribution in the bilayer, ultimately inhibiting micellization.[35] Our case is certainly different because, although penetration was found to be hindered by vesicle charge for SB056 (§3.1.3), no significant differences were found for β-SB056 at the two vesicles compositions investigated. In addition, differently from melittin, no calcein release was observed from purely zwitterionic POPC vesicles (data not shown), which is compatible with the very low affinity observed for our peptides.[4] The

present case is different also from that of the model β-sheet peptide KIGAKI, for which calcein release was found to increase with the content of negative lipids in the vesicles.[36]

In figure 3.10a, the percentage of release was calculated by applying the all-or-none model reported in detail in the methods section. Briefly, the model involves a threshold concentration of vesicle bound peptide molecules to observe the release of all the calcein content from the vesicle. Such threshold can be different for the various bilayer compositions. A normalized Gaussian distribution is associated to each experimental data point to describe the probability of having a given number of bound peptide molecules per liposome. In practice, $[P_l]/[L]$ is converted into the corresponding ratio between the number of bound peptide molecules and the number of vesicles, i.e. the average number of bound peptides per vesicle. Since peptide partition on vesicles made with only POPC was negligible,[4] in our model no additional peptide molecules bind onto a vesicle whose external leaflet was already saturated by bound peptides. In other words, the number of bound peptide molecules required to neutralize the net negative charge of the vesicle external leaflet was set as the limit value for the position of the Gaussian distribution. The threshold was found to increase with the content of POPG in the vesicles: 1354 for 25%POPG, 2001 for 50%POPG, 3052 for 75%POPG, showing how the perturbing ability of the peptide strongly depends on the electrostatics. Previous MD simulations allowed the estimation of the surface area occupied by a single peptide molecule, about 4 $nm^2$. These simulations were performed on the basis of a NMR study, where detergent micelles were used as membrane mimicking model and the peptide was found to assume a parallel β-hairpin conformation (figure 1.5, §1.5).[29] In the simulations, the peptide backbone was rather extended and the positively charged residues on the two branches tended to maximize their relative distance, such that we considered the value of 4 $nm^2$ as close to the maximum surface area occupied by any our peptides. Then, the same value was applied to calculate the external leaflet area occupied by the peptides at the threshold numbers obtained with our calcein release model. The percentage of surface coverage resulted to be 14%, 21% and 30%, respectively, with increasing the negative charge of the vesicles from 25%, to 50% and finally 75% POPG. It has to be considered that the model we applied to describe the release data involved a distribution of the number of peptides per vesicle, meaning that at the last data points of figure 3.10, when [P]/[L] is high, a significant portion of overcrowded vesicles is taken into account, despite the upper limit imposed to the threshold.

It was shown (§3.1.2) that $K_p$ increases with increasing the negative charge of the membrane model. However, from the present data, it is clear how this is not sufficient to give the same degree of perturbation because of the threshold increase. This results in the behaviour of the peptide being remarkably different at the low [P]/[L], where a significant leakage activity was seen at the 25%POPG, while no release was observed at 75%POPG (figure 3.10a). However, our data show two distinct [P]/[L] regimes, indicating that despite more peptide is needed to perturb the more negatively charged vesicles, when peptide concentration is high enough, the higher electrostatics allows a larger fraction of peptide to bind, resulting in a higher fraction of vesicles going beyond the threshold and release their calcein content. To the best of our knowledge, such an inversion of the release efficiency has never been reported so far, and a different mechanism of action depending on the electrostatics cannot be ruled out on the basis of the present results.

In figure 3.10b, the same release model was applied to SB056, even if it was not possible to estimate the $K_p$ values. We decided to use the ones of β-SB056, and comparable threshold values where obtained after applying the all-or-none model: 1131 for 25%POPG and 2818 for 75%POPG.

Interestingly, while at high [P]/[L] the release data were rather similar for the two peptide analogues, on the other hand, significant differences were observed at low [P]/[L]. At 25%POPG SB056 appeared to be less efficient in perturbing the permeability of the bilayer than β-SB056, the contrary applies to 75%POPG (as indicated by the arrows in figure 3.10b).
It is worth mentioning the case from the literature of an interesting natural peptide that shares some features with the two peptides studied in the present work. Tachyplesin-I is an arginine-rich antimicrobial peptide characterized by a β-hairpin folding, which was isolated from the horseshoe crab *Tachyplesus tridentatus*.[37] Its membrane perturbing activity was related to the in-plane mobility, while the conformation seemed not to correlate with the latter.[37] By comparing different analogues, the authors finally suggested that a more regular β-hairpin conformation was responsible for preventing aggregation and promoting a mostly monomeric behaviour, which would ensure, in turn, high in-plane mobility and, correspondingly, bilayer perturbing efficacy. They concluded that, in general, when extended structures are promoted, peptides lose plasticity and their in-plane mobility, with the final consequence of a drastic change in the peptide mode of action, more similar to the classic carpet model.[38,39]

On these basis, and taking into account all the results collected so far on our peculiar branched peptides, it is possible to put forward that the in-plane mobility model presumably applies in the low [P]/[L] regime. Possibly, mobility is reduced by increasing the electrostatic interaction between peptides and lipids, explaining the reduced leakage observed at 75%POPG. In the case of SB056, which seemingly has a higher tendency to aggregate than β-SB056, even in buffer (§3.1.3), aggregation complicates the scenario. Aggregates are probably less mobile than monomeric peptides but, at the same time, they exert a higher lateral pressure on the phospholipids. This would provide a possible explanation for the lower release observed at 25%POPG than for β-SB056, while higher values were observed at 75%POPG. In the former case, the lose of lateral in-plane mobility makes the difference because a certain proportion of mobile monomers "is lost", due to aggregates formation, while in the latter, the aggregates perturb bilayer packing more efficiently than the low-mobility monomers. Of course, lateral mobility measurements would be needed to prove these hypotheses.

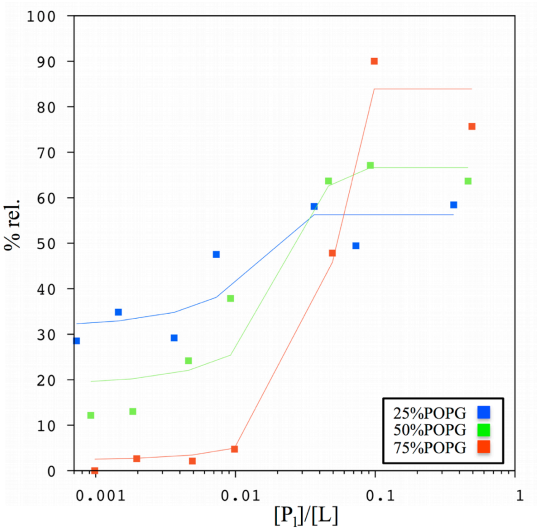


**Figure 3.11.** Calcein release (% rel.) measured for β-SB056 is reported as a function of [P$_l$]/[L]. Experimental data points are shown together with calculated data (lines), as obtained by applying a Monte Carlo least squares fitting procedure of the all-or-none release model reported in the methods section. The experimental data are the same as in figure 3.10a, but the fitting model was applied by considering peptide distribution on both leaflets. Repeatability was 15% (maximum deviation observed over three replicates).

Our data suggested a change in the peptide mechanism upon increasing [P]/[L], since more and more aggregates are probably formed, whether regular or disordered, but increased release are

observed in any case. If a classic carpet model applied, similarly to what was suggested for tachyplesin-I,[37] a redistribution of the peptide among the two leaflets should be considered. Figure 3.11 shows the results obtained for β-SB056 with our calcein release model, when it was applied by taking both leaflets into account to evaluate the electroneutrality point. Comparing the calculated results showed in figure 3.11 to those in figure 3.10a, a slight worsening of the curve fitting on the low [P]/[L] side can be seen, but an improvement on the high [P]/[L] was obtained, especially for the case with the highest %POPG in the vesicles. These results are certainly interesting, even if they cannot be used to prove the actual mode of action of these peptides.

To this end, after pore formation has been ruled out on the basis of the release kinetics (see above), additional calcein leakage experiments were performed for β-SB056 in the presence of vesicles prepared with 100% POPG. Results are shown in figure 3.12 and compared to those obtained at 75%POPG already shown in figure 3.10a and 3.11).

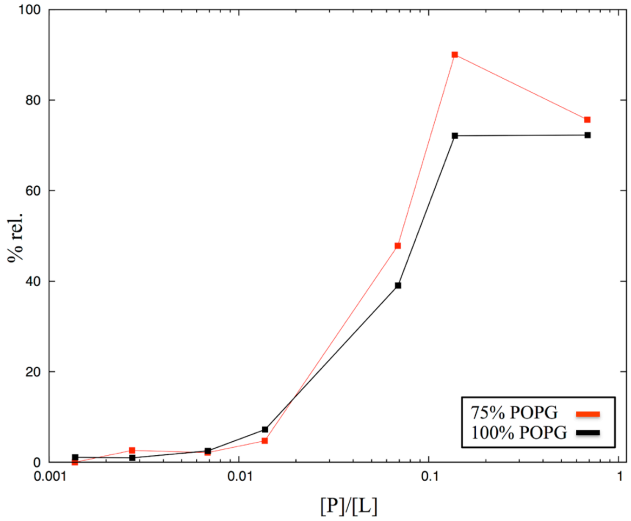


**Figure 3.12.** Calcein release (% rel.) measured for β-SB056 is reported as a function of [P]/[L], i.e. the ratio between the total peptide and total lipid concentration. Solid lines connecting experimental data are not the result of a fitting procedure but they were added only to improve visualization. Repeatability was 15% (maximum deviation observed over three replicates).

Results obtained at 75% and 100% POPG were absolutely comparable, showing no further changes in peptide behaviour with increasing the membrane negative charge beyond 75%. A mechanism of action common to many cationic membrane active peptides is the so-called clustering of anionic lipids. The peptide would attract anionic lipids generating an alteration in the local composition of the bilayer and generating packing defects between different domains.[40] If this was the case of β-SB056, no release had to be expected from 100%POPG vesicles, since anionic lipid clustering would have no effect on a 100% anionic bilayer.[41] Clearly from figure 3.12, this was not the case and, thus, anionic lipid clustering mechanism has been ruled out. In addition, different examples from the literature have shown that peptides acting through this kind of mechanism do not use to induce any vesicle leakage, or the vesicles content release is typically very low,[42] differently from what we observed for the two branched peptides under investigation.

### 3.1.5 Conformation analysis through infrared spectroscopy

Conformation of the two branched peptides SB056 and β-SB056 was performed in comparison with the model peptide KIGAKI[36], which was chosen as reference for extended antiparallel β-sheets.[43] Despite previous NMR/MD investigation had showed that both dendrimeric peptides folded as a twisted β-hairpin in the presence of negatively charged micelles,[29] it was important to extend

conformational analysis. The experimental conditions employed did not allowed to attain information in a more sophisticated membrane model like the vesicles we used in the present work. This was not possible with liquid-state NMR, because LUVs are typically too large for detailed structure determinations. In fact they tumble slowly in solution and cause, in turn, peptide resonances broadening, reducing spectral resolution. Thus, only information about a single peptide monomer are available and, in addition, these were obtained in micelles, whose very high curvature might affect peptide structure. For these reasons, in the present work, we made use of LUVs and infrared spectroscopy in the ATR mode, so to reduce surface curvature of the membrane model and in order to investigate peptide conformation up to high [P]/[L], where probability of forming extended structures is maximized.

Figure 3.13 shows the IR spectra acquired from the samples in the form of rehydrated film (RF), as explained in details in the section of materials and methods. The peptides KIGAKI, β-SB056 and SB056 were analysed in the presence of LUVs with either 25 or 75%POPG. Data are shown for the [P]/[L] 1:20.

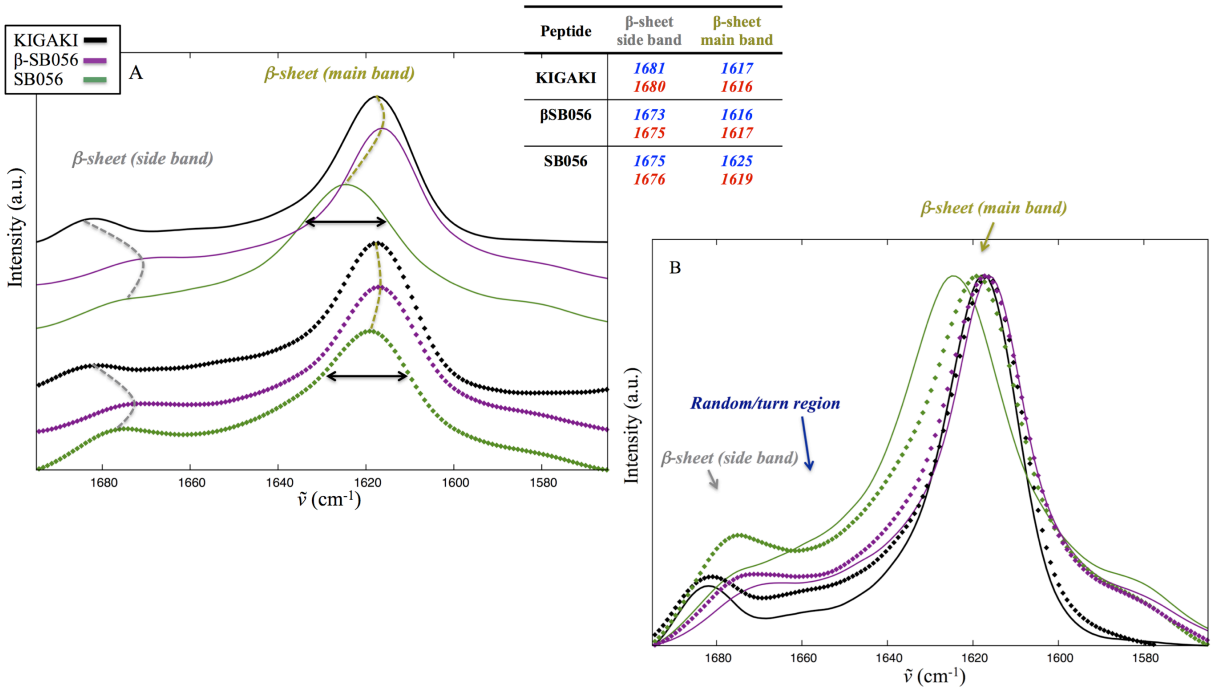


**Figure 3.13.** A) Stacking plot of the normalized amide I band obtained from RF samples of KIGAKI (black), β-SB056 (purple) and SB056 (green). B) Superposition of the same spectral region reported in A. Spectra acquired in the presence of LUVs with 25% and 75% POPG are shown with solid and dotted lines, respectively. The buffer was PBS prepared in $D_2O$. The [P]/[L] ratio was 1:20. The table reports positions of the two components characteristic of β-sheets. Data pertaining at the 25 and 75%POPG are reported in blue and red, respectively.

The amide I band around 1650 $cm^{-1}$, which usually comprised several components, is the most important one for conformational studies. The different secondary structure motif can be correlated to different frequency range within the amide I region. It is indeed particularly sensitive to backbone conformation and rigidity, while it is almost insensitive to the nature of the side chains.[44,45] The spectrum of KIGAKI, as expected, is clearly dominated by the two components due to β-sheets, the most intense one at 1616-1617 $cm^{-1}$ and the so-called secondary component at 1680-1681 $cm^{-1}$. The spectrum obtained in our experimental conditions is in very good agreement

with that reported in the literature by other authors.[36] Similarly, the main and the secondary components typical for β-sheets were identified also for the two branched peptides under investigation, with their wavenumbers within the range reported in the literature.[44–47] However, important differences where found by comparing the model peptide KIGAKI with the two dendrimeric peptides, as well as by comparing the latter.

The main and the secondary component of the KIGAKI amide I band are typical of an antiparallel β-sheet.[46,47] Differently, especially the secondary component of both dendrimeric peptides was found significantly shifted at shorter wavenumbers (1673-1676 $cm^{-1}$), which can be attributed to an higher contribution from parallel β-sheets.[46] This is perfectly reasonable in our opinion because, in spite of a possible antiparallel pairing of different peptide monomers in an extended sheet, the pairing between the two branches of the same peptide has to be parallel, so that the relative content of parallel β-sheet should be 50% at the least.

Despite this similarity shared by the two branched peptides, structural order appeared to be rather different among the two. In particular, β-SB056 show higher order in agreement with all the results reported so far and on the basis of what could be expected from primary sequence regularization. The main component attributed to β-sheets (figure 3.13a) showed both position and width remarkably comparable to KIGAKI, as it can be even more easily seen in figure 3.13b. Band width typically reflects conformational plasticity,[46] indicating that β-SB056 formed ordered β-sheets at both lipid bilayer composition, whether the content of negatively charged lipids were low or high. On the contrary, SB056 showed a significantly different amide I band depending on the membrane model employed. At 25%PG, the main component was found shifted to higher wavenumbers that, despite being still within the range of β-type structures, can be interpreted as due to an increased structural disorder and higher backbone flexibility. This is also bolstered by the higher width of this component.[45,46] Both the shift and the increased width of the main β-sheets component in the case of SB056 is accompanied by an overall increase of the relative intensity in the central portion of the amide I band, as it can be even more easily seen in figure 3.13b. The region between 1660 and 1640 $cm^{-1}$ is usually attributed to turns, loops and random coiled structures,[44,46,47] indicating the higher structural disorder of SB056 once more, when compared to its sequence regularized analogue.

By increasing the amount of negatively charged lipids, an increased structural order was observed for SB056. In particular, the main component shifted to lower wavenumbers and became comparable to that of KIGAKI and β-SB056 (figure 3.13a). However, the level of disorder was higher by the way, as shown by the higher width of the same main β-sheets component and the higher intensity in the central region of the amide I band (figure 3.13b).

Finally, for the sake of completeness, both dendrimeric peptides had a shoulder on the low wavenumbers side of the amide I band (1590-1580 $cm^{-1}$), which was completely absent in the spectra of KIGAKI. This is mostly due to the stretching vibrations of the arginine's guanidine group.[47] This region of the IR spectrum showed no significant difference between SB056 and β-SB056 indeed, as expected from their identical amino acid composition.

Even if ATR-IR spectra acquired from RF samples are usually characterized by a remarkably higher S/N ratio when compared to the corresponding fully hydrated (FH) samples, the former inherently poses concern about possible artefacts induced during the drying stage of the preparation (see material and methods for details). In the particular case under investigation, the fraction of peptides bound on the vesicles surface might increases abnormally upon drying,

exceeding the spontaneous partition between the aqueous and the lipid phase. Such increase in the peptide local concentration on the membrane might force peptides towards self-assembly, possibly giving an overestimated degree of structural order. FH samples are usually more complicated to analyse because of the lower S/N and resolution worsened by broader peaks.[47–49] Nevertheless, they reflect a more physiological condition and the equilibrium partition between the aqueous and the lipid phase, as well as peptide mobility and flexibility. Figure 3.14 shows the IR spectra acquired from the samples in the form of FH samples. The peptides KIGAKI, β-SB056 and SB056 were analysed in the presence of LUVs with either 25 or 75%POPG. Data are shown for the [P]/[L] 1:20.

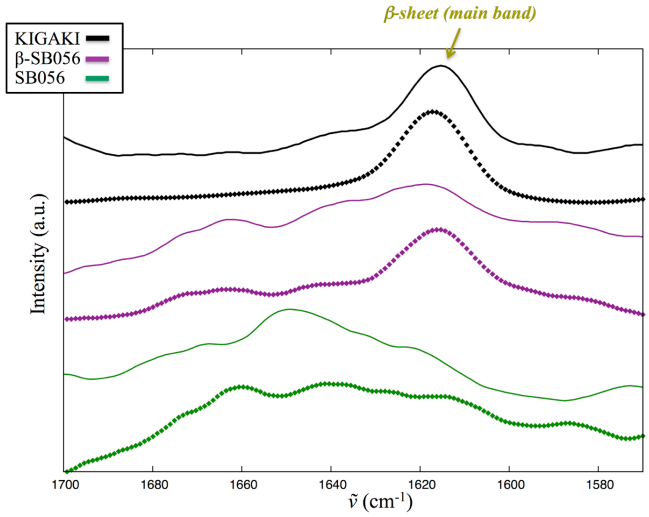


**Figure 3.14**. Stacking plot of the normalized amide I band obtained from FH samples of KIGAKI (black), β-SB056 (purple) and SB056 (green). Spectra acquired in the presence of LUVs with 25% and 75% POPG are shown with solid and dotted lines, respectively. The buffer was PBS prepared in $D_2O$. The [P]/[L] ratio was 1:20.

Despite the overall quality of FH spectra is clearly lower than usually obtained for RF samples, KIGAKI spectra confirm this peptide as a good model for β-sheets in our experimental conditions. The position of the main component of the amide I band and its width are comparable to the results obtained from RF at both vesicles compositions. In addition, a slight intensity decrease was observed in the unstructured region of the amide-I (1660-1640 $cm^{-1}$) when moving from 25% to 75% POPG, showing that the higher the peptide partition in the lipid phase, the higher the ordered peptide fraction. In the case of β-SB056, the degree of structural order is clearly lower but absolutely evident and the effects of peptide partition more pronounced. At 25% POPG, despite the main component attributed to β-sheets is visible below 1620 $cm^{-1}$, together with the putative secondary component below 1680 $cm^{-1}$, the components attributed to turn/loops and coils at about 1660 and 1640 $cm^{-1}$, respectively, are remarkable. On the other hand, the portion of peptides involved in β-sheets significantly increased in the presence of 75% POPG vesicles, with only minor contributions from unordered fractions in the central region of the amide I band. Finally, SB056 was found to be actually only very poorly structured in the presence of both kind of vesicles, as shown by a very broad amide I band characterized by many different components distributed over the whole spectral region.

These results are very important from different perspectives. On the technical side, they clearly showed how RF spectra are able to provide very well resolved spectra but sometimes giving misleading information. Despite the relative ability of the different peptides to fold into ordered structures were the same, RF shall be always be looked carefully and possibly cross-checked with FH spectra. As far as the two peptides under investigation are concerned, these results largely confirm and complement what have been discussed so far on the basis of the different fluorescence

spectroscopy experiments (§3.1.2, 3.1.3 and 3.1.4).

For the sake of completeness, it was also interesting to acquire and inspect the IR spectra of the same peptides in PBS in the absence of any membrane model. Figure 3.15 shows the amide I band spectral region of peptides KIGAKI, β-SB056 and SB056 in PBS.


**Figure 3.15.** Stacking plot of the normalized amide I band obtained from FH samples of KIGAKI (black), β-SB056 (purple) and SB056 (green) in PBS prepared with $D_2O$ ([P] = 2 mM).

The strong tendency of the model peptide KIGAKI to form β-sheets even in the absence of a membrane mimicking model is evident. In agreement with the literature,[43] this peptide was reported to form amyloid-like fibrils already in water. Conversely, both β-SB056 and SB056 spectrum in PBS clearly showed they were completely unordered in solution, indicating that they need a membrane like support to adhere to, pre-organize and oligomerize. The inherently more regular amphipatic profile of the primary sequence of β-SB056 is reflected by a higher tendency to form regular β-sheets. In contrast, SB056 preserve a high level of disorder in spite of the content of negatively charged lipids in the membrane model employed.

### 3.1.6 Surface pressure of lipid monolayers

The mode of action of antimicrobial peptides inherently depends on their ability and kind of interaction with the lipid bilayer, eventually leading to a perturbation of lipid packing.[50] Surface pressure measurements are widely considered a suitable tool for investigating the physical chemistry of lipid monolayers spontaneously formed at the air/water interface, which are comparable, under certain conditions, to the corresponding bilayers.[51] The evolution over time of the surface pressure of a lipid monolayer after peptide addition in the aqueous subphase can provide important information about peptide tendency and ability to adhere and insert through the lipid molecules.[52]

First of all, monolayers formed by the two glycerophospholipids selected in the present work were characterized by recording the π-Γ isotherm of the pure and mixed systems, as described in details in the methods section, where π is the surface pressure, and G is the surface excess of the amphiphiles at the interface. The instrumentation we used was suited to work in the so-called

constant-area mode,[53] i.e. spreading increasing amount of lipids at the air/buffer interface in a constant-area trough. Lipids pack spontaneously and orient with respect to the surface normal in a density dependent fashion. When compared to the more conventional variable-area mode, where a fixed amount of lipids is spread at the interface and an external pressure is applied mechanically, the constant-area mode has the advantage of allowing the study of a monolayer always at equilibrium,[53] but it is hard to be automatized (which was not our case, indeed) and, thus, require quite a lot of time. Figure 3.16 shows a typical π-Γ isotherm obtained with our setup.

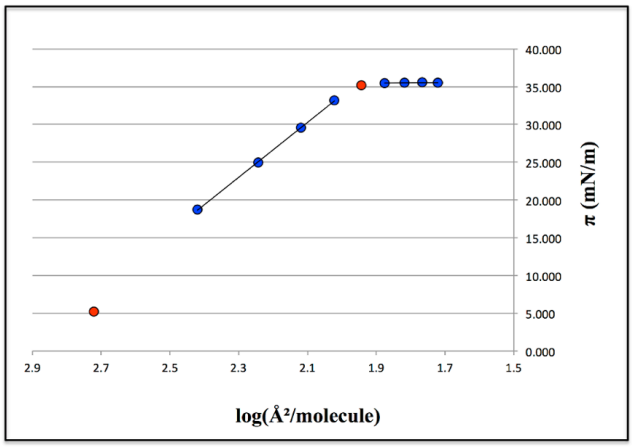


**Figure 3.16.** Example of a π-Γ isotherm (pure POPG in this case). The linear curve-fitting is shown for the region corresponding to the liquid-condensed (L-C) and the saturation (S) phase, respectively. The intersection point gives the area/molecule in a fully packed lipid monolayer.[53] The very first point was not included in the first linear fitting because probably belongs to the liquid-expanded (L-E) phase (see the text). The point located in between the two linear portions of the isotherm was not included in any of the two linear fitting.

The surface area π measured after each lipids addition is reported as a function of moles/area (Γ). Then, it is straightforward to convert this to area per molecule. The experimental π-Γ isotherm showed a typical clear slope change between the so-called liquid-condensed (L-C) and the saturation (S) phase. The two corresponding linear portions of the isotherm share a transition pressure, which is characteristic of the lipid system under investigation. When Γ is very low, the lipids float almost flat at the interface, having an area/molecule available which is significantly larger than molecular size.[53] Lipids start to pack together and eventually flip on one side with progressively increasing Γ. Such monolayer phase is referred to as liquid-expanded (L-E). It is hardly monitored with our setup and it was not of interest for our purposes by the way. Upon further increasing Γ, the monolayer of flipped horizontal lipids passes to the L-C phase. The available area/molecule is progressively reduced and the lipids are forced to flip in order to assume a direction almost perpendicular to the interface, so to accommodate the higher number of molecules within the same space. This packing eventually reaches a saturation point and no further increase of surface pressure is observed with increasing Γ, i.e. the S phase. The lipid molecules are maximally packed and the excess is forced to form aggregates in solution, whose lipids are in exchange equilibrium with the ones present in the interface monolayer.[53] Thus, the transition point between the L-C and S phase allows the estimation of the area/molecule characteristic for the fully packed monolayer under investigation, which is particularly useful to compare monolayers of different composition, or the monolayer stability as a function of different parameters such as pH, ionic strength and temperature.

Results obtained for different mixtures of POPC and POPG are reported in table 3.3. POPC and POPG showed a comparable packing density with the uncertainties of our experimental setup at all the compositions investigated, which is in agreement with their reported ideal miscibility.[54] On average, the results reported in table 3.3 are in agreement with the corresponding data retrieved

from the literature for the two dipalmitoyl analogues, DPPC and DPPG, as well as for the two dimyristoyl ones, DMPC and DMPG. The area/lipid in the S phase is ~85 Å$^2$/molecule.[55] Actually, a lower value can be expected by considering that DPPC/PG have no unsaturated bonds. However, quite surprisingly, we could not find the operative temperature in the work reporting about the dipalmitoyl analogues and, in addition, the authors used the compression method.[56] In the literature, it is reported that acyl chains length often affects packing density more than a single unsaturation. In agreement, the area/lipid in the S phase for DMPC and DMPG was reported to be ~55 Å$^2$/molecule, in experimental conditions similar to ours.[53]

**Table 3.3.** The average area occupied by a lipid molecule in the investigated monolayers (S phase) prepared with different molar ratio of POPC and POPG.

| Lipid composition | Å$^2$/molecule |
|---|---|
| 100% POPC | 73±10 |
| 75%POPC-25%POPG | 78±18 |
| 50%POPC-50%POPG | 75±20 |
| 25%POPC-75%POPG | 81±28 |
| 100%POPG | 80±28 |

This first campaign of characterization was necessary in order to identify the optimal surface pressure regime for the following investigation about peptide insertion capability. The L-E phase is not recommended, since lipid molecules are not packed and peptides can make use of the "free" interface giving an increase in the surface pressure without actually interacting with the lipids. On the contrary, when monolayer surface pressure corresponds to saturation, lipid in the monolayer are in equilibrium with vesicles or other lipid aggregates in solution, meaning that a significant portion of the injected peptides will be potentially "lost" on these aggregates.[53,55] Thus, the initial surface pressure of choice must be within the range corresponding to the L-C phase, where lipids are packed enough to be considered as a real monolayer, but no other aggregates are present in the subphase. For these reasons monolayers were prepared with an initial surface pressure ($\pi_i$) of 25±1 mN/m. After lipid monolayer was prepared with the chosen initial surface pressure and composition, peptide was injected in the subphase at different final concentrations. Peptide interaction with the monolayer and possible intercalation between the lipid molecules causes surface pressure to increase as a function of time, up to an equilibrium final pressure ($\pi_f$). Figure 3.17 shows a typical curve of monolayer surface pressure as a function of time obtained with our setup.

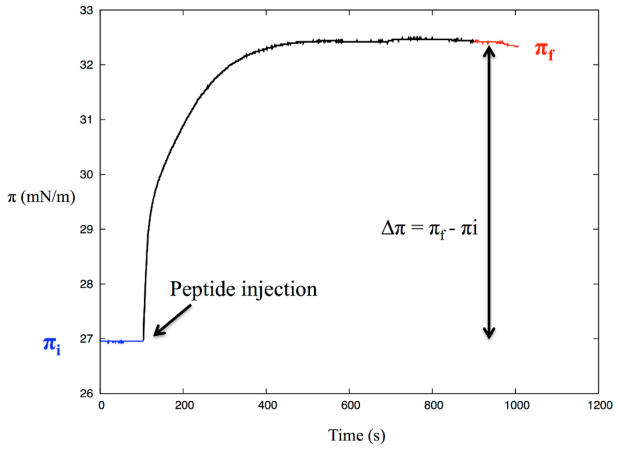


**Figure 3.17.** Typical curve of surface pressure as a function of time obtained after peptide injection in the monolayer subphase (in this case, β-SB056 interacting with 25% POPC / 75% POPG monolayer). The initial surface pressure ($\pi_i$) and the final value ($\pi_f$) are obtained as the average over at least 60 points recorded in the corresponding stationary phase. The difference between final ($\pi_f$) and initial surface pressure ($\pi_i$) is defined as $\Delta\pi$. The black arrow points to the moment of peptide injection.

The difference between final ($\pi_f$) and initial surface pressure ($\pi_i$), calculated as average values over at least 60 points recorded in the corresponding stationary phase of the curve, is defined as $\Delta\pi$. Compared to helical peptides like temporin-L[33] and bombinins,[57] for instance, which are characterized by an extremely fast increase of the surface pressure and also rapid arrival to the final equilibrium, the branched peptides investigated in the present work caused only a moderately rapid increase, reaching the equilibrium rather slowly. This difference suggests a remarkably different behaviour, indicating that our branched peptides change state after binding to the lipid monolayer. In agreement with the results reported so far, an oligomerization process can be put forward. The Gibbs equation (equation 14, §2.3.3) is described in details in the methods section. It was applied to fit the experimental -$\Delta\pi$ values as a function of the logarithm of peptide molar concentration in order to estimate peptide surface excess $\Gamma$. Figure 3.18 shows a typical example.

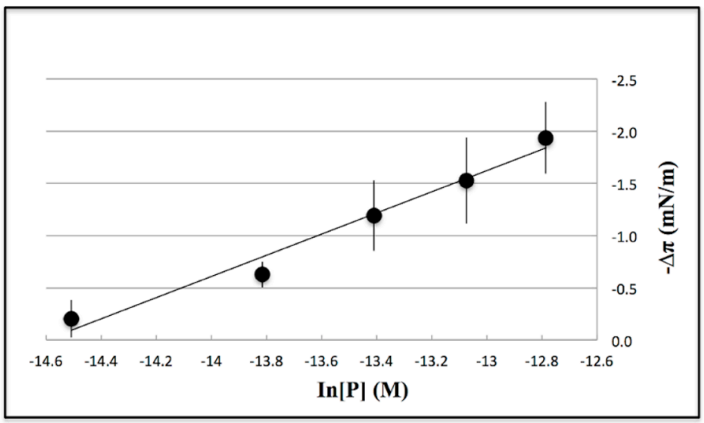


**Figure 3.18.** Application of equation 14 (§2.3.3) to determine peptide surface excess in the presence of a preformed lipid monolayer at the air/buffer interface (in this case, β-SB056 in the presence of a 25% POPG / 75% POPC monolayer). Uncertainty was determined over five replicates.

The surface excess can be easily calculated from the angular coefficient of the straight line fitting the experimental data at the working temperature (300K). Results are obtained as mmol/m$^2$ and then converted to Å$^2$/molecule. Table 3.4 reports all the results for both SB056 and β-SB056 with respect to 25% and 75% POPG monolayers.

**Table 3.4.** Area/molecule and $\Delta\pi$ range for SB056 and β-SB056 with respect to 25% and 75% POPG monolayers.

| **Peptide** | 25% POPG | | 75% POPG | |
|---|---|---|---|---|
| | Å$^2$/molecule | $\Delta\pi$ range (mN/m) | Å$^2$/molecule | $\Delta\pi$ range (mN/m) |
| SB056 | 359 ± 17 | 7.7-9.6 | 202 ± 14 | 6.5-10 |
| β-SB056 | 408 ± 39 | 0.2-1.9 | 270 ± 40 | 3.5-6.4 |

Both peptides showed a decrease of the average area/molecule with increasing the content of negatively charged lipids in the monolayer. This is in perfect agreement with the observation, for β-SB056 at least, that partition constants determined in section 3.1.2 (in LUV dispersions) increased with increasing the lipid bilayer negative charge. In order to accommodate more peptide molecules on the same available area, peptides have to assume a more compact conformation. In the case of

SB056, it was not possible to quantitatively determine the partition constants, but a certain degree of bilayer overcrowding was put forward on the basis of its non-ideal partition curves (§3.1.2), especially at 75%POPG. This is in agreement with the lower values of area/molecule determined by the present surface pressure experiments for SB056 than for its analogue β-SB056, at both 25% and 75%POPG. Finally, it is also very interesting to note that the value of 400 $Å^2$/molecule found for β-SB056 in the presence of 25%POPG monolayer (table 3.4), is in a remarkably good agreement with the value of the monomeric area determined by the research group in a previous combined NMR/MD investigation, where detergent micelles were used as membrane mimicking models. In the MD simulations, the branched peptide lied on the micelle surface by adopting a distorted β-hairpin conformation where the positively charged groups of lysine and arginine residues tented to maximize their relative distance and interacted with the negatively charged groups of the detergent molecules (figure 1.5, §1.5). Thus, while β-SB056 seems to maintain a mostly monomeric behaviour when the content of negatively charged lipids is low, SB056 appeared to aggregate anyway, which is supported by all evidence collected and presented in this manuscript so far.

Also the Δπ values were informative to compare the two peptides. In the literature, for instance, values as high as 10-15 mN/m are reported for helical peptides that exploit an effective insertion through the lipid molecules to form pore-like structures, such as Esculentin-1b,[58] Temporin B and L[59]. In the case of the two branched peptides under investigation, Δπ values were significantly smaller, which is in agreement with the tryptophan fluorescence quenching experiments (§3.1.3) indicating only a superficial insertion. By the way, some differences could be observed among the two analogues. As already mentioned, experimental evidence indicate a mostly monomeric behaviour for β-SB056 in low negative charge lipid layers, where the peptide fits within the void between the headgroups. In section 3.1.3, it was discussed how insertion depth slightly decreased upon increasing the content of negatively charged lipids, so that the observed increase in the Δπ values can only be attributed to the regular β-sheet aggregates formed (§3.1.5), which apply a higher lateral pressure to the lipids. On the other hand, the less regular SB056 was shown to form irregular aggregates, already on low negative charge lipid layers. Indeed, despite penetration depth was likely to be comparable between the two peptide analogues (§3.1.3), Δπ values were significantly larger for SB056 (table 3.4). Finally, with increasing the content of negatively charged lipids, SB056 really overcrowded the lipid layer surface and aggregation is even more pronounced (§3.1.2). The increased size of the aggregates is expected to be accompanied by larger Δπ values, but this was not the case since the increased size of the aggregates was "balanced" by a lower penetration capacity (§3.1.3).

### 3.1.7 Peptide-induced vesicles size variation

In order to gain more information about the mechanism of action for this class of peptides, is was assessed whether they were able to induce any change in vesicles size distribution. Such an effect is expected, for instance, in the case of mechanisms like detergent-like disruption, also referred to as micellization (vesicles size decrease), or vesicles fusion (size increase).[1,60] Vesicles size variation can be monitored with both optical density (OD) measurements and dynamic light scattering (DLS). Figure 3.19 shows results of OD measurements for both β-SB056 and SB056 in the presence vesicles with low (25% POPG) and high (75% POPG) content of negatively charged lipids.

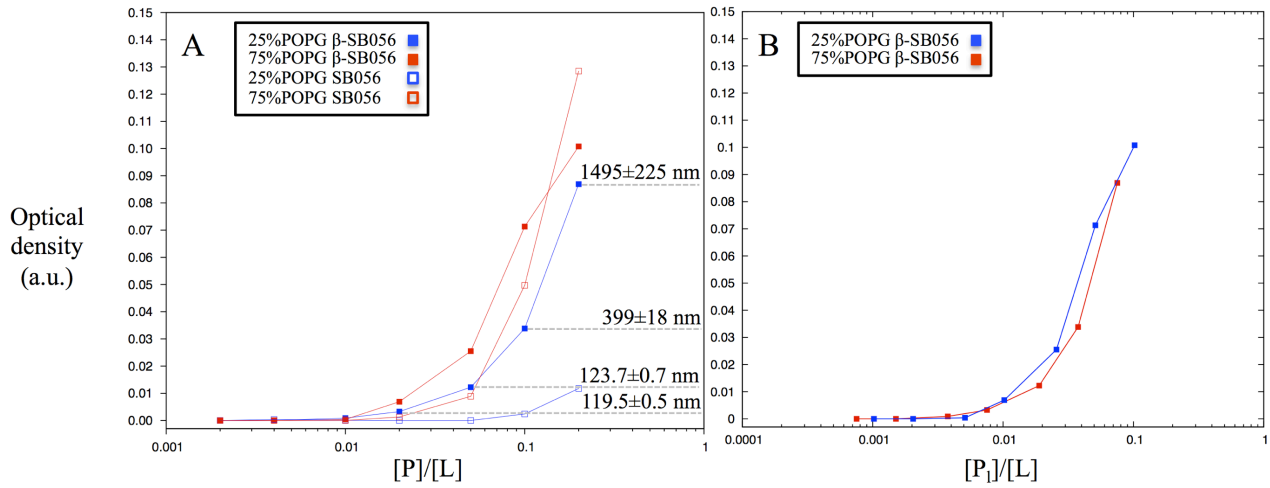


**Figure 3.19.** (a) OD data for both β-SB056 (filled squares) and SB056 (empty squares). Hydrodynamic diameters obtained from DLS in the case of β-SB056 in the presence of 25%POPG LUVs, are indicated together with the standard deviation. (b) Same results shown in panel a for β-SB056 after x-axis was converted into $[P_I]/[L]$. In both panels, results in the presence of LUVs with low (75% POPC / 25%POPG) and high (25% POPC / 75%POPG) content of negatively charged lipids are indicated in blue and red, respectively. Points connecting lines are used only to facilitate visualization. OD data were obtained as average of 10 readings and standard deviation was always ≤ 6%.

A general increase of vesicles size was induced by peptides in all the investigated cases. This is clearly not compatible with a micellization mechanism. Moreover, OD was found to drop down in a ad-hoc experiment performed by adding triton X-100 to LUVs dispersion. This surfactant is known to disrupt lipid vesicles and, indeed, is the same detergent used in calcein leakage assays to provide 100% release level (§3.1.4). Thus, a detergent-like mechanism could be ruled out.

From figure 3.19a, the higher ability of β-SB056 to induce vesicles size increase than its analogue is clear. In both cases, when experimental [P]/[L] is considered, peptides appeared to be more effective when vesicles' negative charge is high. However, neither OD nor DLS measurements are able to discriminate among vesicles active fusion or simple aggregation. If the latter was the only phenomenon responsible for size increase, the curve pertaining to 25% POPG should have started to show aggregation at lower [P]/[L] than the other one, because less peptide would have been needed (even locally) to neutralize vesicles electric charge and promote aggregation. Despite peptide partition constant was taken into account (figure 3.19b), and the actual $[P_I]/[L]$ was used to plot the results, OD curves obtained in the presence of the two different LUV dispersions resulted to superimpose each other, indicating once more that other phenomena than simple aggregation occurred. In addition, it has also to be noted that calcein release curves at 25% and 75% POPG were markedly different (§3.1.4), although the present OD curves showed the same trend. This is probably due to the fact that, as said, OD measurements (as well as DLS size distribution) are not able to discriminate between fusion and aggregation, since particles size increase occurs in both cases. Conversely, calcein release presumably accompanies only peptide-induced membrane fusion.

### 3.1.8 Transmission electron microscopy

In order to shed more light on peptides mode of action, transmission electron microscopy (TEM) images were collected (in collaboration). Investigation of both β-SB056 and SB056 with differently charged vesicles was planned but, unfortunately, due to instrument failure, the experimental

campaign was interrupted and reparation is still on-going. Figure 3.20 shows some images taken from 25% POPG vesicles in the absence and presence of β-SB056 at [P]/[L] 1/100.

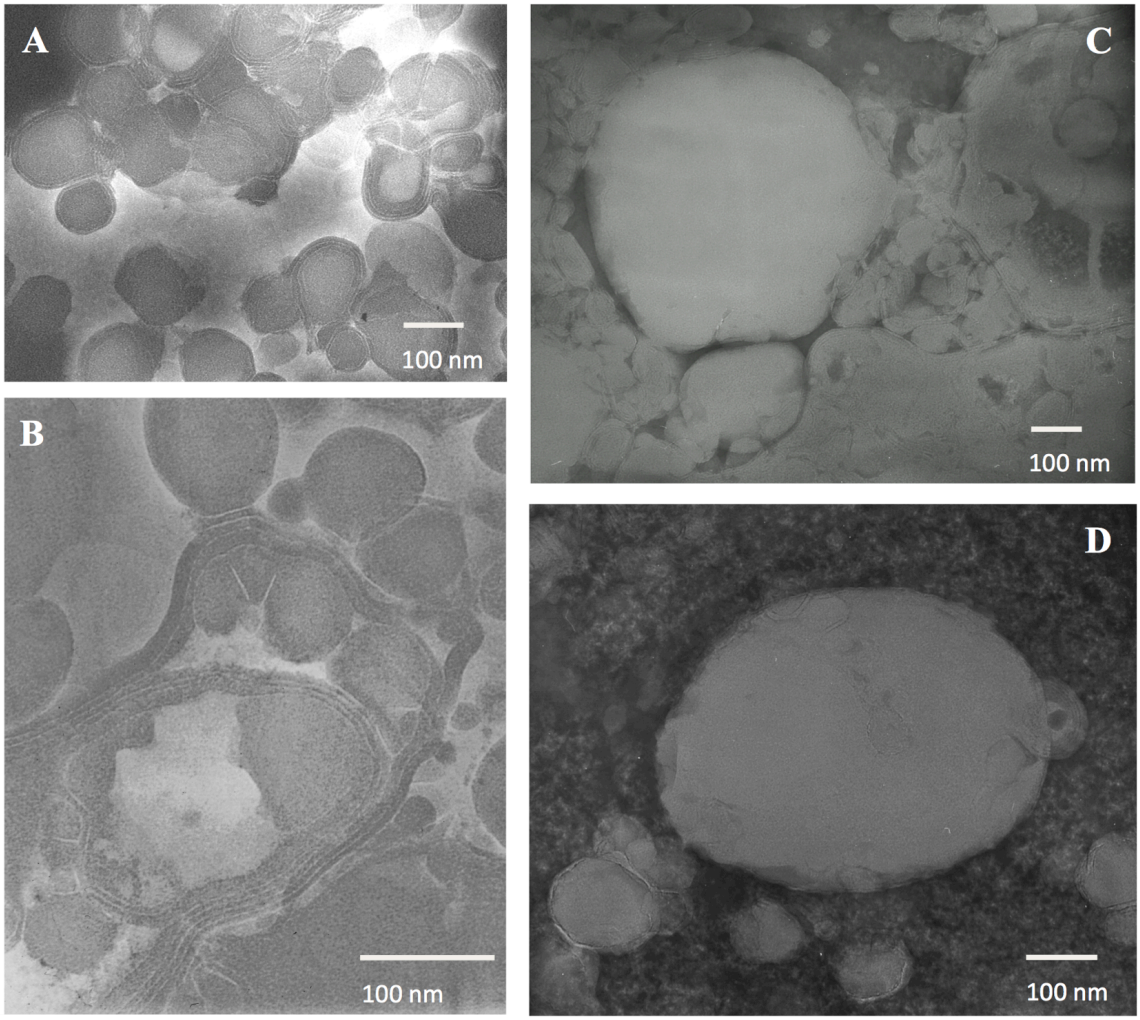


**Figure 3.20.** (A) LUVs (75%POPC / 25%POPG) dispersion in the absence of peptide. (B-D) same as figure A, after incubation with β-SB056 at [P]/[L] of 1:100. TEM images were acquired in the bright-field mode, but figures A and B are the correspondent negatives, for the sake of clarity.

In figure 3.20A, LUVs can be easily identified in the absence of peptide as almost spherical particles with a dark border, which is the phospholipid bilayer. As few as ≤ 3 lamellae were usually observed and size distribution appeared to be quite narrow, around ~100 nm.

After peptide addition (figure 3.20 B-D), size, lamellarity and overall appearance of vesicles were dramatically altered. Although numerous unperturbed vesicles were still visible, extremely long lamellar structures were observed as well. In many cases, these long lipid bilayers were found to incorporate several smaller particles like in figure 3.20B and right side of figure 3.20C. Many spherical vesicles as large as 500-600 nm were also observed. Such particles (figure 3.20 C,D) seemed actually to be formed by fusion of different smaller vesicles. The original lamellae can be still observed, especially on the border of these huge particles where the image contrast is enough.

These images bolster the hypothesis of a fusogenic activity for the investigated dendrimeric peptide. However, for the sake of clarity, the inherent limitations of TEM in this field have to be considered. The sample is deposited on a grid and, thus, it is investigated in a quasi-solid state. Moreover, a staining and protecting agent is required to prevent sample damages under the electron

beam. Last but not the least, several images might not be representative of a complex sample like these as a whole. The results are extremely interesting and encouraging but certainly call for further investigations.

## 3.2 Introduction of an anchoring lipid tail

The regularization of the amphipathic profile led to β-SB056, an analogue of the original SB056 from the Spider Biotech, whose sequence is characterized by perfect alternation of hydrophilic/charged and hydrophobic residues. As discussed in the section 3.1, despite these two peptides differ only for the relative position of the first two residues, the operated amphipathic profile regularization had important consequences. As already reported in the introduction of the present thesis, another important feature of these branched peptides is the presence of an aminooctanamide tail, which was originally designed and introduced with the idea of enhancing peptide interaction with the lipid membrane. However, previous investigations performed by our research group showed that the tail is totally exposed to the aqueous environment,[29] making its actual importance questionable.
For this reason, in the present work we decided to replace it with a more lipophilic tail, a fatty acid like in glycerophospholipids. In the literature, many reports are present where a hydrophobic anchor was introduced in peptide structures to promote membrane binding, sometimes resulting in the alteration of peptide structure and performances.[61–65]

In order to investigate the influence of the tail in the activity of the dendrimeric peptides investigated here, we ordered four new β-SB056 analogues: one analogue without the tail (β-SB056-nt, linker C-term amidated), and three analogues with saturated fatty acid tail of 8, 14 and 18 C atoms (β-SB056-t8, β-SB056-t14, β-SB056-t18), respectively. As reported in the materials and methods section, for synthetic reasons, the introduction of a fatty acid at the linker C-terminus required the addition of one more lysine residue first, whose C-terminus was amidated, and coupling the fatty acid to the ε-amino group of this additional lysine (figure 2.1, §2.1).

### 3.2.1 Biological activity

MIC values were determined (by our collaborators) in the presence of 150 mM of NaCl in the culture broth, against standard bacterial strains, namely, *E. coli* (ATCC 25922), *P. aeruginosa* (ATCC 25923) and *S. aureus* (ATCC 27853), for all the analogues: β-SB056-nt, β-SB056-t8, β-SB056-t14 and β-SB056-t18.

The antimicrobial activity of β-SB056-nt was comparable to that of β-SB056 against all the tested strains. These results clearly bolster our hypothesis of the aminooctanamide tail being not important for peptide activity. Conversely, when the shortest lipophilic tail was introduced in β-SB056-t8, MIC values results as high as 50 mM, and even larger (> 50 mM) for the other two analogues.

Definitely, the introduction of a lipid tail impaired the antimicrobial activity of the analogues, despite the peptide part was identical to the parent β-SB056. Of course, MIC values cannot be taken to infer any molecular level detail, since they reflect a rather complex cell-level response to the peptide action. Nevertheless, some scenarios can be put forward, not necessarily mutually exclusive. The lipid tail could provide the peptide with exaggerated affinity for the outer

membrane, in the case of Gram-negative bacteria, never reaching the plasma membrane. The lipid tail could be an effective anchor in the lipid bilayer, such that a dramatic reduction in peptide mobility could impair its oligomerization or structural rearrangements and, in turn, membrane perturbing activity. Also peptide solubility shouldn't be underrated, which can be reduced by the increased hydrophobicity, ultimately biasing the experimental MIC values. Also, micelles formation cannot be ruled out.

Despite we looked for improved activity analogues, we decided to investigate the molecular reasons for the observed reduction in the activity of the new analogues anyway. Important information can be derived for the future design of additional analogues, and more light might be shaded on the positive characteristics of the parent peptide.

### 3.2.2 Peptide partition between bulk solution and lipid vesicles

Partition studies were performed by following the same approach reported in section 3.1.2. In figure 3.21, results are shown for the four analogues in the presence of vesicles prepared with 25%mol POPG (and 75%mol POPC).

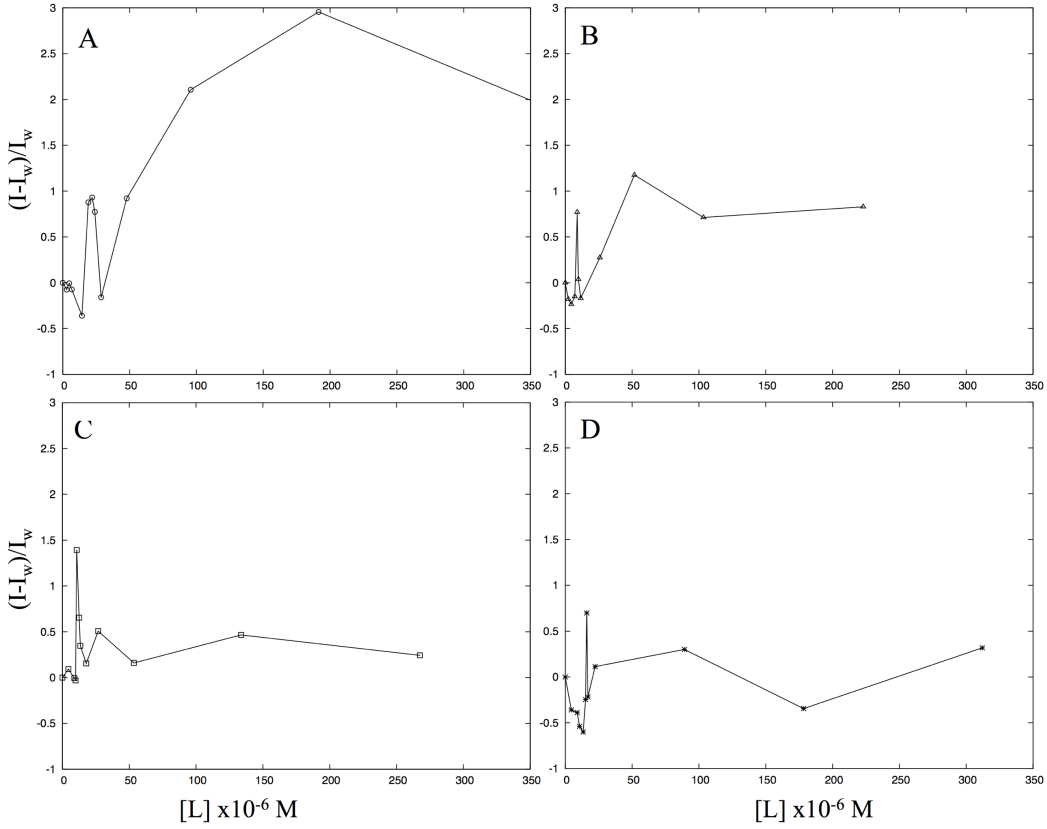


**Figure 3.21.** Partition curves obtained for β-SB056-nt (a), β-SB056-t8 (b), β-SB056-t14 (c) and β-SB056-t18 (d) in the presence of LUVs prepared with 25% POPG. The application of equation 1 was not possible for all these analogues, as they largely deviated from ideal behaviour. Consequently, the determination of $K_p$ was not possible. Experimental data points are linked with a solid line just to facilitate their visualization. Repeatability was 15% (maximum deviation observed over three replicates).

The same two-state partition model[13–15] (equation 1, § 2.3.1.) could not be fitted to the experimental data in these cases. The expected hyperbolic trend for Trp emission intensity as a function of total lipid concentration was clearly not the case, indicating a non-ideal peptide partition between the bulk solution and the vesicles bilayer.[17,21]

Nevertheless, the partition curve of β-SB056-nt (figure 3.21a) shares some features with those obtained for β-SB056 and SB056 (figure 3.3 and 3.4). At high [P]/[L], on the left side of the curve, a clear peak is observed, similarly to SB056 in the presence of vesicles with high content (75%mol) of POPG (figure 3.4). However, differently from SB056, β-SB056-nt showed to recover emission intensity with increasing the lipid concentration, i.e. recovering an almost ideal partition curve and reaching a relative fluorescence level comparable to β-SB056. This kind of partition curve was reported for peptides like omiganan:[17] after an initial fluorescence "spike" due to bilayer overcrowding at low [L], the peptide fully recovered a "normal" fluorescence intensity with the expected hyperbolic trend at high [L].

Overall, the partition curve obtained for β-SB056-nt resembles the one for the parent peptide, but the evident aggregation tendency, already at 25%POPG, with increasing [P]/[L]. The only difference between the two peptides is the tail, thus, the initial spike in the case of β-SB056-nt has to be attributed to the absence of the hydrophilic tail. Interestingly, previous MD simulations of β-SB056 interacting with a mixed micelle composed by 25%mol negatively charged sodium dodecylsulfate and 75%mol dodecylphosphocholine, showed the aminooctanamide tail totally water exposed and highly mobile.[29] Along the MD simulation, the peptide was observed to change conformation after binding on top of the micelle and to finally reach a more stable state. It can be put forward that a water-exposed tail might be helpful for the peptide in finding the right conformation more easily after adhesion on top of the membrane model. In case the adhesion occurred with a non-optimal conformation/orientation, the peptide might be trapped in some local energy minima and not able to escape to a more stable state. Possibly, the hydrophilic flexible tail endowed the peptide with sufficient mobility to change conformation even after adhesion, and finally fold as an ordered β-hairpin conformation. This might explain why, differently from the parent peptide, β-SB056-nt is characterized by a significant propensity to overcrowd the vesicles as soon as the [P]/[L] exceeds a certain limit, as can be observed from its partition curve (figure 3.19). In such conditions, it is plausible that a not perfectly ordered conformation, in terms of regular exposure of hydrophilic residues towards the water/polar headgroups, and hydrophobic residues towards the inner hydrophobic region of the lipid bilayer, might generate cooperative peptide binding leading to unordered aggregates. However, with increasing [L], the peptide local concentration is less and recovery of the ideal partition profile shows that β-SB056-nt has a lower tendency to aggregate than SB056, due to the amino acid sequence regularization.

Partition curve of β-SB056-t8 (figure 3.21b) clearly shows strong deviation from ideal behaviour. It resembles the case of SB056 at 75%POPG (figure 3.4), although β-SB056-t8 showed the same type of partition already at 25%POPG. The "overcrowding peak" is evident and, similarly to SB056, fluorescence intensity was not fully recovered with increasing [L] (figure 3.21b). As discussed throughout section 3.1, in the case of SB056, Trp intensity resulted to be levelled off because of the formation of aggregates already in water, such that Trp residues did not experience a dramatic change of environment polarity upon binding to the vesicles. As shown by quenching experiments with acrylamide (table 3.1), Trp environment was apolar even in the absence of vesicles, and it was similarly apolar in the vesicles bilayer, explaining the small difference between Trp intensity along the partition curve (figure 3.4). Thus, on the basis of the partition curve alone, before collecting more information, we concluded that behaviour of β-SB056-t8 was rather similar to SB056, meaning that despite peptide sequence was regular as in the parent peptide β-SB056,

insertion of lipophilic tail provide the peptide with dramatic structural disorder. In the following sections more details will be presented and the picture will be more comprehensive.

With increasing tail length even further, the situation appeared to be even more problematic. Partition curves obtained for both β-SB056-t14 and β-SB056-t18 show the spike at high [P]/[L], characteristic of vesicle surface overcrowding, but with increasing [L], almost no difference was observed in the Trp fluorescence intensity with respect to the spectrum recorded in the absence of vesicles (figure 3.21c and 3.21d).

In the literature, the interesting case of the helical membrane-active peptide trichogin-GA-IV and its analogues endowed with tails of different length is reported.[63] The authors found a reduction in peptide activity when the chain length was between 10 and 14 C atoms, until almost negligible with 16-18 C atoms.[63] On the basis of complementary biophysical techniques, they proposed peptide self-association as possible explanation.[63]

### 3.2.3 Conformation analysis through infrared spectroscopy

Secondary structure analysis of the analogues with the acyl tails was attempted by using ATR-FTIR spectroscopy, both preparing rehydrated films (RF) and studying the fully hydrated (FH) samples. Unfortunately, we were able to perform the experiments only with β-SB056-t8, i.e. the shortest tail. Despite identical experimental conditions and peptide concentration, signal/noise ratio was very poor in the case of both β-SB056-t14 and β-SB056-t18, such that amide I band was practically not visible. On the other hand, β-SB056-t8 showed S/N comparable to the parent peptide. Our conclusion is that, probably, the two peptides with the long tail were not sufficiently soluble to reach the millimolar concentration range needed for IR spectroscopy. This, together with the biologic activity decrease (§3.2.1), convinced us to leave β-SB056-t14 and β-SB056-t18, and to focus only on β-SB056-t8 in the following investigations.

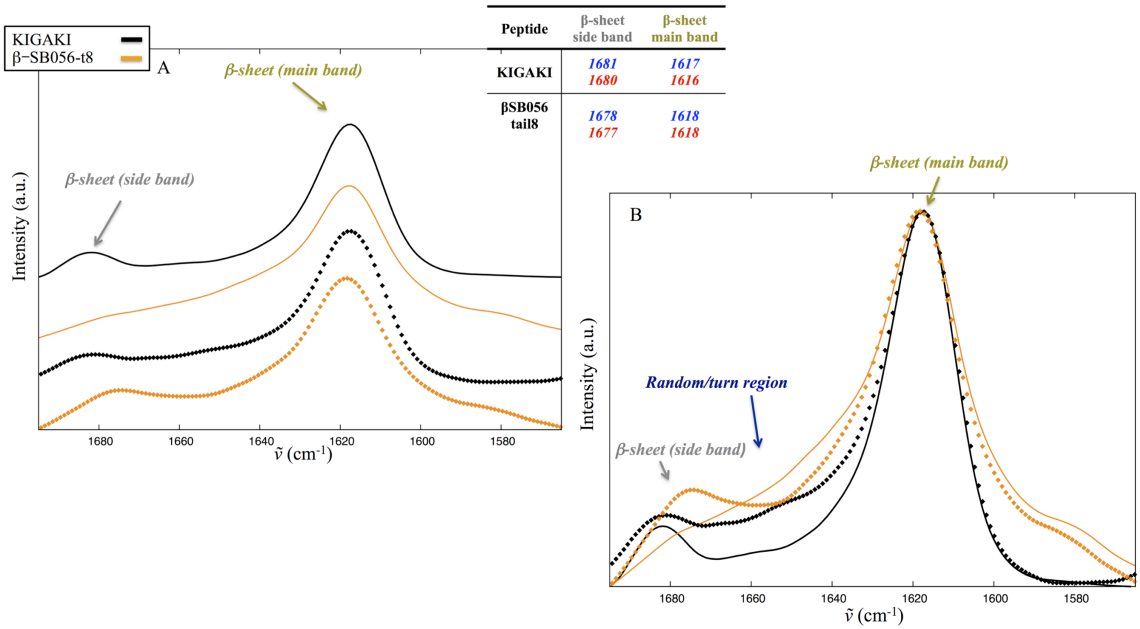


**Figure 3.22.** A) Stacking plot of the normalized amide I band obtained from RF samples of KIGAKI (black) and β-SB056-t8 (orange). B) Superposition of the same spectral region reported in A. Spectra acquired in the presence of LUVs with 25% and 75% POPG are shown with solid and dotted lines, respectively. The buffer was PBS prepared with $D_2O$. The [P]/[L] ratio was 1:20. The table reports positions of the two components characteristic of β-sheets. Data pertaining to 25% and 75% POPG are reported in blue and red, respectively.

Figure 3.22 shows RF spectra acquired in the presence of LUVs with different content of POPG, namely, 25%mol and 75%mol, at a [L]/[P] of 20:1. Results for β-SB056-t8 are compared to those for the peptide KIGAKI, which was chosen as β-sheet peptide model (§3.1.5). Similarly to KIGAKI, as well as to β-SB056 and SB056 (§3.1.5), amide I band of β-SB056-t8 is characterized by a major component at 1618 $cm^{-1}$, which is the typical main band observed for β-sheets in $D_2O$.[46,47] This is usually accompanied by a so-called side-band which results to be located at intermediate wavelength between KIGAKI and the parent peptide β-SB056. Between these two components, we identified two additional contributions to amide I band, namely, turn/loop like conformations at ~1660 $cm^{-1}$ and random coil at ~1640 $cm^{-1}$. In figure 3.22b, the overall contribution of these non-β conformations can be better appreciated. KIGAKI was the peptide with the lowest proportion of such unordered structures. Peptide β-SB056-t8 resulted in between β-SB056 and SB056 (figure 3.13b), the latter being the one with the highest proportion of unordered components in the amide I band. Similarly to the case of the parent peptide, the position of the β-sheet components for β-SB056-t8 did not change with the vesicles negative charge, but they were more prominent with 75%POPG, suggesting a higher degree of structural order. Finally, for the sake of completeness, the shoulder on the lower wavenumber side of amide I, which is absent in the spectra of KIGAKI, is due to stretching vibrations of the arginine's guanidine group.[47]

However, as already discussed in section 3.1.5, it is always advisable to cross-check results by inspecting FH samples, despite the lower S/N. The latter are usually characterized by broader peaks, making spectra analysis more difficult [47–49] but, on the other hand, an abnormal degree of structural order might appear in the RF spectra, due to sample overconcentration during dehydration.[66] Figure 3.23 shows the spectra obtained from FH samples of KIGAKI and β-SB056-t8 in the presence of LUVs with either 25% or 75% POPG, at [L]/[P] 20:1.

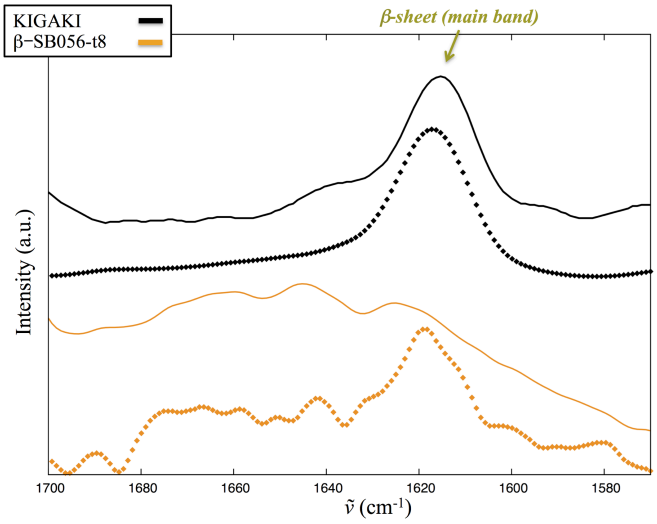


**Figure 3.23.** Stacking plot of the normalized amide I band obtained from FH samples of KIGAKI (black) and β-SB056-t8 (orange). Spectra acquired in the presence of LUVs with 25% and 75% POPG are shown with solid and dotted lines, respectively. The buffer was PBS prepared with $D_2O$. The [P]/[L] ratio was 1:20.

These spectra confirmed the following points: i) similarly to both the parent β-SB056 and SB056, structural order increase with increasing the content of negatively charged lipids in the vesicles; ii) insertion of the lipophilic tail in the peptide structure dramatically reduced the peptide ability to assume regular conformation and, in turn, regular oligomers and, eventually, extended β-sheets. The first point reflects the higher partition constant expected when in presence of vesicles with

higher negative charge. This means a proportionally higher fraction of bound peptides on the vesicles bilayer, thus, higher local concentration and probability to self-assemble into β-sheets. As far as the second point is concerned, the lipophilic tail of β-SB056-t8 is expected to have a high affinity for the hydrophobic core of the lipid bilayer, in contrast to the aminooctanamide tail of the parent peptide, which was found to be hydrophilic.[29] Therefore, the acyl chain of β-SB056-t8 is expected to deeply insert between the lipids in order to avoid contacts with both the solvent molecules and the lipid headgroups, ultimately acting as a strong anchoring element of the dendrimeric architecture. A significant reduction of peptide mobility is possible, impacting peptide ability to rearrange its conformation after binding and adopt an ordered structure. Finally, FH spectra acquired in the absence of vesicles are reported in figure 3.24 for both KIGAKI and β-SB056-t8.

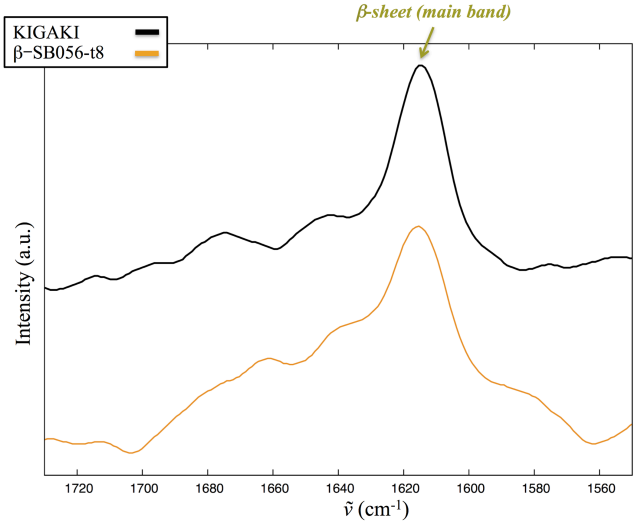


**Figure 3.24.** Stacking plot of the normalized amide I band obtained from FH samples of KIGAKI (black) and β-SB056-t8 (orange) in PBS prepared with $D_2O$ ([P] = 2 mM).

Surprisingly, β-SB056-t8 showed a spectrum comparable to that of KIGAKI, who is known to form amyloid-like fibrils even in the absence of a membrane model.[43] The position of the main component is absolutely comparable, although relative intensity of the unordered components at ca. 1660 and 1640 cm-1 is higher for β-SB056-t8. This result is surprising especially when it is compared to the corresponding spectra acquired for β-SB056 and SB056 (figure 3.15). As typically observed for relatively short peptides in buffer, the latter showed IR spectra indicative of a mostly random coiled conformation. Such a difference with respect to the parent peptide has to be ascribed to the acyl tail. In the absence of any membrane model, it probably promotes peptide self-assembly to escape the solvent, which induces also the peptide branches to organize themselves in a quite ordered aggregate. Further focused investigations would be needed to unveil what kind of aggregates is formed in solution by β-SB056-t8, beyond the aims of the present work.

### 3.2.4 Tryptophan insertion depth

Important information on peptide localization in the vesicles bilayer were obtained for β-SB056-t8 by adopting the same strategy as for β-SB056 and SB056 (§3.1.3). Trp emission intensity was monitored after the addition of either hydrophilic or hydrophobic quenchers. Experiments using acrylamide, a hydrophilic probe, were performed in PBS both in the presence and absence of

differently charged vesicles. In the absence of vesicles, a quenching constant of 3.4±0.1 $M^{-1}$, which is significantly lower than free Trp (15.8 $M^{-1}$)[23] or other reference peptides reported in table 3.1, but higher than obtained for the parent peptide (2.7±0.1 $M^{-1}$). This confirms peptide tendency to form aggregates in solution, but these are characterized by Trp residues being on average more exposed to water than for the parent peptide. This is compatible with the conclusions inferred from the IR analysis (see the previous section). In order to avoid contacts between the solvent and the acyl tail, the peptide portion of the dendrimeric assembly was, in turn, more solvent exposed, as it is seen by Trp that, located on the opposite side of the molecule, resulted more sensible to acrylamide quenching. In the presence of lipid vesicles, the same results obtained for both β-SB056 and SB056 were for β-SB056-t8, i.e Trp residues were not accessible to the hydrophilic acrylamide, confirming peptide partition into the lipid phase. The previously employed spin-labelled phospholipids 5-NS and 16-NS (§3.1.3) were used to gain more information about Trp insertion depth. Results obtained for β-SB056-t8 are shown in figure 3.25.

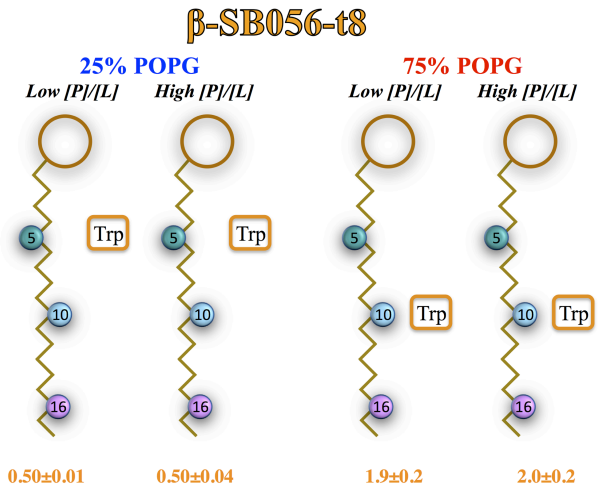


**Figure 3.25.** Schematic representation of the results obtained from Trp quenching experiments with the two lipid probes 5-NS and 16-NS. The same lipid model of figure 3.5 was used. Results for β-SB056-t8 are shown in the presence of LUVs with two different membrane compositions and at two [P]/[L] (low [P]/[L] = 0.003; high [P]/[L] = 0.06). A label "Trp" is placed next to the $C_5$, $C_{10}$ or $C_{16}$ to indicate its insertion depth in the bilayer as inferred from the corresponding $K_{16\text{-NS}}/K_{5\text{-NS}}$ (§3.1.3).

Differently both from β-SB056 and SB056 (figure 3.6), no reduction in $K_{16\text{-NS}}/K_{5\text{-NS}}$ was observed by moving from low to high [P]/[L], indicating that Trp localization did not change upon increasing peptide local concentration. In the case of 25% POPG, Trp residues resulted located absolutely closer to the $C_5$ than to $C_{16}$, as indicated by the $K_{16\text{-NS}}/K_{5\text{-NS}} < 1$. Interestingly, in the case of the parent peptide, a value as low as 0.5 was obtained only in the presence of cholesterol, which was able to hinder peptide insertion between the lipids. This means that in the present case of the analogue β-SB056-t8, despite the peptide sequence is exactly the same, Trp residues are forced to stay in the outermost region of the bilayer. It worth to remind here that, despite the rather simple model we applied to interpret the different values obtained for $K_{16\text{-NS}}/K_{5\text{-NS}}$ (as depicted in figure 3.25, for instance), the hydrophobic probes we used are free fatty acids, not glycerophospholipids. As already discussed in section 3.1.3, 5-NS is typically taken as a rather superficial probe,[26] meaning that actually, in the present case, Trp residues are forced to stay within the headgroups, thus significantly less inserted than observed for the parent peptide. This is absolutely consistent with all of the previous considerations, since the high hydrophobic character of the acyl tail will drive it to insert in the inner core of the bilayer. In turn, Trp residues, which are located exactly on the opposite side of the dendrimeric assembly, could not insert as much as for the parent peptide, which was conversely endowed with a hydrophilic tail. An overall tilted orientation (of the peptide

portion) probably pertains to both parent peptide (§3.1.3) and the acylated analogue, but a sort of competition for insertion emerged from the present study. In the parent peptide, the tail is rather hydrophilic because of the terminal amide group, so that the Trp end of the molecular assembly can insert. On the other hand, in β-SB056-t8, the situation is reversed, the tail is markedly hydrophobic and, thus, inserts deeper than Trp end. No difference of $K_{16\text{-}NS}/K_{5\text{-}NS}$ was observed with increasing [P]/[L], meaning that average Trp insertion depth was not significantly affected by peptide overcrowding, as seen from partition curve (figure 3.21). This would explain also why Trp fluorescence intensity did not change markedly along the partition curve (§3.2.2). A significant change is expected when Trp population progressively moves from the polar aqueous to the unpolar lipid phase, like in the case of β-SB056. However, the results presented so far for the analogue β-SB056-t8 indicated that Trp population moved from the polar aqueous to the polar headgroups region, where dipolar interactions can still effectively relax the excited state.[6]

By increasing the content of negatively charged lipids in the vesicles, electrostatics became more important and the peptide appeared to change localization by moving deeper, despite the highly hydrohobic acyl tail still needed to be accommodated in the bilayer inner core. Quenching constants were similar to those obtained for the parent peptide, β-SB056, suggesting a possible change in the overall peptide orientation. However, it has to be reminded that structural order was only poor and absolutely not comparable to that observed for the parent peptide by IR spectroscopy (figure 3.23 and 3.14, respectively). In conclusion, the behaviour of β-SB056-t8 appeared strongly dependent on the high hydrophobic character of the tail, impairing ideal partition between the aqueous and lipid phase and, in turn, conformational rearrangements needed to assume the order structure promoted by the regular amphipathicity of the peptide portion.

### 3.2.5 Surface pressure of lipid monolayers

In order to complete the investigation on β-SB056-t8, the lipid monolayer technique was employed monitoring variation of surface pressure after peptide injection in the aqueous subphase. Similarly to the parent peptide, a moderately rapid increase of the surface pressure was followed by a rather long phase of final equilibration (figure 3.17). The application of Gibbs equation (equation 14, §2.3.3) to fit experimental $-\Delta\pi$ values as a function of the logarithm of peptide concentration, allowed the estimation of the peptide surface excess $\Gamma$, which was finally converted into area/molecule. Results are 161±5 and 126±5 $Å^2$/molecule in the case of 25% and 75% POPG, respectively. The corresponding range of $\Delta\pi$ was 6-11 and 5-11 mN/m. When these are compared to the results reported hereinbefore for β-SB056 and SB056 (table 3.4), the extremely high tendency for monolayer overcrowding is evident. The values obtained for the area/molecule are exceptionally low with respect to the monomeric β-hairpin value of ~400 $Å^2$/molecule extracted from MD simulations.[29] One may hypothesize a vertical insertion of the peptide between the lipid molecules, but this would be unfavourable from a thermodynamic point of view since positively charged residues should be accommodated within the hydrophobic region. Therefore, it is much more plausible that such low values of area/molecule simply reflect overcrowding of the monolayer, in agreement with the partition curve obtained, at least, for the vesicle with 25% POPG. With respect to both β-SB056 and SB056, the lipophilic tail of β-SB056-t8 is expected to effectively intercalate the lipids, and this is reflected by higher $\Delta\pi$ values.

## References


1. Nguyen, L. T., Haney, E. F. & Vogel, H. J. The expanding scope of antimicrobial peptide structures and their modes of action. Trends Biotechnol. 29, 464–472 (2011).
2. Kyte, J. & Doolittle, R. F. A simple method for displaying the hydropathic character of a protein. J. Mol. Biol. 157, 105–132 (1982).
3. Manzo, G. et al. Enhanced Amphiphilic Profile of a Short β-Stranded Peptide Improves Its Antimicrobial Activity. PLOS ONE 10, e0116379 (2015).
4. Batoni, G. et al. Rational modification of a dendrimeric peptide with antimicrobial activity: consequences on membrane-binding and biological properties. Amino Acids 48, 887–900 (2015).
5. Pini, A. et al. A novel tetrabranched antimicrobial peptide that neutralizes bacterial lipopolysaccharide and prevents septic shock in vivo. FASEB J. 24, 1015–1022 (2010).
6. Zhao, H. & Kinnunen, P. K. J. Binding of the Antimicrobial Peptide Temporin L to Liposomes Assessed by Trp Fluorescence. J. Biol. Chem. 277, 25170–25177 (2002).
7. Christiaens, B. et al. Tryptophan fluorescence study of the interaction of penetratin peptides with model membranes. Eur. J. Biochem. 269, 2918–2926 (2002).
8. Mangoni, M. L. et al. Comparative Analysis of the Bactericidal Activities of Amphibian Peptide Analogues against Multidrug-Resistant Nosocomial Bacterial Strains. Antimicrob. Agents Chemother. 52, 85–91 (2008).
9. Simões, M., Simões, L. C. & Vieira, M. J. A review of current and emergent biofilm control strategies. LWT - Food Sci. Technol. 43, 573–583 (2010).
10. Mah, T.-F. C. & O'Toole, G. A. Mechanisms of biofilm resistance to antimicrobial agents. Trends Microbiol. 9, 34–39 (2001).
11. Percival, S. L., Suleman, L., Vuotto, C. & Donelli, G. Healthcare-associated infections, medical devices and biofilms: risk, tolerance and control. J. Med. Microbiol. 64, 323–334 (2015).
12. Luca, M. D., Maccari, G., Maisetta, G. & Batoni, G. BaAMPs: the database of biofilm-active antimicrobial peptides. Biofouling 31, 193–199 (2015).
13. Santos, N. C., Prieto, M. & Castanho, M. A. R. B. Quantifying molecular partition into model systems of biomembranes: an emphasis on optical spectroscopic methods. Biochim. Biophys. Acta BBA - Biomembr. 1612, 123–135 (2003).
14. Matos, P. M., Franquelim, H. G., Castanho, M. A. R. B. & Santos, N. C. Quantitative assessment of peptide–lipid interactions.: Ubiquitous fluorescence methodologies. Biochim. Biophys. Acta BBA - Biomembr. 1798, 1999–2012 (2010).
15. Santos, N. C., Prieto, M. & Castanho, M. A. R. B. Interaction of the Major Epitope Region of HIV Protein gp41 with Membrane Model Systems. A Fluorescence Spectroscopy Study. Biochemistry 37, 8674–8682 (1998).
16. Loura, L. M. S., de Almeida, R. F. M., Coutinho, A. & Prieto, M. Interaction of peptides with binary phospholipid membranes: application of fluorescence methodologies. Chem. Phys. Lipids 122, 77–96 (2003).
17. Melo, M. N. & Castanho, M. A. R. B. Omiganan interaction with bacterial membranes and cell wall models. Assigning a biological role to saturation. Biochim. Biophys. Acta BBA - Biomembr. 1768, 1277–1290 (2007).
18. Henriques, S. T. & Castanho, M. A. R. B. Environmental factors that enhance the action of the cell penetrating peptide pep-1: A spectroscopic study using lipidic vesicles. Biochim. Biophys. Acta BBA - Biomembr. 1669, 75–86 (2005).
19. Ferre, R. et al. Synergistic Effects of the Membrane Actions of Cecropin-Melittin Antimicrobial Hybrid Peptide BP100. Biophys. J. 96, 1815–1827 (2009).
20. Breukink, E. et al. The Orientation of Nisin in Membranes. Biochemistry 37, 8153–8162 (1998).

21. White, S. H., William C. Wimley, Alexey S. Ladokhin & Kalina Hristova. Protein folding in membranes: determining energetics of peptide-bilayer interactions. Methods Enzymol. 295, 62–87 (1998).
22. Wimley, W. C. et al. Folding of β-sheet membrane proteins: a hydrophobic hexapeptide model1. J. Mol. Biol. 277, 1091–1110 (1998).
23. Moro, F., Goñi, F. M. & Urbaneja, M. A. Fluorescence quenching at interfaces and the permeation of acrylamide and iodide across phospholipid bilayers. FEBS Lett. 330, 129–132 (1993).
24. Gopal, R., Seo, C. H., Song, P. I. & Park, Y. Effect of repetitive lysine–tryptophan motifs on the bactericidal activity of antimicrobial peptides. Amino Acids 44, 645–660 (2012).
25. Franquelim, H. G., Loura, L. M. S., Santos, N. C. & Castanho, M. A. R. B. Sifuvirtide Screens Rigid Membrane Surfaces. Establishment of a Correlation between Efficacy and Membrane Domain Selectivity among HIV Fusion Inhibitor Peptides. J. Am. Chem. Soc. 130, 6215–6223 (2008).
26. Nicol, F., Nir, S. & Szoka, F. C. Effect of cholesterol and charge on pore formation in bilayer vesicles by a pH-sensitive peptide. Biophys. J. 71, 3288–3301 (1996).
27. Aniket Magarkar et al. Cholesterol level affects surface charge of lipid membranes in saline solution. (2014).
28. Strandberg, E., Tiltak, D., Ehni, S., Wadhwani, P. & Ulrich, A. S. Lipid shape is a key factor for membrane interactions of amphipathic helical peptides. Biochim. Biophys. Acta BBA - Biomembr. 1818, 1764–1776 (2012).
29. Manzo, G. et al. The singular behavior of a β-type semi-synthetic two branches polypeptide. Three-dimensional structure and mode of action. Phys Chem Chem Phys (2016). doi:10.1039/C6CP05464A
30. Mazzuca, C. et al. Fluctuations and the Rate-Limiting Step of Peptide-Induced Membrane Leakage. Biophys. J. 99, 1791–1800 (2010).
31. Andrea C. Rinaldi & Andrea Giuliani. Antimicrobial Peptides:methods and protocols. 618, (Methods in molecular biology).
32. Marcellini, L. et al. Esculentin-1b(1–18) – a membrane-active antimicrobial peptide that synergizes with antibiotics and modifies the expression level of a limited number of proteins in Escherichia coli. FEBS J. 276, 5647–5664 (2009).
33. Rinaldi, A. C. et al. Temporin L: antimicrobial, haemolytic and cytotoxic activities, and effects on membrane permeabilization in lipid vesicles. Biochem. J. 368, 91–100 (2002).
34. Gregory, S. M., Cavenaugh, A., Journigan, V., Pokorny, A. & Almeida, P. F. F. A Quantitative Model for the All-or-None Permeabilization of Phospholipid Vesicles by the Antimicrobial Peptide Cecropin A. Biophys. J. 94, 1667–1680 (2008).
35. Benachir, T. & Lafleur, M. Study of vesicle leakage induced by melittin. Biochim. Biophys. Acta BBA - Biomembr. 1235, 452–460 (1995).
36. Blazyk, J. et al. A Novel Linear Amphipathic β-Sheet Cationic Antimicrobial Peptide with Enhanced Selectivity for Bacterial Lipids. J. Biol. Chem. 276, 27899–27906 (2001).
37. Doherty, T., Waring, A. J. & Hong, M. Dynamic Structure of Disulfide-Removed Linear Analogs of Tachyplesin-I in the Lipid Bilayer from Solid-State NMR. Biochemistry 47, 1105–1116 (2008).
38. Strandberg, E. & Ulrich, A. S. NMR methods for studying membrane-active antimicrobial peptides. Concepts Magn. Reson. Part A 23A, 89–120 (2004).
39. Shai, Y. Mechanism of the binding, insertion and destabilization of phospholipid bilayer membranes by α-helical antimicrobial and cell non-selective membrane-lytic peptides. Biochim. Biophys. Acta BBA - Biomembr. 1462, 55–70 (1999).
40. Epand, R. M., Rotem, S., Mor, A., Berno, B. & Epand, R. F. Bacterial Membranes as Predictors of Antimicrobial Potency. J. Am. Chem. Soc. 130, 14346–14352 (2008).

41. Epand, R. M. & Epand, R. F. Bacterial membrane lipids in the action of antimicrobial agents. J. Pept. Sci. 17, 298–305 (2011).
42. Epand, R. M. et al. Lipid clustering by three homologous arginine-rich antimicrobial peptides is insensitive to amino acid arrangement and induced secondary structure. Biochim. Biophys. Acta BBA - Biomembr. 1798, 1272–1280 (2010).
43. Wadhwani, P. et al. Self-Assembly of Flexible β-Strands into Immobile Amyloid-Like β-Sheets in Membranes As Revealed by Solid-State 19F NMR. J. Am. Chem. Soc. 134, 6512–6515 (2012).
44. Haris, P. I. & Chapman, D. The conformational analysis of peptides using fourier transform IR spectroscopy. Biopolymers 37, 251–263 (1995).
45. Hiramatsu, H. & Kitagawa, T. FT-IR approaches on amyloid fibril structure. Biochim. Biophys. Acta BBA - Proteins Proteomics 1753, 100–107 (2005).
46. Barth, A. Infrared spectroscopy of proteins. Biochim. Biophys. Acta BBA - Bioenerg. 1767, 1073–1101 (2007).
47. Tamm, L. K. & Tatulian, S. A. Infrared spectroscopy of proteins and peptides in lipid bilayers. Q. Rev. Biophys. 30, 365–429 (1997).
48. Menikh, A., Saleh, M. T., Gariépy, J. & Boggs, J. M. Orientation in Lipid Bilayers of a Synthetic Peptide Representing the C-Terminus of the A1 Domain of Shiga Toxin. A Polarized ATR-FTIR Study. Biochemistry 36, 15865–15872 (1997).
49. Martin, I., Goormaghtigh, E. & Ruysschaert, J.-M. Attenuated total reflection IR spectroscopy as a tool to investigate the orientation and tertiary structure changes in fusion proteins. Biochim. Biophys. Acta BBA - Biomembr. 1614, 97–103 (2003).
50. Straus, S. K. & Hancock, R. E. W. Mode of action of the new antibiotic for Gram-positive pathogens daptomycin: Comparison with cationic antimicrobial peptides and lipopeptides. Biochim. Biophys. Acta BBA - Biomembr. 1758, 1215–1223 (2006).
51. Maget-Dana, R. The monolayer technique: a potent tool for studying the interfacial properties of antimicrobial and membrane-lytic peptides and their interactions with lipid membranes. Biochim. Biophys. Acta BBA - Biomembr. 1462, 109–140 (1999).
52. Zhang, L., Rozek, A. & Hancock, R. E. W. Interaction of Cationic Antimicrobial Peptides with Model Membranes. J. Biol. Chem. 276, 35714–35722 (2001).
53. MacDonald, R. C. & Simon, S. A. Lipid monolayer states and their relationships to bilayers. Proc. Natl. Acad. Sci. 84, 4089–4093 (1987).
54. Miscibility of Phospholipid Binary Mixtures | Avanti Polar Lipids https://avantilipids.com/tech-support/physical-properties/miscibility/.
55. Marsh, D. Lateral pressure in membranes. Biochim. Biophys. Acta BBA - Rev. Biomembr. 1286, 183–223 (1996).
56. Lad, M. D. et al. Antimicrobial Peptide-Lipid Binding Interactions and Binding Selectivity. Biophys. J. 92, 3575–3586 (2007).
57. Coccia, C. et al. Membrane interaction and antibacterial properties of two mildly cationic peptide diastereomers, bombinins H2 and H4, isolated from Bombina skin. Eur. Biophys. J. 40, 577–588 (2011).
58. Manzo, G. et al. Folded Structure and Insertion Depth of the Frog-Skin Antimicrobial Peptide Esculentin-1b(1–18) in the Presence of Differently Charged Membrane-Mimicking Micelles. J. Nat. Prod. 77, 2410–2417 (2014).
59. Zhao, H., Rinaldi, A. C., Di Giulio, A., Simmaco, M. & Kinnunen, P. K. J. Interactions of the Antimicrobial Peptides Temporins with Model Biomembranes. Comparison of Temporins B and L. Biochemistry 41, 4425–4436 (2002).
60. Henriques, S. T. & Castanho, M. A. R. B. Consequences of Nonlytic Membrane Perturbation to the Translocation of the Cell Penetrating Peptide Pep-1 in Lipidic Vesicles. Biochemistry 43, 9716–9724 (2004).

61. Khandelia, H., Ipsen, J. H. & Mouritsen, O. G. The impact of peptides on lipid membranes. Biochim. Biophys. Acta BBA - Biomembr. 1778, 1528–1536 (2008).
62. Pedersen, T. B., Sabra, M. C., Frokjaer, S., Mouritsen, O. G. & Jørgensen, K. Association of acylated cationic decapeptides with dipalmitoylphosphatidylserine–dipalmitoylphosphatidylcholine lipid membranes. Chem. Phys. Lipids 113, 83–95 (2001).
63. Toniolo, C. et al. Effect of Nα-Acyl Chain Length on the Membrane-Modifying Properties of Synthetic Analogs of the Lipopeptaibol Trichogin GA IV. J. Am. Chem. Soc. 118, 4952–4958 (1996).
64. Mak, P. et al. The increased bactericidal activity of a fatty acid-modified synthetic antimicrobial peptide of human cathepsin G correlates with its enhanced capacity to interact with model membranes. Int. J. Antimicrob. Agents 21, 13–19 (2003).
65. Kurtzhals, P. et al. Albumin binding of insulins acylated with fatty acids: characterization of the ligand-protein interaction and correlation between binding affinity and timing of the insulin effect in vivo. Biochem. J. 312, 725–731 (1995).
66. Jackson, M. & Mantsch, H. H. The Use and Misuse of FTIR Spectroscopy in the Determination of Protein Structure. Crit. Rev. Biochem. Mol. Biol. 30, 95–120 (1995).

# 4. Summary and Conclusions

## 4.1 Main findings

The aim of the present work was the biophysical characterisation of the SB056 peptide family, a new class of short branched polypeptides. By making use of different and complementary techniques, the behaviour of these peptides was investigated in different experimental conditions. Further details about structure-activity relationship were obtained, allowing a deeper comprehension of their mode of action and efficacy in membrane perturbation as due to the peptide part or the tail.

Dendrimeric peptides have shown several advantages over the linear ones with the same amino acid sequence. From the literature, the superior stability to proteases and peptidases degradation was already known. The present work have shown also a higher activity against several bacterial strains together with the characteristic of preserving such activity in the presence of electrolytes at physiological concentrations.[1] From a strictly biophysical point of view, this seems to be due to the maintained affinity for negatively charged lipid bilayers even at relatively high ionic strength[1] (§3.1.1).

Both the linear and the dendrimeric peptides showed β-type folding upon interaction with the membrane models.[2,3] However, structure was found to be more or less ordered, and the behaviour attributable to monomers or aggregates, depending on the environment. In particular, the bilayer (or monlayer) content of negatively charged lipids played major role, depending also on the local (bound) peptide concentration, of course.

The amino acid sequence, in terms of its characteristic alternation of hydrophilic/charged and hydrophobic residues, was found to be fundamental for the peptide to assume a regular β-conformation. With such a conformation, indeed, upon adhesion on top of the membrane, the polar side chains can point to the aqueous phase and the polar outermost region of the membrane, while the apolar ones are embedded into the hydrophobic core. It was striking to see how amphipathic profile regularization, which was obtained by exchanging only the position of the first two residues of the peptide sequence, impacted both structure and general behaviour of these polypeptides. It is worth noting that overall net positive charge was exactly the same, so that it can't be invoked to explain the observed differences.
In particular, both fluorescence (§3.1.2) and infrared spectroscopy (§3.1.5) showed that β-SB056, which is endowed with the regular amphipathic profile, had a regular and ordered behaviour. Both at low and high [P]/[L], neither membrane overcrowding nor amorphous aggregation was observed, but regular extended β-sheets were formed with progressively increasing peptide bound concentration. Also surface pressure measurements bolstered these findings, with peptide surface excess showing no monolayer overcrowding.

Conversely, the former analogue SB056 was shown to be more prone to form amorphous aggregates, both in solution and especially on top of the lipid membrane models. The expression 'amorphous aggregates' is here used to indicate those peptide aggregates due to self-assembly without structure order. In particular, partition curves obtained from Trp fluorescence (§3.1.2) were clearly far from the ideal hyperbolic trend predicted by the model equations. Peptide insertion depth (§3.1.3) into the lipid bilayer was found to change dramatically with increasing the proportion of negatively charged

lipids, clearly showing peptide inability to penetrate with increasing local peptide concentration and, presumably, aggregates size. Finally, surface excess values evaluated from surface pressure measurements were overly high, when compared to those found for β-SB056.

Both branched peptides share the same octanamide tail, which was originally designed by Spider Biotech to improve membrane affinity. Probably due to synthesis procedures, together with both economic reasons and availability of the starting materials on the market, the tail resulted with a terminal amide group. From the very beginning of the collaboration with our research group, the actual role as an anchoring tail was questioned, despite evidences of better antimicrobial activity with respect to other analogues (as assessed during the starting design stage by the SB company). The amide group is clearly polar and capable of forming H-bonds, thus, it was not surprising to find the tail not inserting in the membrane models.[3] Interestingly, by removing the tail from the regularized analogue, β-SB056, the tendency to amorphous aggregation appeared with increasing membrane bound peptide concentration (§3.2.2).

This clearly suggested that a not-anchoring tail was able to impact structure order somehow. On the basis of previous NMR/MD investigations,[3] the tail was found exposed to the solvent and highly dynamic, providing the peptide branches with conformational plasticity and flexibility on the same side of the molecular structure (i.e. the C-terminal portion). It is possible to speculate that a hydrophilic tail helps the peptide to escape from local energy minima and finally fall into a deeper minimum, which corresponds to a higher structural order fully compatible with the intrinsic amphipathic profile of the peptide sequence. In the literature, whether peptides folding occurs immediately before or after membrane adhesion is still an open point. The evidence of a sort of peptide "pre-folding" in solution were provided and thought to favour peptide, both thermodynamically and kinetically, to reach the "final" state in membrane.[4] Thus, in other words, it is quite reasonable to assume that a significant fraction of peptides might adhere to the membrane surface with a conformation that does not correspond to the most energetically favourable state. Due to the importance of electrostatics in this first step of the peptide-membrane interaction, it is plausible that positively charged side chains point to and interact directly with the negatively charged lipid head groups. However, this is exactly the opposite to what is typically found to be the "bound state", where hydrophobic side chains are directed towards the membrane, while hydrophilic ones point to the solvent. Definitely, there should be a stage when the peptide changes orientation and escape from the very first interaction minimum to the final deeper one.

Summarizing, from the results obtained during my PhD work, it seems that the octanamide tail provides β-SB056 with enough mobility to make full use of its inherent structural order. Conversely, it appeared that, despite the same flexible solvent exposed tail, SB056 is not able to adopt an ordered conformation, definitely due to its non-regular amphipathic profile.

The superior structural order of β-SB056 is reflected by a significantly higher microbiological activity (§3.1.1). I am aware that parameters such as MIC and MBC are due to several processes and reflect the overall peptide activity. Nevertheless, during my PhD I tried to apply simplified models to understand what is the kind of mode of action of these branched peptides with respect to lipid bilayer perturbation. Finally, I could rule out several mechanisms: pore formation (§3.1.4), detergent-like disruption (§3.1.7) and the clustering of anionic lipids (§3.1.4). Due to peptides remarkably high

positive charge (+10 net charge over 21 amino acid residues), contribution from membrane depolarization cannot be neglected. Evidence collected during the present work points to a fusogenic mechanism, in agreement with vesicles leakage (§3.1.4), vesicles size increase as shown by both UV-vis (§3.1.7) and DLS (§3.1.7), and bolstered by TEM images (§3.1.8). Further experiments are now needed to proof this, but the route to take is extremely interesting and I look forward to continue this research.

I have also investigated the effects of introducing a lipophilic tail on the most active β-SB056. The idea was to check whether activity enhancement could be obtained by improving membrane affinity. Results contradicted the hypothesis, as a general decrease in antimicrobial activity was observed for all the analogues with a lipophilic tail (§3.2.1). A dramatic increase in membrane overcrowding tendency (§3.2.2) and structural disorder (§3.2.3) was found, which is in agreement with the interpretation of the tail role proposed above. The lipophilic tails appeared to act as a really anchoring moiety. Membrane strong binding presumably reduces peptide mobility and prevents it from finding the correct structure order despite the regular amphipathic profile of the peptide branches.

In conclusion, this PhD work has shed more light on this new class of β-type branched polypeptides. The results presented here are important from two different general points of view: (i) β-peptides are definitely less studied than α-helical ones, and (ii) structure-function investigations on dendrimeric peptides are almost absent from the literature. Certainly, numerous open points remain but I hope that my work might stimulate and encourage further investigations on such interesting and functionally flexible peptide family.

## 4.2 Outlook

The present study involved the combination of several biophysical techniques, providing very interesting and sometimes unexpected results. Different open points are still open, that require further investigations. Some ideas for the next future are sketched hereinafter.

The investigated dendrimeric peptides showed to maintain activity in the presence of electrolytes at physiological concentrations, in contrast to the linear analogues. The actual reason for this has still to be deciphered. When the dendrimeric peptide is compared to the linear one, a higher number of counterions have to be considered to effectively shielding the net positive charge. One may argue that such larger counterions cloud is less favourably formed, since it would need a given number of ions with the same charge in a relatively small volume. However, also shielding of the membrane charge by positive ions should be considered, which would be absolutely peptide independent. In addition, positive charge density is almost the same for the dendrimeric and the linear peptide, such that it is much more reasonable to think that the above mentioned different susceptibility to ionic strength is mostly due to a different stability of the membrane bound state.

Let us think to the peptides investigated in this work when they form a β-sheet. In such a case, all the positively charged lysine and arginine residues would face each other, especially in the case of parallel strand pairing. Of course, positive charges would repel each other, making the overall structure unstable. It is thus possible that counterions from the surrounding solution play a stabilization role,

enhancing the stability of β-sheets and ultimately resulting in higher stability of the peptide bound state. Thus, it would be interesting to investigate whether the presence and nature of the counterions might influence peptide structure, membrane affinity and perturbing activity, without neglecting possible ion-specific effects.

As far as the mechanism of action is concerned, β-SB056 was suggested to have fusogenic activity. Fluorescence spectroscopy might be the method of choice for a new measurements campaign aimed at confirming and characterizing better such activity. In addition, it is interesting to note that amino acid sequence of each branch of β-SB056 is characterized by two lysine and two arginine residues. In the literature, a different H-bonding propensity is reported for these two residue types, with influence on peptide activity in terms of induce membrane curvature and fusogenic propensity.[5–7] It would be extremely interesting, thus, to study new analogues with four Lys and four Arg, respectively, in order to compare their behaviour and shed more light on the residue specific contribution. Then, starting from the most active analogue identified, we could extend the dendrimeric structure to a higher number of bioactive units to see whether better performance correlates with dendrimer size.

From this PhD thesis, in the specific case of the SB056 peptide family, a lipophilic tail worsened the activity, in contrast to other examples reported in literature.[8–10] Despite the hydrophilic tail appeared to be beneficial for peptide structure order, the effect on overall activity were not dramatic. This open the possibility to substitute the octanmide tail with other hydrophilic moieties, to provide the dendrimeric architecture with further properties, such as a fluorescent reporting group, for instance. Alternatively, the C-terminus of the lysine linker could be used as anchoring point to functionalize the surface of biomaterials[11–13] and nanoparticles.[14–16]

**References:**


1. Batoni, G. et al. Rational modification of a dendrimeric peptide with antimicrobial activity: consequences on membrane-binding and biological properties. Amino Acids 48, 887–900 (2015).
2. Manzo, G. et al. Enhanced Amphiphilic Profile of a Short β-Stranded Peptide Improves Its Antimicrobial Activity. PLOS ONE 10, e0116379 (2015).
3. Manzo, G. et al. The singular behavior of a β-type semi-synthetic two branches polypeptide. Three-dimensional structure and mode of action. Phys Chem Chem Phys (2016). doi:10.1039/C6CP05464A
4. D'Abramo, M. et al. Conformational behavior of temporin A and temporin L in aqueous solution: A computational/experimental study. Biopolymers 81, 215–224 (2006).
5. Mishra, A. et al. Translocation of HIV TAT peptide and analogues induced by multiplexed membrane and cytoskeletal interactions. Proc. Natl. Acad. Sci. 108, 16883–16888 (2011).
6. Schmidt, N. W. et al. Criterion for Amino Acid Composition of Defensins and Antimicrobial Peptides Based on Geometry of Membrane Destabilization. J. Am. Chem. Soc. 133, 6720–6727 (2011).
7. Schow, E. V. et al. Arginine in Membranes: The Connection Between Molecular Dynamics Simulations and Translocon-Mediated Insertion Experiments. J. Membr. Biol. 239, 35–48 (2011).
8. Khandelia, H., Ipsen, J. H. & Mouritsen, O. G. The impact of peptides on lipid membranes. Biochim. Biophys. Acta BBA - Biomembr. 1778, 1528–1536 (2008).

9. Kurtzhals, P. et al. Albumin binding of insulins acylated with fatty acids: characterization of the ligand-protein interaction and correlation between binding affinity and timing of the insulin effect in vivo. Biochem. J. 312, 725–731 (1995).
10. Pedersen, T. B., Sabra, M. C., Frokjaer, S., Mouritsen, O. G. & Jørgensen, K. Association of acylated cationic decapeptides with dipalmitoylphosphatidylserine–dipalmitoylphosphatidylcholine lipid membranes. Chem. Phys. Lipids 113, 83–95 (2001).
11. Gao, G. et al. The biocompatibility and biofilm resistance of implant coatings based on hydrophilic polymer brushes conjugated with antimicrobial peptides. Biomaterials 32, 3899–3909 (2011).
12. Etienne, O. et al. Multilayer Polyelectrolyte Films Functionalized by Insertion of Defensin: a New Approach to Protection of Implants from Bacterial Colonization. Antimicrob. Agents Chemother. 48, 3662–3669 (2004).
13. Costa, F., Carvalho, I. F., Montelaro, R. C., Gomes, P. & Martins, M. C. L. Covalent immobilization of antimicrobial peptides (AMPs) onto biomaterial surfaces. Acta Biomater. 7, 1431–1440 (2011).
14. Wang, H. et al. The efficacy of self-assembled cationic antimicrobial peptide nanoparticles against Cryptococcus neoformans for the treatment of meningitis. Biomaterials 31, 2874–2881 (2010).
15. Bi, L., Yang, L., Narsimhan, G., Bhunia, A. K. & Yao, Y. Designing carbohydrate nanoparticles for prolonged efficacy of antimicrobial peptide. J. Controlled Release 150, 150–156 (2011).
16. Pan, H., Soman, N. R., Schlesinger, P. H., Lanza, G. M. & Wickline, S. A. Cytolytic peptide nanoparticles (‘NanoBees’) for cancer therapy. Wiley Interdiscip. Rev. Nanomed. Nanobiotechnol. 3, 318–327 (2011).

**Table S1** Minimal inhibitory concentrations (MIC) of both linear and dendrimeric peptides, reported in μM. *E. coli* ATCC 25922 and *S. aureus* ATCC 25923 were chosen as representatives of Gram-negative and Gran-positive bacteria, respectively. Measurements were performed in Mueller–Hinton broth (MHB) with and without additional NaCl 150 mM. Reproduced from the reference.[1]

| **Peptide** | *E. coli* ATCC 25922 | | *S. aureus* ATCC 25923 | |
|---|---|---|---|---|
| | MHB | MHB+NaCl | MHB | MHB+NaCl |
| *SB056-linear* | 25 | >100 | >100 | >100 |
| β-SB056-*linear* | 6.25 | 12.5 | 12.5 | >100 |
| *SB056-dendrimeric* | 3.125 | 6.25 | 12.5 | 25 |
| β-SB056-*dendrimeric* | 6.25 | 3.125 | 12.5 | 6.25 |

**Table S2** Hemolitic activity of both linear and dendrimeric peptides, reported in μM. Reproduced from the reference.[1]

| **Peptide** | **% hemolysis** | | | | | | | | |
|---|---|---|---|---|---|---|---|---|---|
| | Peptide concentration (μM) | | | | | | | | |
| | 50 | 25 | 12.5 | 6.25 | 3.125 | 1.56 | 0.78 | 0.39 | 0.195 |
| *SB056-linear* | 4 | 2 | 2 | 2 | 2 | 0 | ND | ND | ND |
| *β-SB056-linear* | 11 | 11 | 6 | 6 | 2 | 2 | 2 | ND | ND |
| *SB056-dendrimeric* | 62 | 36 | 20 | 14 | 5 | 5 | 4 | ND | ND |
| *β-SB056-dendrimeric* | 34 | 24 | 21 | 16 | 15 | 15 | 11 | 8 | 4 |

**Table S3** Minimal bactericidal concentration (MBC) of both linear and dendrimeric peptides. *E. coli* ATCC 25922 and *S. aureus* ATCC 25923 were chosen as representatives of Gram-negative and Gran-positive bacteria, respectively. MBC values, reported in μM, were determined after 90-min of incubation in MHB medium at a temperature of 310K. Reproduced from the reference.[1]

| **Peptide** | *E. coli* ATCC 25922 | *S. aureus* ATCC 25923 |
|---|---|---|
| *SB056-linear* | 100 | >100 |
| *β-SB056-linear* | 12.5 | 50 |
| *SB056-dendrimeric* | 3.125 | 25 |
| *β-SB056-dendrimeric* | 6.25 | 12.5 |

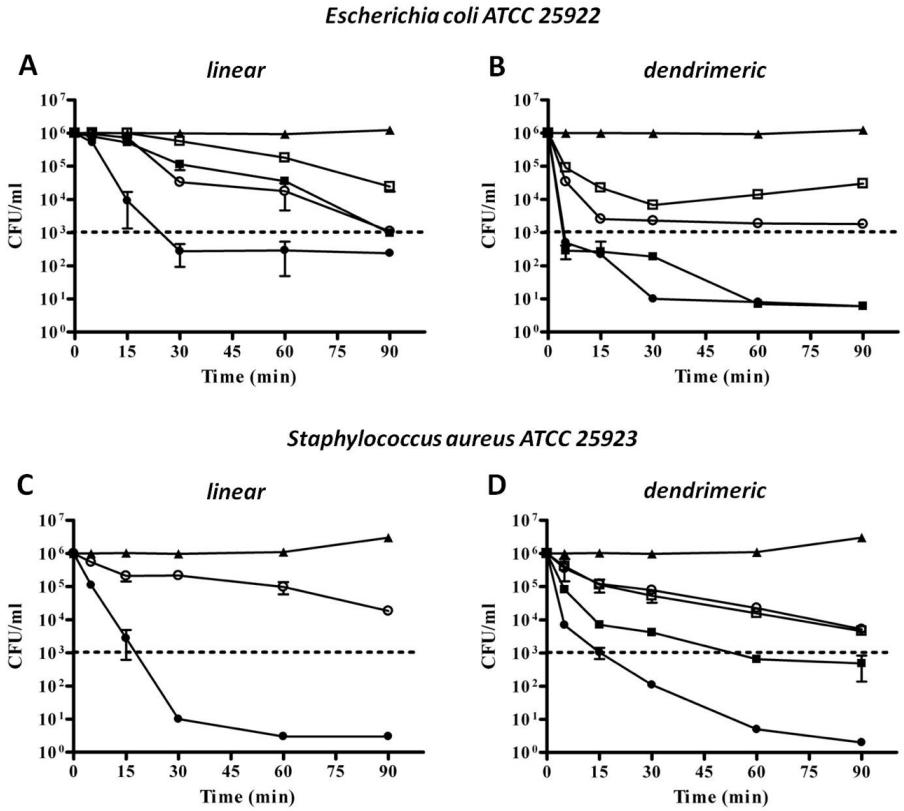


**Figure S1** Killing kinetics of linear (on the left) and dendrimeric (on the right) peptides on *E. coli* (on the top, a and b) and *S. aureus* (on the bottom, c and d). SB056, β-SB056 and the control without peptide are represented by square, circle and triangle symbols, respectively. The dotted lines indicate the killing of 99.9% of bacteria. Filled and empty symbols, respectively, indicate bacteria (1 x 106 CFU/mL) incubation at MBC or MBC/2 concentrations in MHB at a temperature of 310K. Reproduced from the reference.[1]

**Table S4** Minimal inhibitory concentrations (MIC) of both linear and dendrimeric peptide analogues against *S. epidermidis* ATCC 35984 and *Pseudomonas aeruginosa* ATCC 27853. MIC values are reporetd in μM and determined in biofilm-like conditions (stationary phase cells in 50% TSB/Glc 0.25%). Reproduced from the reference.[1]

| **Peptide** | *S. epidermidis* ATCC 35984 | *P. aeruginosa* ATCC 27853 |
|---|---|---|
| *SB056-linear* | >40 | >40 |
| *β-SB056-linear* | 10 | >40 |
| *SB056-dendrimeric* | 40 | >40 |
| *β-SB056-dendrimeric* | >40 | >40 |

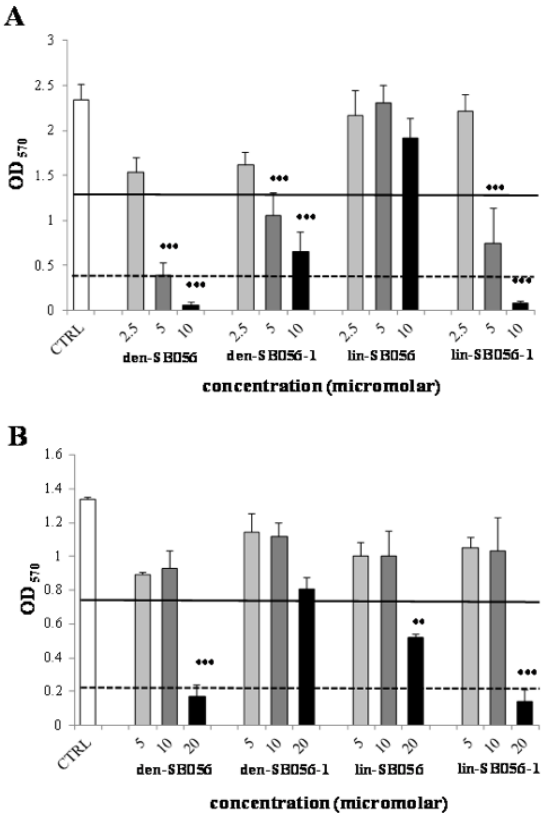


**Figure S2** Results relative to the evaluation of peptides ability to inhibit biofilm formation by *S. epidermidis* ATCC 35984 (a) and *Pseudomonas aeruginosa* ATCC 27853 (b) after 24 h of strain incubation at the temperature of 310K in a 96-well plate. Different peptide concentrations were tested and the culture in the absence of peptides was used as positive control (CTRL). Biofilm reduction was evaluated by crystal violent staining and expressed as $OD_{570}$. A reduction of 50% and 90% of biofilm mass is represented using solid and dotted lines, respectively. Data are expressed as the mean of three independent experiments ± the standard error of the mean (SEM). Stars were used to indicate statistically significant differences between the control and the biofilm values obtained for all the peptide concentration investigated, in particular $^{**}p < 0.01$ and $^{***}p < 0.001$ (one-way ANOVA followed by Tukey–Kramer multiple comparison test). Reproduced from the reference.[1]

# HPLC chromatogram and mass spectrum of β-SB056 as received from PPR

Column: XB-C18 Kinetex 2.6u 100A
Method: C1_FA0-80_60.M
Instrument: Instrument 3
Flow Rate: 1.5mls/min
Injection Volume: 20ul
Method Info: Analysis carried out using a 100A 4.6 x 50mm column, gradient from 0% - 80% Acetonitrile, in 8 minutes. At 60C.

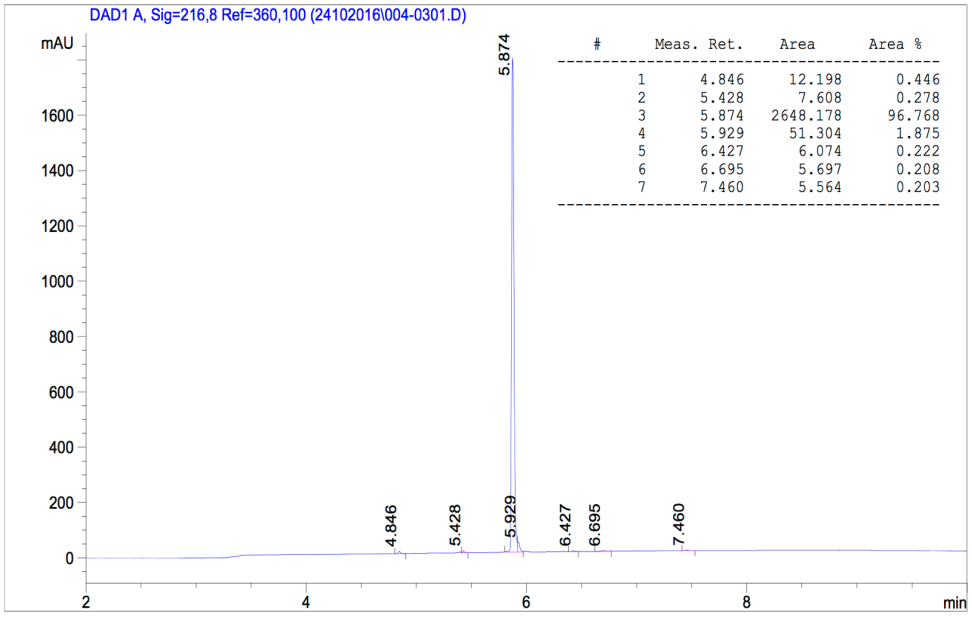


| # | Meas. Ret. | Area | Area % |
|---|---|---|---|
| 1 | 4.846 | 12.198 | 0.446 |
| 2 | 5.428 | 7.608 | 0.278 |
| 3 | 5.874 | 2648.178 | 96.768 |
| 4 | 5.929 | 51.304 | 1.875 |
| 5 | 6.427 | 6.074 | 0.222 |
| 6 | 6.695 | 5.697 | 0.208 |
| 7 | 7.460 | 5.564 | 0.203 |

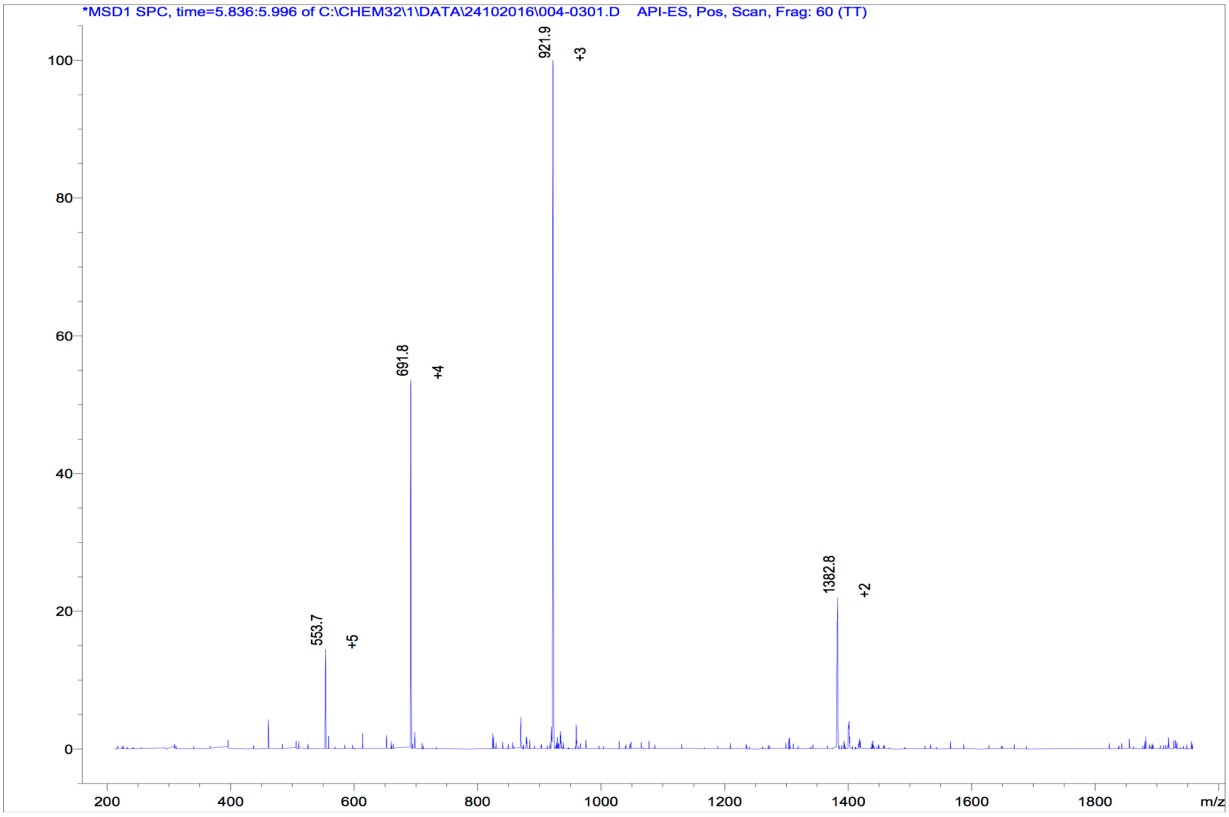

HPLC chromatogram and mass spectrum of SB056 as received from PPR

| | |
|---|---|
| Column: | Kinetex 2.6u XB-C18 A100 |
| Method: | C1_FA0-80_60.M |
| Instrument: | Instrument 1 |
| Flow Rate: | 1.5mls/min |
| Injection Volume: | 20ul |
| Method Info: | Analysis carried out using a 100A 4.6 x 50mm column, gradient from 0% - 80% Acetonitrile, in 8 minutes. |

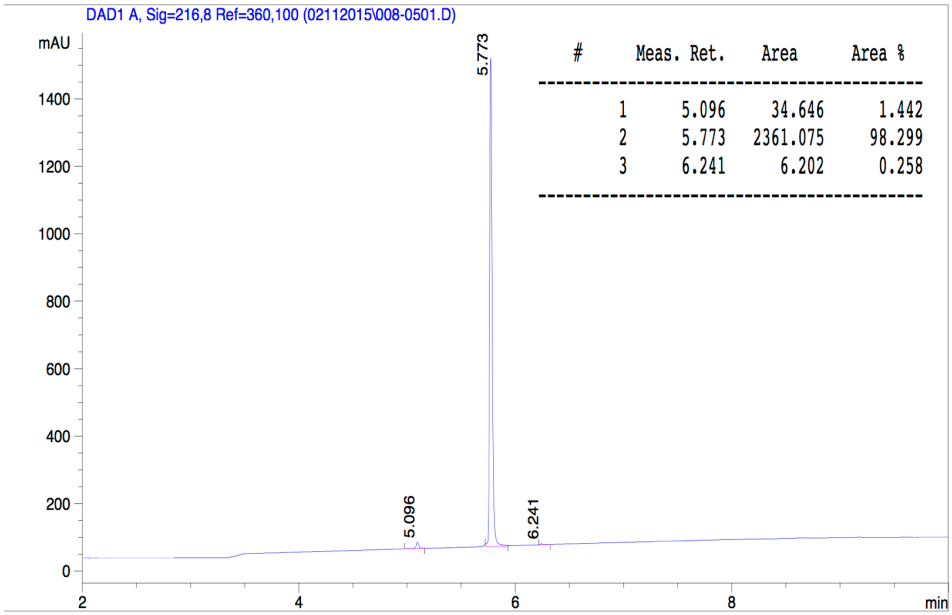


| # | Meas. Ret. | Area | Area % |
|---|---|---|---|
| 1 | 5.096 | 34.646 | 1.442 |
| 2 | 5.773 | 2361.075 | 98.299 |
| 3 | 6.241 | 6.202 | 0.258 |

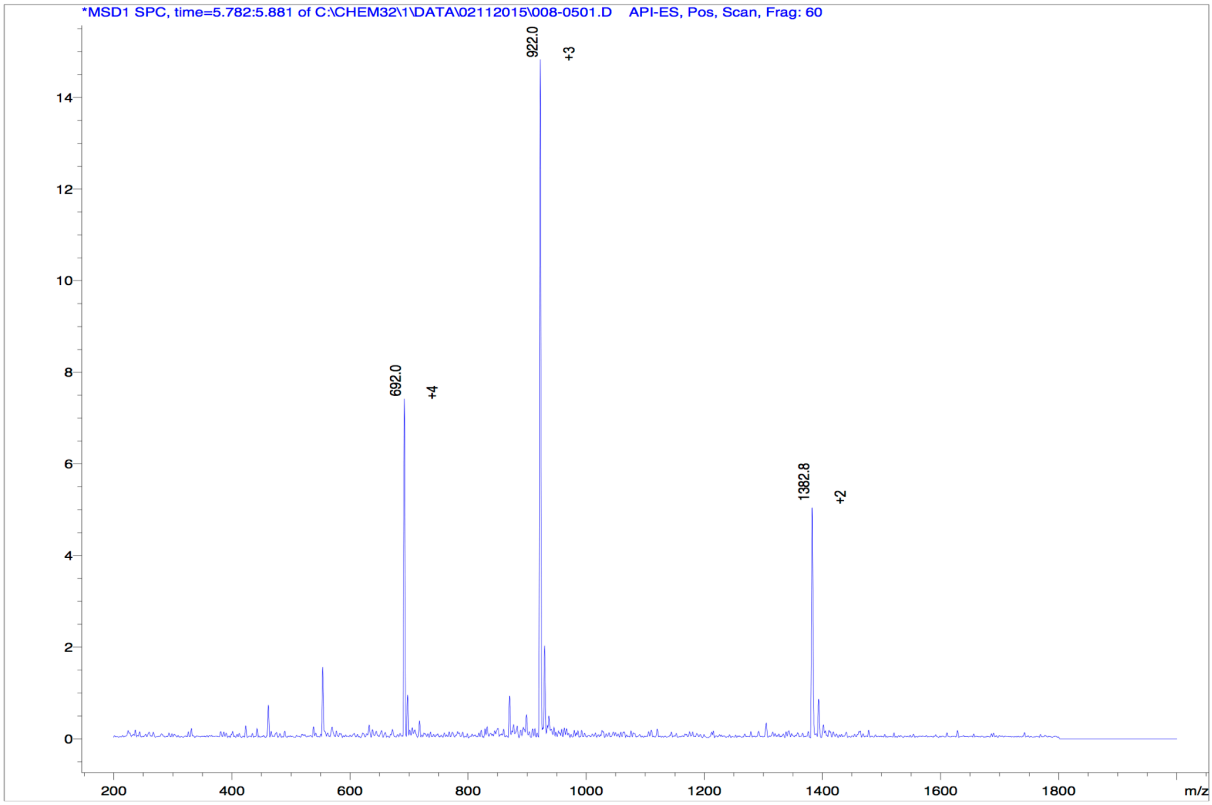

# HPLC chromatogram and mass spectrum of β-SB056-nt as received from PPR

Column: Kinetex 2.6u C18 100A
Method: C1_FA10-90_60.M
Instrument: Instrument 2
Flow Rate: 1.5mls/min
Injection Volume: 60ul
Method Info: Analysis carried out using a 100A 4.6 x 50mm column, gradient from 2% - 80% Acetonitrile, in 8 minutes.

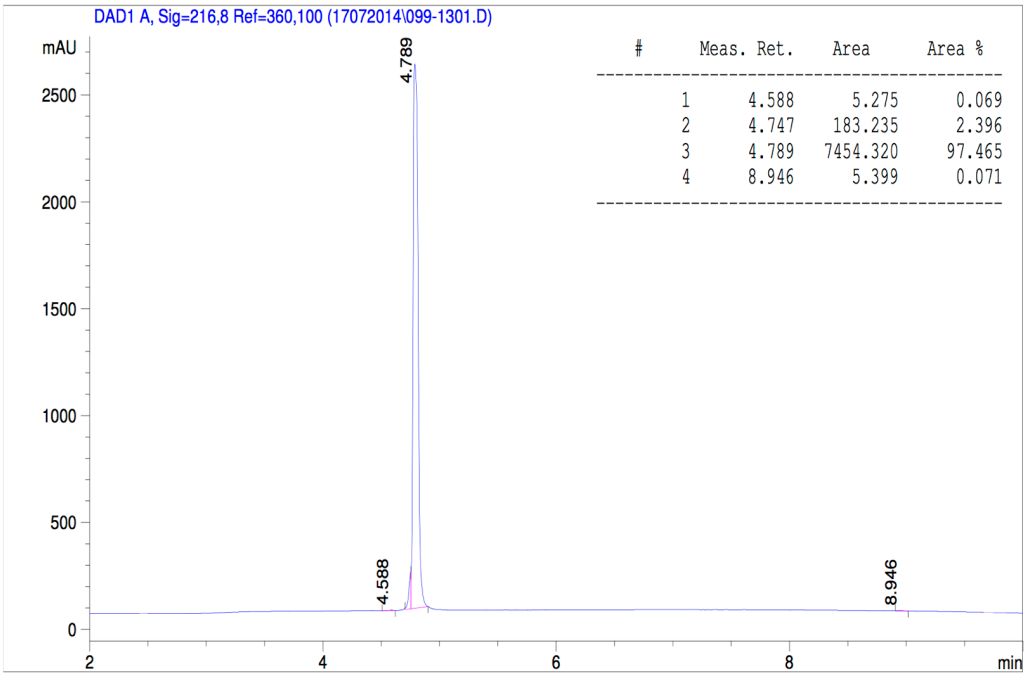


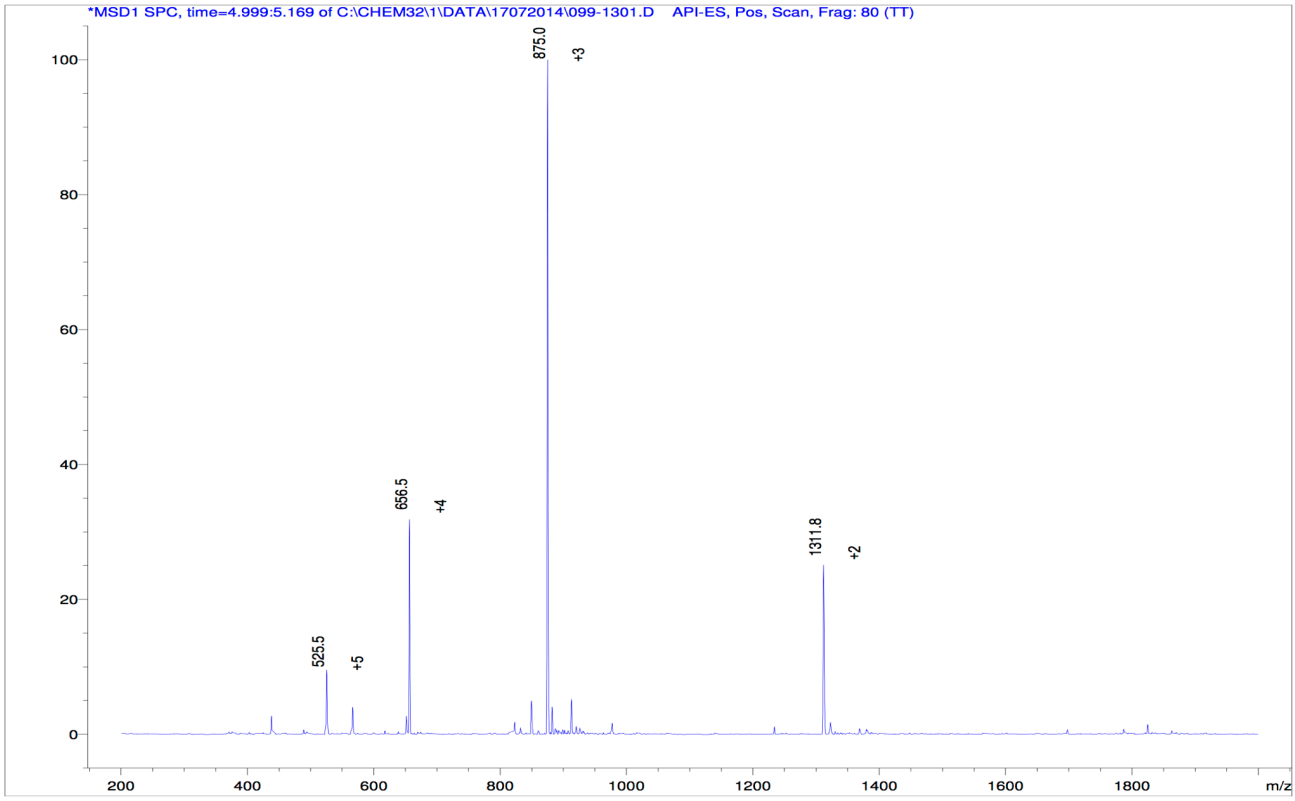

# HPLC chromatogram and mass spectrum of β-SB056-t8 as received from PPR

| | |
|---|---|
| Column: | Kinetex 2.6u C18 100A |
| Method: | C2_FA10-90_80_DMSO. |
| Instrument: | Instrument 1 |
| Flow Rate: | 1.5mls/min |
| Injection Volume: | 20ul |
| Method Info: | Analysis carried out using a 100A 4.6 x 50mm column, gradient from 10% - 90% Acetonitrile, in 8 minutes. At 60°C. Dissolved in DMSO. |

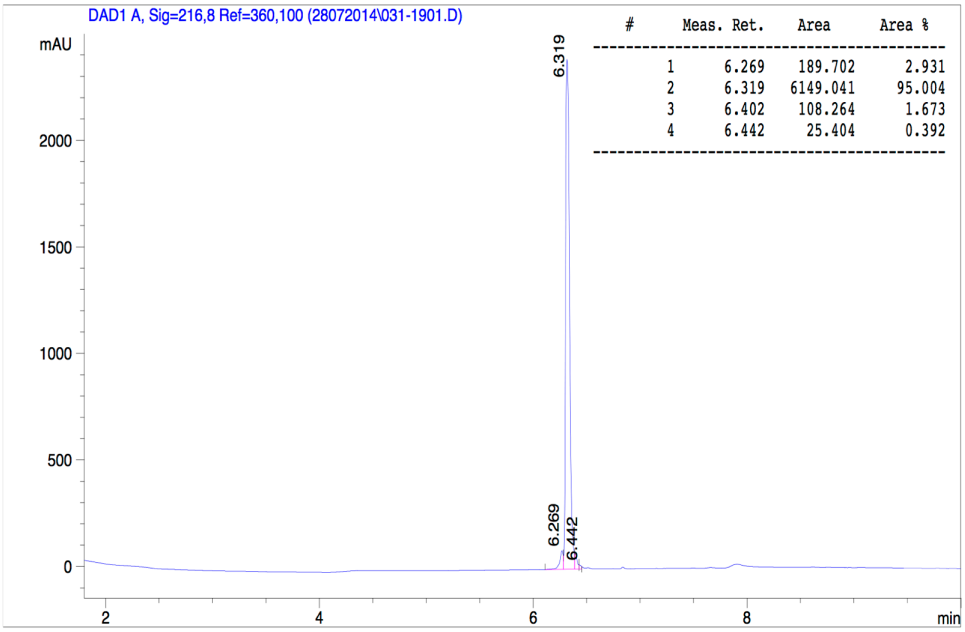


| # | Meas. Ret. | Area | Area % |
|---|---|---|---|
| 1 | 6.269 | 189.702 | 2.931 |
| 2 | 6.319 | 6149.041 | 95.004 |
| 3 | 6.402 | 108.264 | 1.673 |
| 4 | 6.442 | 25.404 | 0.392 |

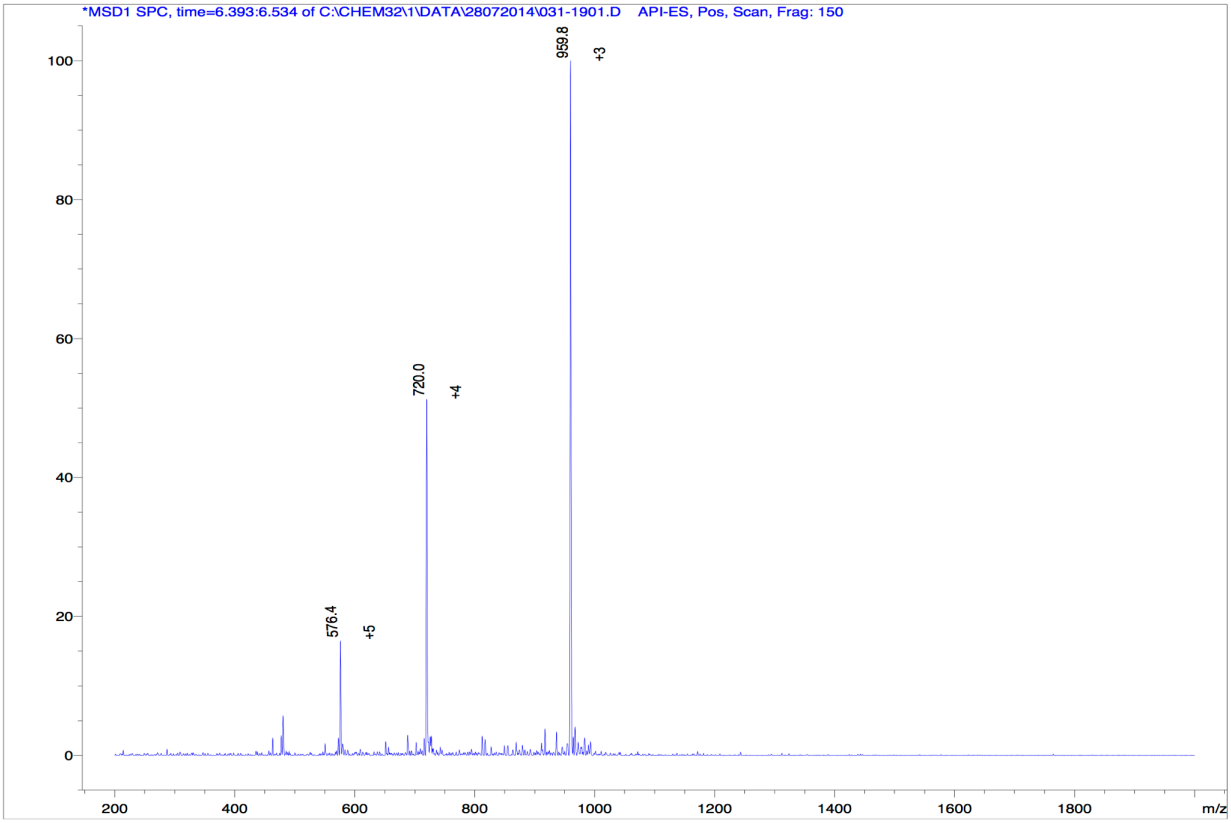

# HPLC chromatogram and mass spectrum of β-SB056-t14 as received from PPR

Column: Kinetex 2.6u C18 100A
Method: C2_FA10-90_80_DMSO.
Instrument: Instrument 1
Flow Rate: 1.5mls/min
Injection Volume: 20ul
Method Info: Analysis carried out using a 130A 4.6 x 50mm column, gradient from 10% - 90% Acetonitrile, in 8 minutes. At 80C.

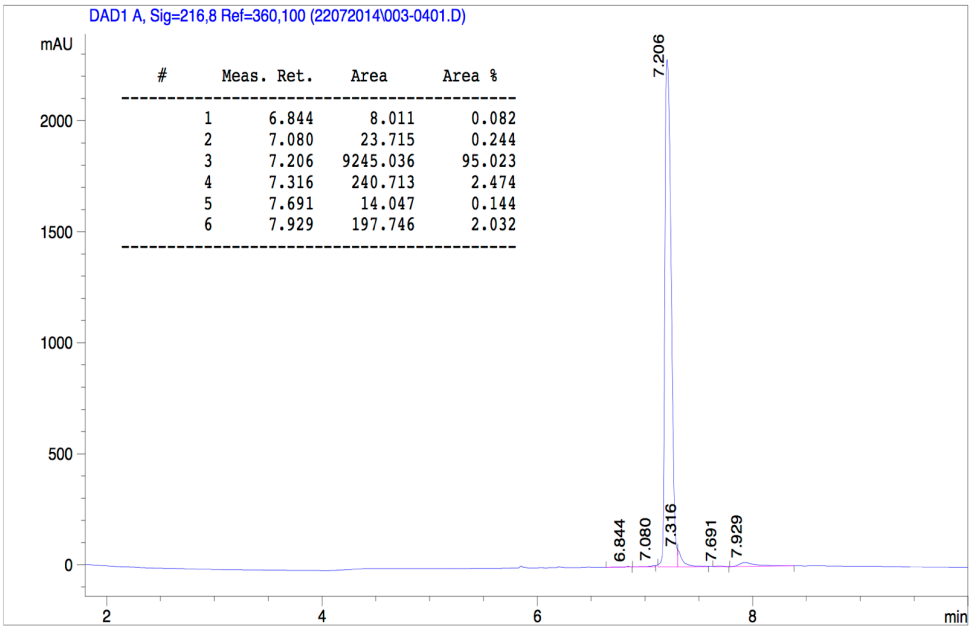


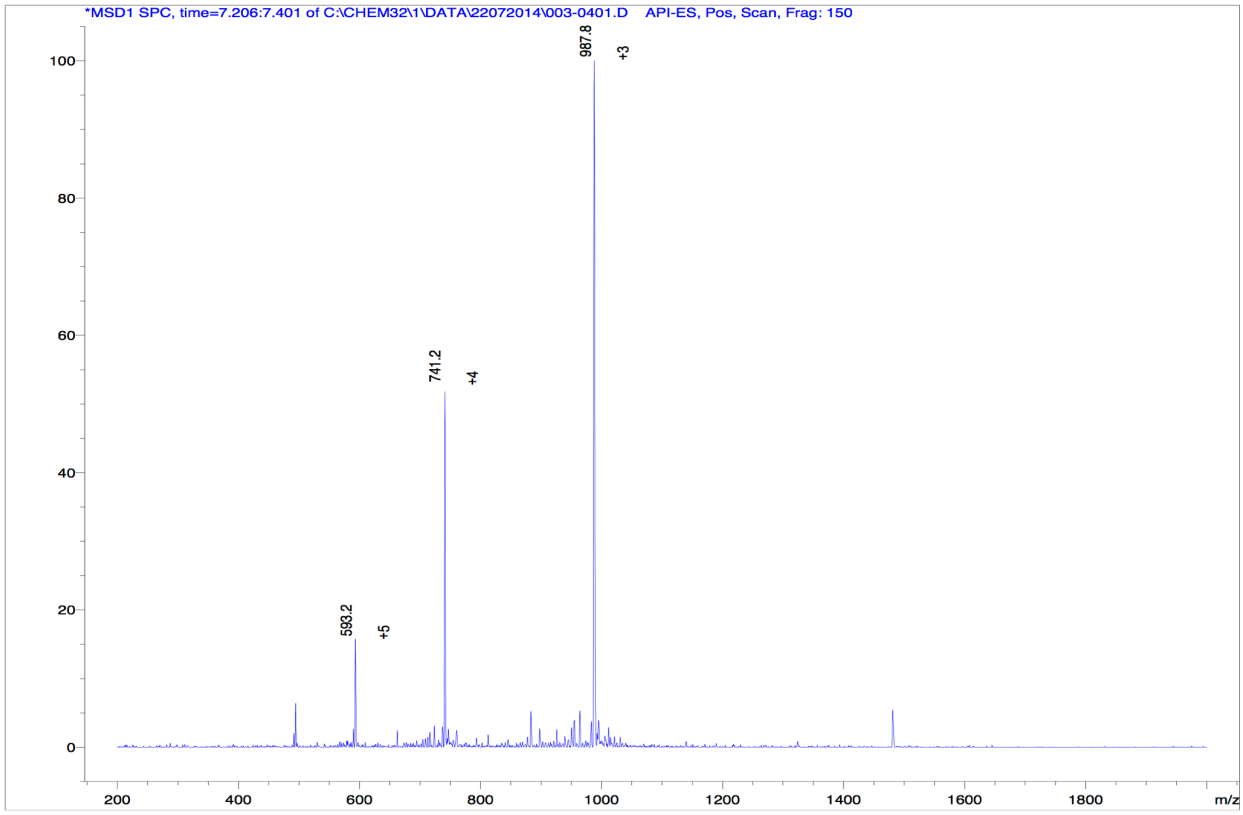

HPLC chromatogram and mass spectrum of β-SB056-t18 as received from PPR

| | |
|---|---|
| Column: | Kinetex 2.6u C18 100A |
| Method: | C2_FA10-90_80_DMSO. |
| Instrument: | Instrument 1 |
| Flow Rate: | 1.5mls/min |
| Injection Volume: | 20ul |
| Method Info: | Analysis carried out using a 130A 4.6 x 50mm column, gradient from 10% - 90% Acetonitrile, in 8 minutes. At 80C. |

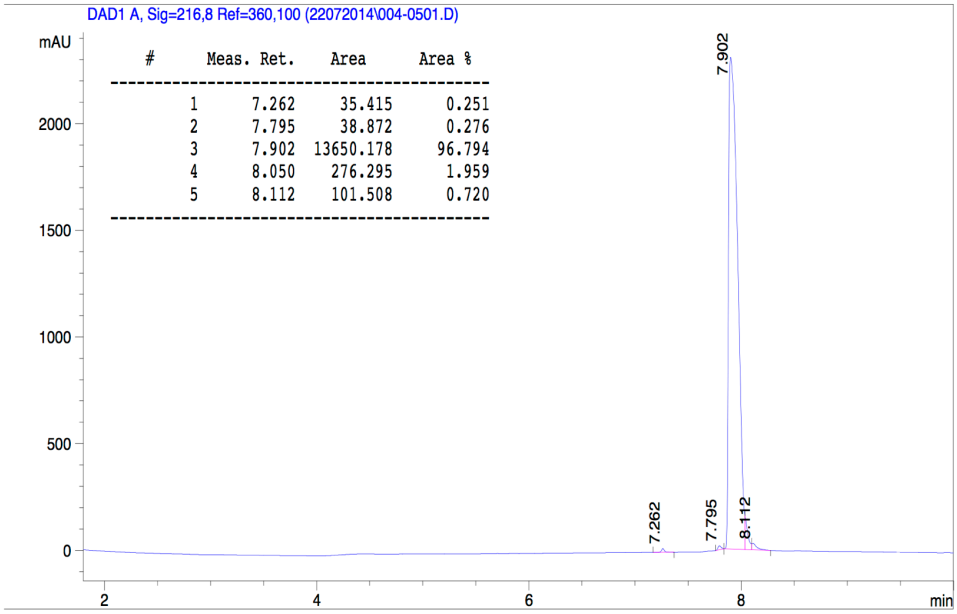


| # | Meas. Ret. | Area | Area % |
|---|---|---|---|
| 1 | 7.262 | 35.415 | 0.251 |
| 2 | 7.795 | 38.872 | 0.276 |
| 3 | 7.902 | 13650.178 | 96.794 |
| 4 | 8.050 | 276.295 | 1.959 |
| 5 | 8.112 | 101.508 | 0.720 |

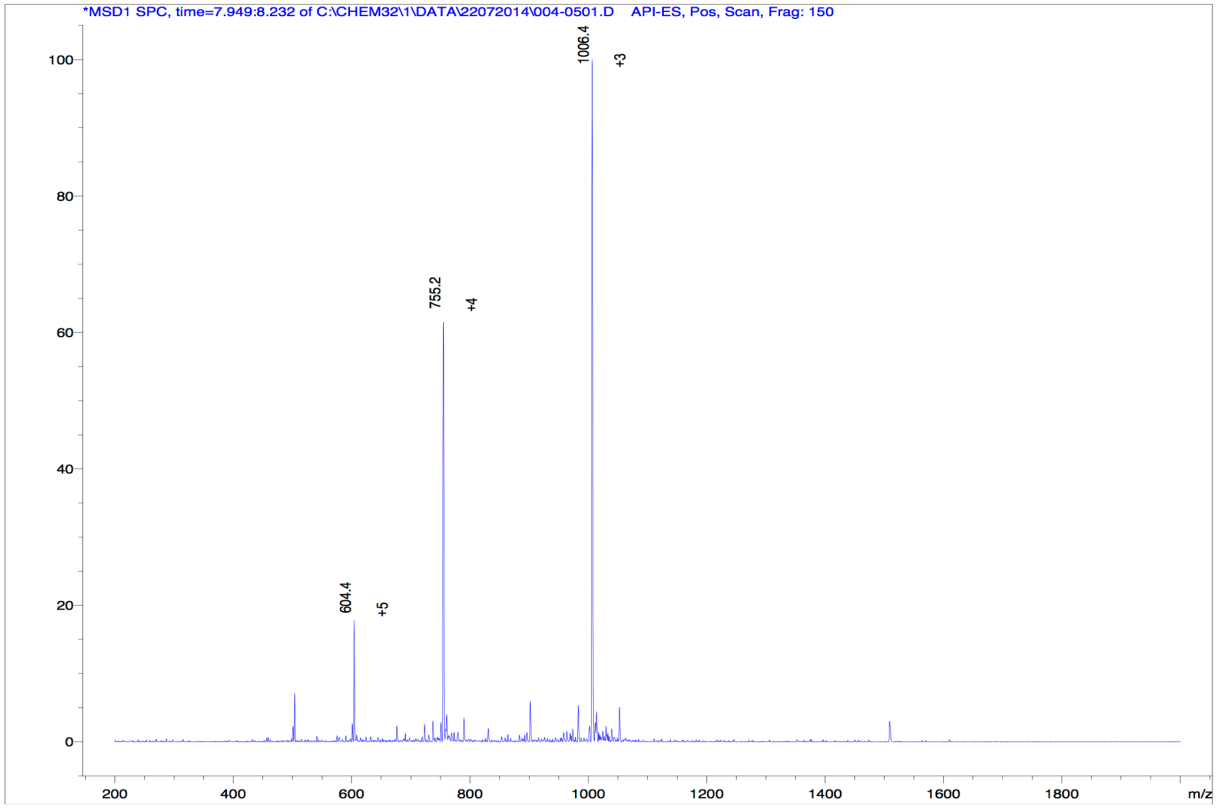

**References:**

1. Batoni, G. *et al.* Rational modification of a dendrimeric peptide with antimicrobial activity: consequences on membrane-binding and biological properties. *Amino Acids* 48, 887–900 (2015).